

https://dspace.org/

Optimisation of the offset distance between idler rolls to minimise stress within conveyor belting

De Andrade, Nelson Sergio

2017

https://hdl.handle.net/10539/25505

De Andrade, Nelson Sergio (2017) Optimisation of the offset distance between idler rolls to minimise stress within conveyor belting, University of the Witwatersrand, <https://hdl.handle.net/10539/25505>

Downloaded from a DSpace repository. https://dspace.org/

Optimisation of the Offset Distance Between Idler Rolls to Minimise Stress Within Conveyor Belting.

by

Nelson Sergio De Andrade

698166

A Research Report submitted to the Faculty of Engineering and the Built Environment in partial fulfilment of the requirements for the degree of

MASTER OF SCIENCE IN ENGINEERING

In

MECHANICAL ENGINEERING

at the

UNIVERSITY OF WITWATERSRAND

Supervisor: Prof John Sheer

Johannesburg
June 2017

Declaration

I, Nelson Sergio De Andrade, hereby declare that this research report is wholly my own work and has not been submitted anywhere else for academic credit either by myself or by another person.

I understand what plagiarism implies and declare that this research report is my own ideas, words, phrases, arguments, graphics, figures, results and organisation except where reference is explicitly made to another person's work.

I understand further that any unethical academic behaviour, which includes plagiarism, is seen in a serious light by the University of Witwatersrand and is punishable by disciplinary action.

…….…… …..……

Signed Date

N De Andrade

Abstract

This research report describes the creation of a unique experimental facility for investigating localised stresses that can develop in conveyor belting during operation. High localised stresses can cause premature failure of conveyor belts, requiring expensive replacement. A key objective of carrying out research in this field is to gain a fundamental understanding of the stress that develops in various types of conveyor belting as it crosses over idler rollers. An experimental facility was developed that will be able to measure the stress and the deformation for different types of belting, such as solid woven/PVC and ply belting, with different belt classes. Particular attention was given to the various effects at the junction point caused by different idler configurations.

Idler arrangements are configurable in the 24m–long test facility for inline, offset and belt-friendly types. Belt stresses at the idler junctions of these configurations are measured by applying strain gauges and load cells. The offset distance can be varied to determine the effect this has on the developing idler junction stress. This will allow comparison of the stresses as the class of belt increases, for each type of belt. The value of doing so is to determine the effect that the weft strength or stiffness has as the belt is forced into the idler junction.

The test facility that was designed and built was shown to meet the requirements of the project. The instruments were calibrated to an acceptable uncertainty. The test facility can handle the full range of planned tests in terms of the design strength and is modular enough to handle a variety of other research initiatives. This establishment of a large, specialised experimental facility constitutes the first phase of an ongoing research programme into improving the design standards for belt conveyor systems.

Acknowledgements

I would like to extend my deepest gratitude to all the sponsors and volunteers that donated and assisted with this research project. Cowles Engineering for supplying the steel work and manufacturing guidance. Flexco for the loan of a suitable testing site with the necessary provisions to conduct the research. The IMHC, CMA and the University of the Witwatersrand for their financial support. Melco, Tectra Automation and Dunlop for their assistance in providing equipment. A special thanks to those who went above and beyond the call of duty to finalise the installation and setup of the testing facility.

Table of Contents:

1 INTRODUCTION 1

1.1 PURPOSE OF THE STUDY 1
1.2 RESEARCH BACKGROUND 2
1.3 RESEARCH MOTIVATION 4
1.4 PROBLEM STATEMENT 4
1.5 RESEARCH OBJECTIVES AND SCOPE 5
1.6 THE METHODOLOGY USED 6
1.7 ASSUMPTIONS 7

2 LITERATURE REVIEW 8

2.1 HISTORY 8
2.2 BELT CONSTRUCTIONS 11
2.2.1 Carcass 13
2.2.2 Covers 16
2.3 BELT TENSION DETERMINATION 18
2.4 IDLER JUNCTION FAILURE 20
2.4.1 Belt Tension and Load Support 20
2.4.2 Belt Rigidity 21
2.4.3 Trough Angle 22
2.4.4 Transition Distance 23
2.4.5 Idler junction failure in Inline idlers with Steel Cord Belts 23
2.5 STRAIN GAUGES APPLIED TO BELTS 29

3 DESIGN AND DEVELOPMENT OF THE EXPERIMENTAL TEST FACILITY 31

3.1 CONCEPTS GENERATION 31
3.2 THE FINAL DESIGN OF THE EXPERIMENTAL FACILITY 34
3.3 EXPERIMENTAL PROGRAMME 41
3.4 CALIBRATION 42

4 COMMISSIONING, TESTING AND VERIFICATION OF THE TEST FACILITY 43

4.1 STRAIN GAUGE CALIBRATION 43
4.1.1 Obtaining a Useable Calibration Factor 43
4.1.2 Calibration Method and Procedure 44
4.1.3 Strain Gauge Calibration Results 52
4.2 LOAD CELL CALIBRATION 56
4.3 TEST FACILITY COMMISSIONING 62
4.3.1 The Structure 62
4.3.2 The Belt Profiler Design 64
4.3.3 The Belt Profiler Assembly Accuracy 69
4.4 OVERALL TESTING OF THE FACILITY 78
4.5 SAFETY MEASURES DESIGNED INTO THE TEST FACILITY 87
4.6 OBSTACLES THAT WERE OVERCOME DURING THE COMMISSIONING PROCESS 88
4.6.1 Sample Preparation 88
4.6.2 Strain Gauge Constraints 88
4.6.3 Lifting the belt under Tension 90
4.6.4 Test Facility Alignment 90

5 DISCUSSION OF THE WORK CARRIED OUT 91

5.1 RANGE AND SCOPE OF THE TEST FACILITY 92
5.2 NEXT STEPS 93

6 RECOMMENDATIONS FOR FURTHER WORK 94

7 REFERENCES 95

8 APPENDICES 98

8.1 DESIGN CALCULATIONS 98
8.1.1 Determination of the Radius of the Convex Curve 98
8.1.2 FEA Analysis of Key Components 100
8.1.3 Deflection Calculations 102
8.1.4 Stress Calculation in the Belt Gantry Lifter 105
8.2 ENGINEERING DRAWINGS 107
8.2.1 Test Facility Overview 107
8.2.2 Belt Attachment 109
8.2.3 Sheave Frame Assembly 110
8.2.4 Belt Gantry Lifter 112
8.2.5 Column Supports 114
8.2.6 Belt Profiler 116
8.3 EQUIPMENT USED 117
8.3.1 Test Instrumentation 117
8.3.2 Calibration Instrumentation 118
8.4 LOAD CELL DATA 121
8.4.1 Readings for the 2 Ton Loadcells 121
8.4.2 Readings for the 20 Ton Loadcell 123

List of Figures:

FIGURE 1-1: 3 ROLL INLINE TROUGHING IDLER (LORBRAND, 2008). 2
FIGURE 1-2: 3 ROLL OFFSET TROUGHING IDLER (LORBRAND, 2008). 2
FIGURE 1-3: ROLL OFFSET BELT FRIENDLY TROUGHING IDLER (LORBRAND, 2008). 3
FIGURE 1-4: ILLUSTRATION OF OFFSET DISTANCE (SANS 1313-1, 2012). 4
FIGURE 2-1: ILLUSTRATION OF THE MAJOR PIECES OF A CONVEYOR SYSTEM (CKIT, 2015). 9
FIGURE 2-2: A DETAILED VIEW OF THE WEFT AND WARP FIBRES IN BELT CONSTRUCTION (HYC, 2016). 11
FIGURE 2-3: SCHEMATIC OF A CROSS SECTION OF PLIED BELT (HENAN PINGYUAN MINING MACHINERY CO. LTD., 2016). 11
FIGURE 2-4: SCHEMATIC CROSS SECTION OF A PLIED CONVEYOR BELT (SATYENDRA, 2013). 12
FIGURE 2-5: DIFFERENT WEAVE CONSTRUCTIONS (KEVRA, 2016). 15
FIGURE 2-6: TENSION DISTRIBUTION FOR STEADY STATE CONDITIONS (WHEELER, 2012). 19
FIGURE 2-7: A CONVEX CURVE BELT (CKIT, 2017). 20
FIGURE 2-8: THE TENSION ON A CONVEX CURVE WILL FORCE THE UNSUPPORTED BELT AREA INTO THE GAP BETWEEN THE IDLERS AS INDICATED BY THE ARROWS (FAYED & SKOCIR, 1997). 21
FIGURE 2-9: THREE-ROLL TROUGH ILLUSTRATING THE SUPPORTED AND UNSUPPORTED BELT TROUGH (AC-TEK, 2017). 22
FIGURE 2-10: WING IDLERS AT 30^0. 22
FIGURE 2-11: WING IDLERS AT 90^0. 22
FIGURE 2-12: IN-LINE OR FULL TROUGH TRANSITION (LEMMON, 2015) 23
FIGURE 2-13: BELT CONTACTING IDLER EDGE, WHICH CAN ACT LIKE A KNIFE EDGE AND DAMAGE THE BELT (ZHANG, 2015). 24
FIGURE 2-14: ILLUSTRATION OF THE ASYMMETRIC PRESSURE DISTRIBUTION, THAT RESULTS IN THE INDENTATION ROLLING RESISTANCE (WHEELER, 2012). 25
FIGURE 2-15:DAMAGE ON BOTTOM COVER DUE TO HIGH CONTACT PRESSURE (ZHANG, 2015). 25
FIGURE 2-16: WEAR ON BOTTOM COVER CAUSED BY THE FORWARD TILT OF THE WING ROLLS (ZHANG, 2015). 26
FIGURE 2-17: EQUIVALENT (VON MISES) STRAIN IN THE BELT COVER OF A STEEL CORD BELT FROM FINITE ELEMENT MODELLING (ZHANG, 2015). 27
FIGURE 2-18: IDLER JUNCTION DAMAGE OCCURRING ON A BELT FRIENDLY IDLER CONFIGURATION, SIDE VIEW. 28
FIGURE 2-19: IDLER JUNCTION DAMAGE OCCURRING ON A BELT FRIENDLY IDLER CONFIGURATION, FRONT VIEW. 28
FIGURE 2-20: ILLUSTRATION OF METHOD USED TO DETERMINE THE BELT ELONGATION. 29
FIGURE 2-21: BENDING STRAIN OF THE TOP STRAND DUE TO A CONICAL PULLEY, 125MM BELT WIDTH, MEASURED BY STRAIN GAUGES COMPARED WITH THE CALCULATED DISTORTION (EGGER M, 2002). 30
FIGURE 3-1: POSSIBLE CONCEPT FOR A TEST FACILITY. 32
FIGURE 3-2: ILLUSTRATION OF HOW THE DIGITAL IMAGE CORRELATION (DIC) TECHNIQUE WORKS (DANTEC DYNAMICS, 2015). 33
FIGURE 3-3: COMPONENTS OF THE TEST FACILITY. 35
FIGURE 3-4: IMAGE OF THE SHEAVE STRUCTURE AND BELT ATTACHMENT. 36
FIGURE 3-5: BELT ATTACHMENT IN OPERATION. 37
FIGURE 3-6: MAGNETIC ENCODER USED ON THE TESTING FACILITY. 38
FIGURE 3-7: ILLUSTRATION OF IMPORTANT ZONES IN THE TEST SETUP, TOP VIEW. 39
FIGURE 3-8: EXPERIMENTAL FACILITY DEPICTING THE STRAIGHT SETUP, DIMETRIC VIEW. 39
FIGURE 3-9: EXPERIMENTAL FACILITY DEPICTING THE STRAIGHT SETUP, FRONT VIEW. 39
FIGURE 3-10: EXPERIMENTAL FACILITY DEPICTING THE CONVEX SETUP, DIMETRIC VIEW. 40
FIGURE 3-11: EXPERIMENTAL FACILITY DEPICTING THE CONVEX SETUP, FRONT VIEW. 40
FIGURE 3-12: LOCATION FOR STRESS MEASUREMENT, TOP VIEW. 41
FIGURE 4-1: CONVENTIONAL SAMPLE WITH CONTINUOUSLY VARYING CROSS SECTIONAL AREA. 44

FIGURE 4-2: SAMPLE WITH MODIFIED GAUGE LENGTH TO HAVE PARALLEL SIDES. 45
FIGURE 4-3: GRAPH OF VARIATION OF AMPLITUDE OF THE LOAD AS A FUNCTION OF ELONGATION (ISO 9856, 1989). 46
FIGURE 4-4: BELT SAMPLE IN TENSILE TESTER WITH EXTENSOMETER ATTACHED. 47
FIGURE 4-5: SETUP OF BELT SAMPLE WITH IN A TENSILE TESTING MACHINE. 48
FIGURE 4-6: QUARTER BRIDGE CONFIGURATION SENSITIVE TO BOTH THE NORMAL FORCE AND BENDING MOMENTS, WITH TEMPERATURE COMPENSATION (HOFFMANN, 2015). 49
FIGURE 4-7: TOP AND BOTTOM COVERS OF THE BELT SAMPLE, ILLUSTRATING GAUGE LOCATION. 49
FIGURE 4-8: BELT SAMPLE WITH GAUGES ATTACHED 50
FIGURE 4-9: ILLUSTRATION OF POSSIBLE OUTCOMES OF THE TESTING, WITH REGARD TO THE COVER ELONGATION. 51
FIGURE 4-10: STRAIN GAUGE ARRANGEMENT PATTERNS. 51
FIGURE 4-11: BAR GRAPH OF FORCE VS CUMULATIVE LENGTH. 52
FIGURE 4-12: SCATTER GRAPH OF FORCE VS CUMULATIVE LENGTH. 53
FIGURE 4-13: STRAIN VERSUS CUMULATIVE LENGTH FOR THE LOADING CYCLE FOR THE TOP COVER. 54
FIGURE 4-14: STRAIN VERSUS CUMULATIVE LENGTH FOR THE UNLOADING CYCLE FOR THE TOP COVER. 55
FIGURE 4-15: SCHEMATIC ILLUSTRATION OF THE 2 TON LOAD CELL CALIBRATION PROCESS. 57
FIGURE 4-16: ILLUSTRATION OF THE SETUP, USED FOR THE CALIBRATION OF THE LOAD CELLS. 58
FIGURE 4-17: 2 TON LOADCELL CALIBRATION RESULTS. 59
FIGURE 4-18: 20 TON LOADCELL CALIBRATION RESULTS. 60
FIGURE 4-19: OVERVIEW OF THE SETUP FOR THE CALIBRATION PROCESS FOR THE 20 TON LOAD CELL. 61
FIGURE 4-20: OVERVIEW STEPS OF HOW THE RIG WAS ALIGNED. 63
FIGURE 4-21: OVERVIEW OF BELT PROFILER DESIGN. 64
FIGURE 4-22: ILLUSTRATION OF AN I BEAM WITH A NATURAL CAMBER (EXAGGERATED) IN THE LENGTH OF THE UNIT. 64
FIGURE 4-23: SLOTTED RECTANGULAR TUBES. 65
FIGURE 4-24: ILLUSTRATION OF THE RECTANGULAR TUBES CONNECTED TO THE I-BEAMS AND PER 90X90 ALUMINIUM BEAM 65
FIGURE 4-25: WORKINGS OF THE STEPPER MOTOR ON THE BELT PROFILER. 66
FIGURE 4-26: ILLUSTRATION OF THE BELT PROFILER PROBE 67
FIGURE 4-27: PATH THE PROBE WILL FOLLOW ON EACH TEST 67
FIGURE 4-28: MOVEMENT OF THE BELT PROFILER STEM BY MEANS OF THE ALUMINIUM RAIL (BROWN) AND CAM ROLLER BEARING (GREEN). 68
FIGURE 4-29: LASER LINE ON BELT PROFILER STEM. 69
FIGURE 4-30: ADJUSTMENT POSITIONS ON BELT PROFILER. 70
FIGURE 4-31: A SCHEMATIC OF LASER DIVERGENCE; THE LASER SPREADS BY AN ANGLE OF Φ SO OVER A DISTANCE D, THE LASER SPREADS TO A WIDTH OF 2R. 70
FIGURE 4-32: RULER ATTACHED TO THE STEM OF THE BELT PROFILER 71
FIGURE 4-33: THE COLOURED WATER SHOWS EXACTLY WHERE THE LINE ON THE RULER WAS. 73
FIGURE 4-34: A PHOTOGRAPH TAKEN FROM THE CORRECT ANGLE PROVIDES SYMMETRY, MAKING IT EASY TO FIND THE CENTRE OF THE READING. 73
FIGURE 4-35: OVERVIEW OF THE WATER TROUGH LEVELLING METHOD 74
FIGURE 4-36: THE SETUP OF THE FINAL WATER AIDED PROBE MOVEMENT PLANE CALIBRATION 75
FIGURE 4-37: SCHEMATIC OF THE PROFILER PROBE MOVEMENT PLANE. 76
FIGURE 4-38: IMAGE OF THE HYDRAULIC CYLINDERS IN OPERATION 78
FIGURE 4-39: BELT GANTRY LIFTER DEPICTING THE HOW THE BELT WILL BE RAISED OFF THE IDLERS. 79
FIGURE 4-40: ILLUSTRATION OF THE BELT TROUGH CENTROID. 80
FIGURE 4-41: SHEAVE STRUCTURE WILL THE MAIN SHEAVE AND GUIDING SHEAVE IN PLACE. 80
FIGURE 4-42: GUIDING SHEAVE DIRECTING THE STEEL WIRE ROPE 81
FIGURE 4-43: DASHBOARD FOR LABVIEW DATA ACQUISITION FOR THE STRAIN GAUGES. 82
FIGURE 4-44: NATIONAL INSTRUMENTS HARDWARE 83
FIGURE 4-45: LABVIEW AND NI SAMPLE SET-UP TO ACQUIRE DATA 84

FIGURE 4-46: MOTOR USED ON THE TEST FACILITY. 85
FIGURE 4-47: VFD USED ON THE TEST FACILITY. 85
FIGURE 4-48: TIRFOR USED TO MOVE THE CABLE AND BELT AROUND THE STRUCTURE. 86
FIGURE 4-49: ILLUSTRATION OF IMPORTANT ZONES IN THE TEST SETUP, TOP VIEW. 89
FIGURE 8-1: FEA ANALYSIS OF THE UNIVERSAL IDLER BASE FRAME 100
FIGURE 8-2: FEA ANALYSIS OF THE BELT ATTACHMENT. 100
FIGURE 8-3: FEA ANALYSIS OF THE SHEAVE FRAME STRUCTURE. 101
FIGURE 8-4: SIMPLE SUPPORTS WITH A CENTRE LOAD (NISBETT, 2011). 102
FIGURE 8-5: SIMPLE SUPPORTS WITH A UNIFORMLY DISTRIBUTED LOAD (NISBETT, 2011). 102
FIGURE 8-6: 90X90 ALUMINIUM BEAM SECTION, FOR THE BELT PROFILER. 104
FIGURE 8-7: I BEAM SECTION, FOR THE BELT PROFILER. 104
FIGURE 8-8: I BEAM SECTION, FOR THE BELT GANTRY LIFTER. 104
FIGURE 8-9: DOUBLE 180X90 ALUMINIUM BEAM SECTION, FOR THE BELT PROFILER. 104
FIGURE 8-10: SECTIONED VIEW OF BELT GANTRY LIFTER BEAM. 106
FIGURE 8-11: OVERVIEW OF THE CONVEX TEST FACILITY CONFIGURATION. 107
FIGURE 8-12: OVERVIEW OF THE FLAT TEST FACILITY CONFIGURATION. 108
FIGURE 8-13: GENERAL ARRANGEMENT DRAWING OF THE BELT ATTACHMENT. 109
FIGURE 8-14: GENERAL ARRANGEMENT DRAWING OF THE SHEAVE FRAME SECTION. 110
FIGURE 8-15: GENERAL ARRANGEMENT DRAWING OF THE SHEAVE FRAME ASSEMBLY. 111
FIGURE 8-16: GENERAL ARRANGEMENT DRAWING OF THE BELT GANTRY LIFTER. 112
FIGURE 8-17: GENERAL ARRANGEMENT DRAWING OF THE BELT GANTRY LIFTER'S MAIN BEAM. 113
FIGURE 8-18: GENERAL ARRANGEMENT DRAWING OF THE COLUMN SUPPORT WITH THE UNIVERSAL IDLER FRAME. 114
FIGURE 8-19: DETAILED VIEW OF THE COLUMN SUPPORT WITH 2TON LOAD CELLS. 115
FIGURE 8-20: GENERAL ARRANGEMENT DRAWING OF THE BELT PROFILER. 116
FIGURE 8-21: ILLUSTRATION OF AN MTS CRITERION C45 TENSILE TESTER. 118
FIGURE 8-22: CALIBRATION CERTIFICATE OF MTS CRITERION C45 TENSILE TESTER. 119
FIGURE 8-23: FARO GAGE USED IN THE LEVELLING FOR THE BELT PROFILER (FARO, 2017). 120

List of Tables:

TABLE 2-1: TYPES OF CARCASSES (SATYENDRA, 2013). 13
TABLE 2-2: EVALUATION OF PLIES (SATYENDRA, 2013). 14
TABLE 2-3: TYPES OF COVER DEFINED IN SANS CONVEYOR BELTING STANDARDS (PITCHER, 2012)..... 17
TABLE 3-1: LAYOUT OF DATA TO BE COLLECTED FROM TEST FACILITY. 42
TABLE 4-1: VARIANCE BETWEEN THE READINGS FOR STRAIN FOR A GIVEN LOAD. 55
TABLE 4-2: UNCERTAINTY AT EACH LOAD TESTED FOR THE LOAD CELL CALIBRATION. 60
TABLE 4-3: PROCESS OF OBTAINING READINGS PHOTOGRAPHICALLY WITH THE LASER METHOD. 72
TABLE 4-4: PROCESS OF OBTAINING READINGS PHOTOGRAPHICALLY WITH THE WATER METHOD..... 76
TABLE 4-5: RESULTS FROM THE PROFILER PROBE MOVEMENT PLANE CALIBRATION, ALONG THE 90X90 ALUMINIUM BEAM..... 77
TABLE 4-6: RESULTS FROM THE PROFILER PROBE MOVEMENT PLANE CALIBRATION, ACROSS THE 90X90 ALUMINIUM BEAM..... 77
TABLE 8-1: FACTORS TO CALCULATE THE MINIMUM RADIUS FOR VARIOUS TOUGH ANGLES (WHEELER, 2012). 98
TABLE 8-2: TABLE OF VARIOUS BELT CLASS AND ITS CORRESPONDING BELT MODULUS (INTERFLEX CONVEYOR BELTS, 2012). 99
TABLE 8-3: MINIMUM RADIUS FOR AN INCREASING BELT CLASS. 99
TABLE 8-4: DEFLECTION CALCULATION FOR THE I BEAM SECTION, FOR THE BELT GANTRY LIFTER. 103
TABLE 8-5: DEFLECTION CALCULATION FOR THE DOUBLE 180X90 ALUMINIUM BEAM SECTION, FOR THE BELT PROFILER..... 103
TABLE 8-6: DEFLECTION CALCULATION FOR THE 90X90 ALUMINIUM BEAM SECTION, FOR THE BELT PROFILER. 103
TABLE 8-7: DEFLECTION CALCULATION FOR THE I BEAM SECTION, FOR THE BELT PROFILER. 103
TABLE 8-8: RESULTS FOR THE BENDING AND SHEAR STRESSES IN THE BELT GANTRY LIFTER BEAM. 105
TABLE 8-9: DESCRIPTION OF THE INSTRUMENTS USED FOR THE PROJECT. 117
TABLE 8-10: CALIBRATION READINGS (IN MV/M) FOR THE 18, 2 TON LOAD CELLS. 121
TABLE 8-11: CALIBRATION READINGS (IN MV/M) FOR THE 20 TON LOAD CELL. 123

List of Symbols:

A = Area (m^2)
B = Belt width (m)
E = Modulus of elasticity of the conveyor belt ($N / m / ply$)
E = Modulus of elasticity (Pa)
F = Force (N)
F_H = Main resistances (N)
F_N = Secondary resistances (N)
F_{st} = Slope resistances (N)
F_{s1} = Special main resistances (N)
F_{s2} = Special secondary resistances (N)
F_U = Force required to convey a bulk material (N)
$FactorC$ = Factor provided (-)
$FactorD$ = Factor provided (-)
I = Polar moment of inertia (m^4)
l = Length of beam (m)
M = Bending Moment (Nm)
p = Number of plys in the belt (-)
$R_{\min}$ = Minimum convex radius (m)
T = Tension (kN/m)
T_c = Tension at point of interest during normal running (N)
T_r = Rated belt tension (N)
V = Shear Force (N)
v = Strain gauge voltage output (V)
y = Perpendicular distance from neutral axis (m)
$y_{\max}$ = Maximum deflection (m)
κ = Calibration Factor (kN/mV)
σ = Bending Stress (Pa)
τ = Shear stress (Pa)
ω = Uniformly distributed load (N / m)

1 INTRODUCTION

Conveyors are the arteries of the bulk material handling industry, moving large amounts of material from the source point to its destination. The basic components of a conveyor are the idlers, conveyor belt, pulleys and drives. The most important component, because of its relatively high cost and wear rate, is the belt itself.

The conveyor belt is subjected to different dynamic loading actions as it rides loaded on the carrying idler rolls in the one direction and unloaded on the return idler rolls in the other direction. The interaction between the conveyor belt and the idler rolls is therefore extremely important as the idler rolls come into contact with the belt most frequently. If there are additional stresses experienced during the belt-idler interaction these would be compounded due to the number of idlers and could fatigue the belt more rapidly.

1.1 Purpose of the Study

The aim of this investigation is to initiate a research programme to better understand the stresses occurring within the conveyor belt, in particular in the idler junction area. The junction point is defined as the area local to the point of intersection where the wing rollers are placed at an angle to the centre roll for the purpose of increasing the cross-sectional area of the material on the conveyor belt and thereby increasing the carrying capacity of the conveyor.

How do the various idler configurations impart stress into this area and which configuration would impart the least? The context of why this is important is described in more detail in Section 1.2 and Section 1.3. The fact that despite a long history of the development of design theories, designers still need to apply the accepted (high) safety factors of 10 for fabric belts and 6.67 for steel cord belts (CKit, 2015) reveals that there remains great scope for improvement in the field of conveyor design.

By gaining a greater understanding of the dynamic forces acting on a conveyor belt, designers will be in a position to design idler configurations which reduce the stresses in conveyor belting. This in turn will allow conveyor designers to reduce the class of conveyor belt for a particular application, thereby offering the industry considerable savings, not only in the capital but also in the operational cost over the life of a conveyor belt.

1.2 Research Background

The debate in the bulk material handling industry on whether offset idlers are "gentler" on the belt as compared to inline idlers, has raged for many years. This debate was exacerbated by the introduction of the so called "belt friendly idler" which has an even greater offset between the rolls than the conventional offset idler, as noted in the national standard, (SANS 1313-1, 2012).

Damage and delamination of the conveyor belt layers is on the rise (Pitcher, 2015) and an emerging trend in the industry is that this increase in belt damage is thought to be related to the dynamic action occurring at the junction between idler rolls.

Of the single roll, two roll vee, three roll and five roll carrying idler configurations being used in the industry, the three-roll idler configuration is by far the most common. In the carrying idler designs, there are three methods of arranging the idler rolls in relation to the cross member. This research focuses on the three configurations:

1. **Inline**

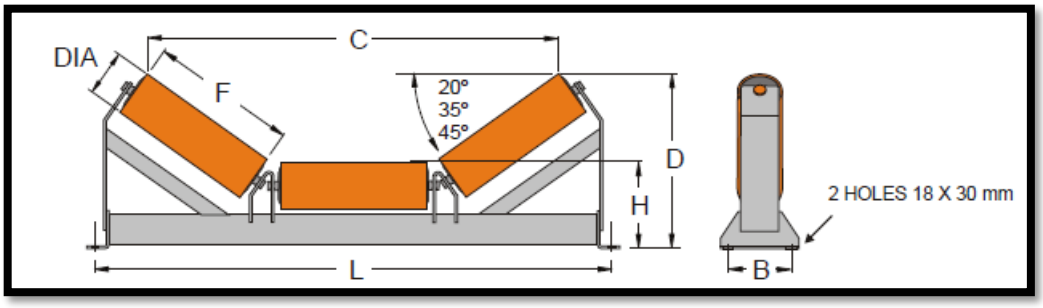


Figure 1-1: 3 Roll inline troughing idler (Lorbrand, 2008).

As the name suggests the three rolls are arranged in a troughing configuration (at the desired angle) with the rolls being inline, as can be seen in the side view of the above illustration.

2. **Offset**

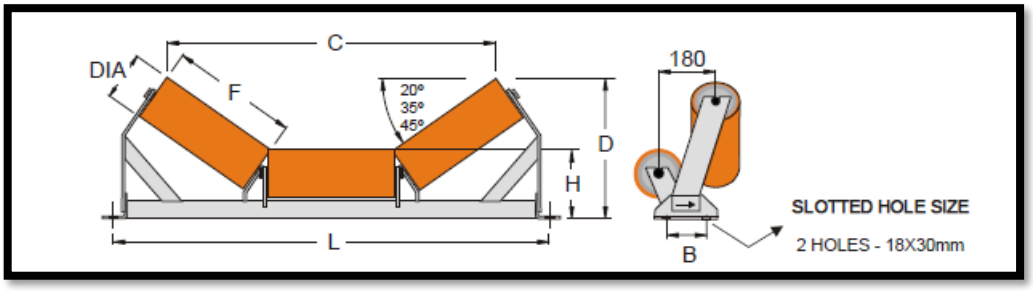


Figure 1-2: 3 Roll offset troughing idler (Lorbrand, 2008).

In the offset configuration the centre roll is offset relative to the wing rolls. The offset distance is governed in South Africa by SANS 1313-1 standard, which stipulates that: "*the horizontal distance between the axis of the centre roll and the axis of an offset roll, when the rolls are aligned parallel to each other, shall, subject to a tolerance of +5mm be as follows:*

a. *150mm in the case of idlers the nominal diameter of which is less than or equal to 150mm, and*
b. *180mm in the case of idlers the nominal diameter of which exceeds 150mm."* (SANS 1313-1, 2012)

3. Offset belt friendly

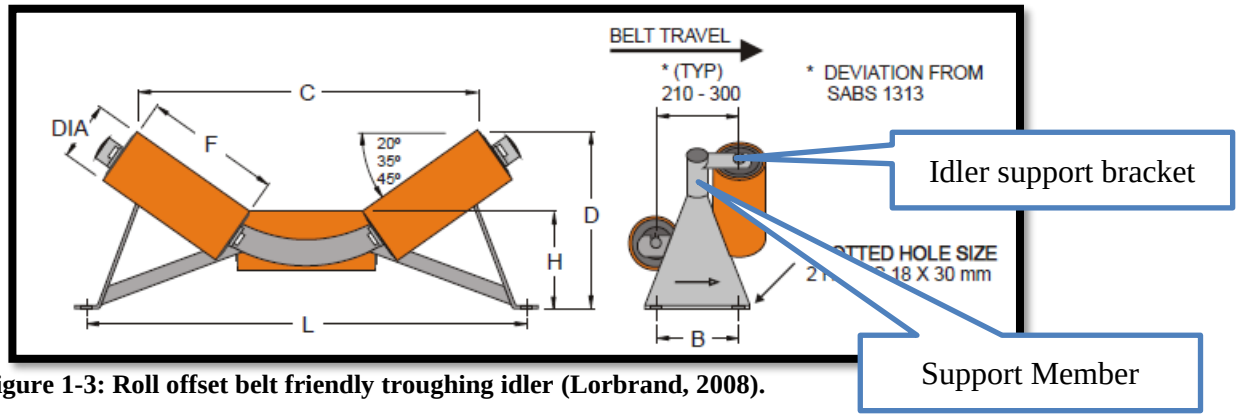


Figure 1-3: Roll offset belt friendly troughing idler (Lorbrand, 2008).

The offset distance in the "Belt Friendly" configuration, as shown in Figure 1-3 is greater than that of the standard offset idler, in that the diameter of the support member should be taken to be included in the offset distance.

The concept of the "belt friendly" idler is that if the centre roll was to be dislodged, then the cross member would effectively carry the belt across the full length where the roll is supposed to be, preventing the roller carrying brackets from cutting into the belt, as would occur on a conventional offset idler. It is important to note that there is no documented historical data to support the supposition that this mode of belt damage is a major threat or cost to the industry.

1.3 Research Motivation

The primary purpose of this investigation is determine the influence on the stress in the belting with respect to the positioning of the support rollers for the respective configurations mentioned above.

In particular, what should the distance between the centre roll and the wing roll shown in Figure 1-4 be to optimise the performance (in terms of stress reduction) of a conveyor belt and does that distance vary with the type of conveyor belt employed for a particular application?

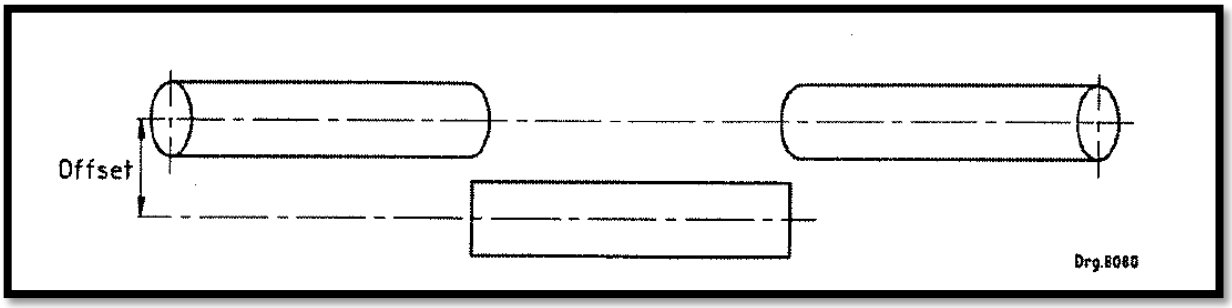


Figure 1-4: Illustration of offset distance (SANS 1313-1, 2012).

As the focus of the study is on determining which of the idler configurations has the least effect in terms of stress within the belt, comparing the range of idlers from inline to various distances between centre lines of offset, only three roll idler configurations will be evaluated.

1.4 Problem Statement

This research focuses specifically on the area of the idler junction on the carrying side. As the conveyor belt passes over the idler junction the belt first has to rise up (i.e. work is done to lift the conveyor up) and it then crosses the idler junction. The junction is defined as the position where two idler roll ends come close to each other forming the belt into the carrying curve, normally in sets of 3 or 5.

The most popular range of totally included troughing idler angles is between 25 and 45 degrees. This translates to the angle between any two rollers to range between 12.5 and 22.5 degrees for a five-roll trough. There has been a trend in recent years of designing deep troughing idlers.

The degree of weft or transverse strength definitely plays a role in that the greater the stiffness in the weft direction the less likely it is that the belt will be forced into the idler junction for a given load. In years gone by very thin belts were used on inline idlers and the belt, due to load, was forced into this idler junction, resulting in severe damage in the form of the belt "splitting" along the junction lines.

This was largely the motivation for the development of the offset idler configuration in which the ends of the rolls overlap, eliminating the gap between the rolls. What needs to be realised though is that by offsetting the rolls, the belt is forced to be first "lifted", assuming the centre roll in front of the set and then "folded" as it strikes the wing rolls.

The comparison of dynamic actions is therefore: with an inline idler the belt is simultaneously lifted and folded, effectively creasing (pinching) the belt between the roll ends, whereas on offset idlers the belt is first lifted (and "flattened out") then folded into the troughing angle but not creased (pinched) between the rolls.

An informed decision needs to be made regarding the stress induced in the belt as it goes past the idler junction. It is important to understand that repetitive nature of this dynamic action is such that whatever the stresses induced amount to, it is continuously repeated at each and every carrying idler, resulting in a compounding effect being applied.

Consider a fairly standard plant conveyor with a 1000m length and an average idler spacing of 1.2m. The number of troughing idlers sets is 833 representing a huge fatigue cycle and in turn greatly influencing the life of the conveyor belting.

1.5 Research Objectives and Scope

The goal of this research is to set up the foundation for a truly comprehensive model that can help conveyor designers, and afford conveyor maintenance operators the knowledge and insight into the best choice of idler configuration for a given conveyor belt, in order to maximise the belt life by reducing stress.

The problem identified is that the stress which develops, as the belt passes over the idlers, is not yet clearly understood. This study attempts to define the different stresses developed on the most commonly utilised idler configurations in South Africa. i.e. three roll inline, offset and belt friendly idlers.

In order for factual information to be compiled, the need exists for data to be collected for analysis. To this end, a comprehensive test facility needed to be constructed, complete with sensing and measuring instruments to make interpretable data available.

The integrity of the data must not be compromised by the fact that the test facility needs to designed and constructed taking into consideration a variety of constraints namely: cost, complexity and limitations on current instrumentation, yet still reflect a true application.

Further consideration must be given to understanding how the selected instruments function to obtain maximum value in terms of the quality of the data. The research has three definite phases:

1. Design and manufacture of the test facility, and validate that the design meets the desired outcomes. This is the subject of this research report.
2. Running the tests to capture the data and finally the conversion of the data into information.
3. Compare with the results obtained from FEA modelling. Ideally the comparison will validate the FEA studies, resulting in high levels of confidence in the use of FEA modelling to other belt widths and idler configurations.

This Research Report covers the first aspect of the entire research scope (which is phase 1 mentioned above) while further studies will be conducted to complete the following two phases.

1.6 The Methodology Used

The test facility described above was to be designed and built to induce the stresses normally experienced by the belt passing over the idlers.

The instrumentation, which is integral to both the belt and the test facility, was to be used to measure temperature, strain, load and displacement. The tests were to be conducted to incorporate the following parameters:

1. The three idler configurations:
    a. Inline
    b. Offset
    c. Belt friendly
2. At various wing roll angles:
    a. 35 degrees
    b. 45 degrees
    c. 0 degrees
3. At a range of loads related to the belt class.
4. For two types of belting
    a. Solid woven/PVC
    b. Fabric ply belting

In summary the objectives were to:

1. Design and construct a test facility.
2. Validate that all the equipment is fit for purpose. This was to be done by calibrating the instrumentation, ensuring that the various pieces of equipment are capable of the loads to which they will be subjected and that all the interfacing components of the test facility work together as expected.

1.7 Assumptions

Certain assumptions were made that would help to simplify the test parameters and guide the design. The most pertinent ones are listed below:

1. The operating range of the conveyor belting is in the linear region. The strain is linearly proportional to the stress in the test operating conditions.

2. These configurations will be evaluated in terms of load; with different types of conveyor belting, namely fabric, solid woven; other factors such as roll diameter and they type of roll (polymer or steel) are assumed to not have any tangible effect on the evaluation and will thus be ignored.

3. The weft strength or stiffness will influence results and this needs to be accounted for; the selection of a high and low class belt, for each type of belt, should accommodate for this issue.

4. The reason for steel cord belting having not been included in this research is the fact that delamination does not occur between the cords and the rubber filler material. A probable reason for this is that the carcass is made of cords and surrounded by rubber, which can withstand a large amount of elongation; therefore, the carcass cannot “crease” and over time fatigue until delamination takes place.

Although the scope and direction of the research has been laid out, an understanding of the history of conveyor belts and idlers and the development thereof is advantageous to understand the reasons why this research holds value. This is outlined in Chapter 2.

2 LITERATURE REVIEW

Conveyors are used in a great many applications. They are robust systems that take a pounding and severe abuse and continue to function and serve human needs. But where did they start? And how did they develop into the systems available today?

The history presented here highlights some of the milestones in the movement of bulk material handling. There has been improvement in the strength of the belting and making the cover more wear resistant, flame retardant and energy efficient.

But has industry given the conveyor system the attention it deserves with respect to the deeper understanding of the stress propagation and failures that can occur? This literature review attempts to give an understanding of where the developments of conveyors have been and highlight gaps so one can better understand the need for this type of research.

2.1 History

It is difficult to assign the invention of the conveyor to an exact date or person since many technical advancements would have set the scene for the creation of the conveyor (HabaTec, 2011). The Figure 2-1 gives a general overview of the major typical pieces of a conveyor system.

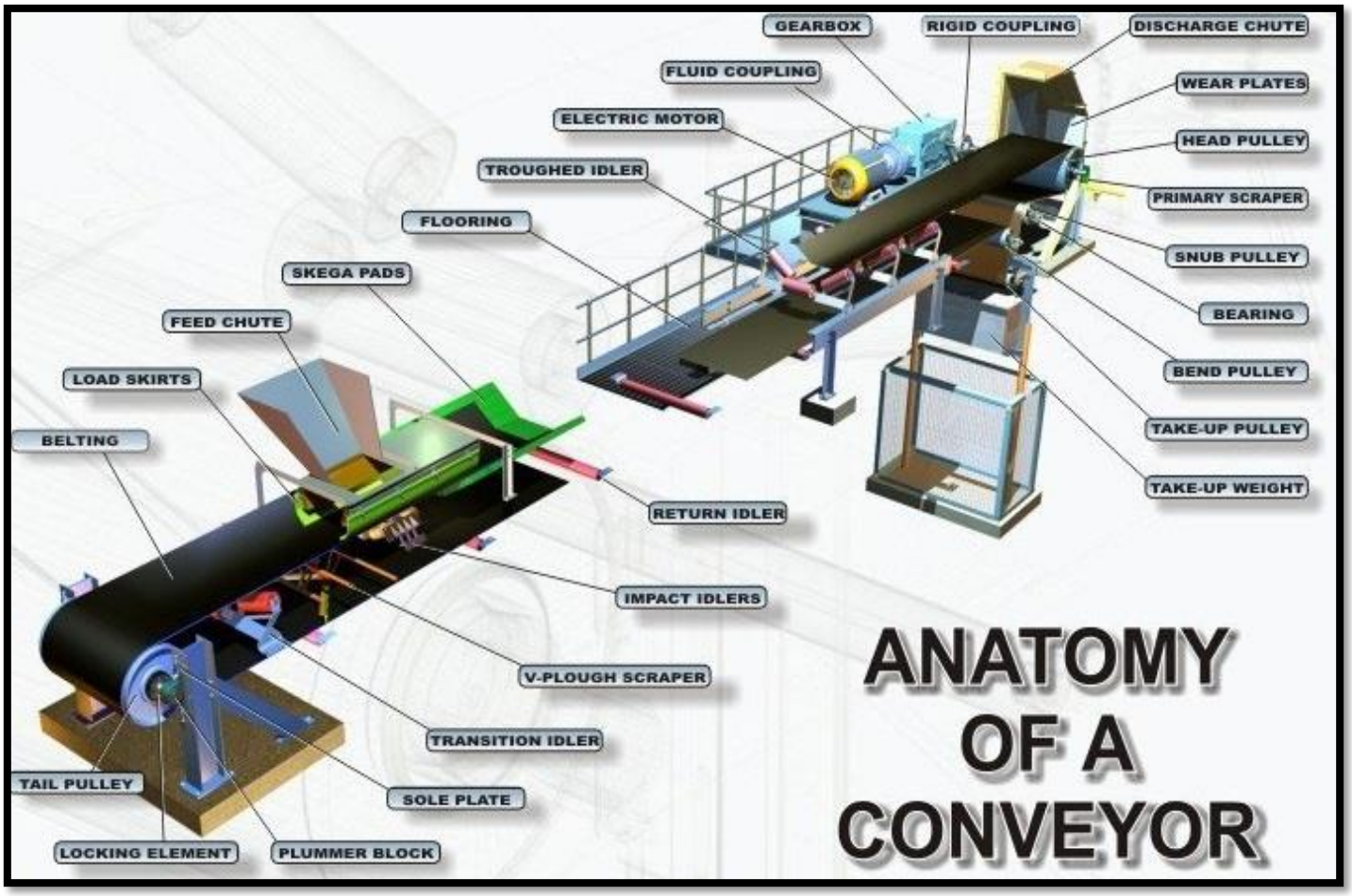


Figure 2-1: Illustration of the major pieces of a conveyor system (Ckit, 2015).

Conveyor belts can be traced back to the latter half of the 17th century and it has since been an invaluable asset in the transportation of material (EasiKit, 2012). The earliest versions of conveyor belts were used to transport grains over short distances (MHEDA, 2004). The earliest conveyor systems utilised belts that were primitive; there was a belt of rubber, leather or canvas that was pulled over a flat bed of wood. It was a popular system since it eased the transportation of bulk material from one location to the next (EasiKit, 2012) (MHEDA, 2004).

In 1892, the American inventor Thomas Robins, started with a series of developments which led to a conveyor belt which was used to carry coal and other ores as is done by today's conveyors. The conveyor belt that Thomas Robins developed in 1892 was used for carrying raw materials such as ore and coal. Nine years later the Swedish firm Sandvik commenced with the production of conveyor belts constructed from steel. Richard Suttcliffe was a British mining engineer who, in 1905, designed the first conveyor that would be used to carry coal in underground mines. This invention revolutionised the mining industry (HabaTec, 2011).

In 1908 Hymle Goddard was granted the first patent on the roller conveyor and in 1913 conveyor belts were used in car manufacturing assembly lines by Henry Ford (HabaTec, 2011). Conveyor belts became common in the 1920s and many advancements were made. Conveyors were designed to carry material over longer distances. A conveyor belt composed of cotton layers and rubber covers was used to carry bulk material over a length of 8 km underground (MHEDA, 2004). A turning point in conveyor history was when synthetic conveyor belts were introduced in WWII mainly because natural materials such cotton and rubber were scarce. Synthetic belts have become popular ever since (EasiKit, 2012). The first safety standard pertaining to conveyor safety was developed in 1947 by the American Standards Association (MHEDA, 2004).

Early conveying systems generated excessive noise and it was the Occupational Safety and Health Administration's priority to curb conveyor noise; this requirement gave rise to the employment of quiet rollers with precision bearings (MHEDA, 2004).
Another conveyor advancement was the implementation of service teams in order to maintain the conveyor structure and look out for symptoms of component failure such as rattling, since maintenance used to cause extensive downtime due to a lack of monitoring and conveyors were often replaced long before the predicted service life (MHEDA, 2004).

Today, conveyor belts can be found in almost every industry where materials are stored, handled or dispensed (MHEDA, 2004). Conveyor belting is manufactured from a long list of natural materials and synthetic polymers, these include: cotton, EPDM (ethylene propylene diene terpolymer), canvas, leather, nylon, neoprene, polyester, urethane, polyurethane, rubber, PVC (polyvinyl chloride) and silicone (EasiKit, 2012). These polymers are configurable for various requirements and the use of conveyor belts has increased dramatically.

Today, the longest conveyor belt system in the world is used in the phosphate mines of Western Sahara and measures over 100km long (Conveyor Belt Guide, 2005) (MHEDA, 2004) (EasiKit, 2012). One of the longest single-flight conveyors in the world is located at Impumelelo colliery, in Secunda, Mpumalanga and measures 26.9km (Meijers, 2013).

2.2 Belt constructions

Conveyor belting is a reinforced elastomer that when installed on a belt conveyor system and joined into an endless loop is used to convey items (Pitcher, 2012). The belt is made up of the carcass which is the reinforced member and the belt covers. The external covering provides wearability and is where the elastomer is contained. The carcass, which is enclosed by the covers, is the strength bearing component of the belt and provides support for the load on the belt (Global Belting Technologies, 2015).

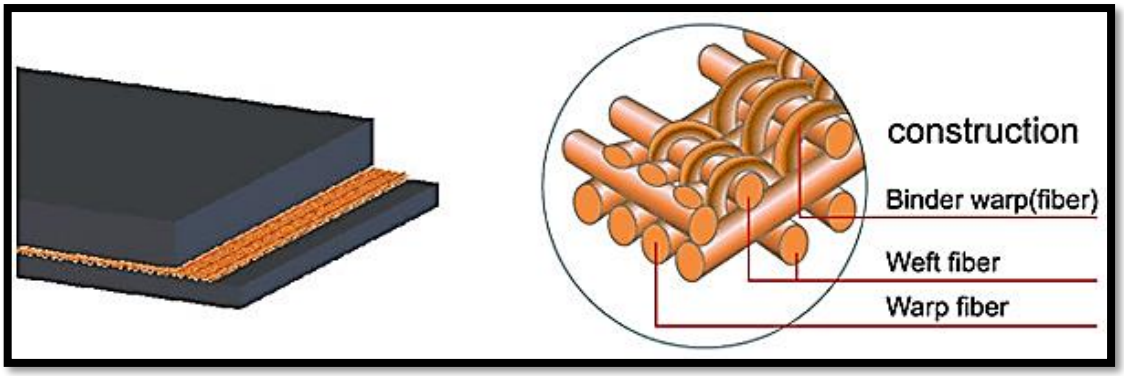


Figure 2-2: A detailed view of the weft and warp fibres in belt construction (HYC, 2016).

The most important part of conveyor installation is the belt itself. The belt has a multitude of functions; it absorbs stresses as the drive starts up, transports load, absorbs loading point impact energy, withstands chemical erosion and provides features such as being flameproof and being antistatic (Satyendra, 2013). Conveyor belts are constructed as a combination of warp and weft yarns and plastic or rubber components as shown in Figure 2-2 (Global Belting Technologies, 2015).

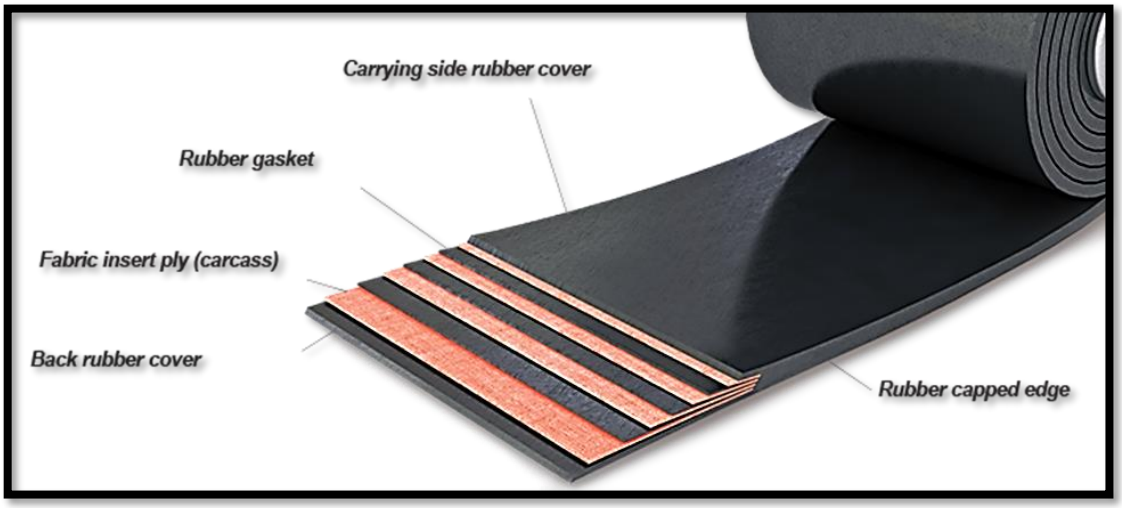


Figure 2-3: Schematic of a cross section of plied belt (Henan Pingyuan Mining Machinery Co. Ltd., 2016).

A plied conveyor belt as shown in Figure 2-3 will have multiple layers of carcass. The layers are separated by rubber layers as shown in Figure 2-3. In certain cases a single ply belt would suffice but it would be unsuitable for a heavier duty application. The selection of the conveyor belt specification depends on its application. The schematic cross section of a plied conveyor belt is shown in Figure 2-4.

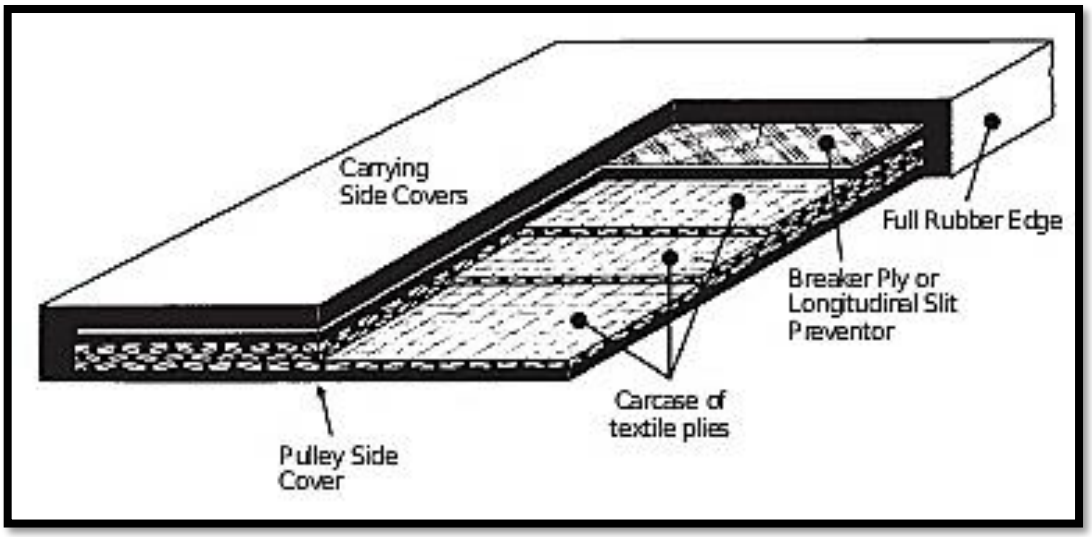


Figure 2-4: Schematic cross section of a plied conveyor belt (Satyendra, 2013).

Conveyor belts have the following components: (Satyendra, 2013)

- Carcass: These are textile plies, steel cord or steel weave.
- Covers: Rubber or PVC of different qualities are used to produce these.
- Additional components such as longitudinal slitting prevention, edge protection, and impact protection.
- Special construction elements for steep incline belts, corrugated edges or cleats etc. (Satyendra, 2013).

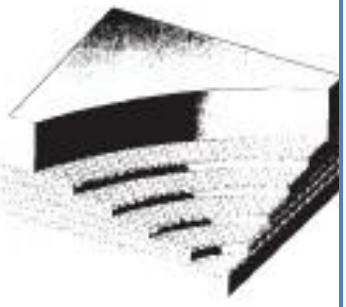
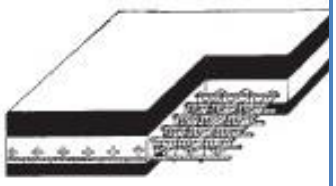
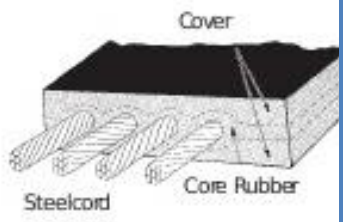
2.2.1 Carcass

The carcass of the conveyor belt could be made of various materials with different constructions. The carcasses are usually textile ply and steel cord carcasses. Textile ply carcasses have one or more textile plies. The maximum numbers of plies is up to 6 (Satyendra, 2013). In monoply belts, a textile carcass is impregnated with PVC.

Depending on the required tensile strength, the carcass fibres are produced from polyamide, polyester or aramid. In a steel weave carcass steel cords are laid parallel to one another in the same plane, above it is a transverse layer of other steel cords that are held in place by binder cords of polyamide.

In a steel cord carcass, the cords are transversely bound together by only the intermediate layer of rubber, which prevent longitudinal slitting and impact damage (Satyendra, 2013). Different types of carcasses are shown in Table 2-1.

Table 2-1: Types of carcasses (Satyendra, 2013).

		
2 Ply	**3 Ply**	**Multiply**
		
Monoply Solid Woven	**Steel Weave**	**Steel Cord**

Each different type of carcass has its own strength. Polyester plies are strong in the warp direction, polyamide plies are strong in the weft direction, aramid plies have high tensile strength, steel cord belts have low elongation factors and synthetic plies have good service life. Various types of plies are evaluated in Table 2-2.

Table 2-2: Evaluation of plies (Satyendra, 2013).

Characteristics	Cotton	Polyamide	Polyester	Polyester-Polyamide	Aramid	Steel weave	Steel cord
Tensile strength	•	**	**	**	***	**	***
Adhesion	•	**	**	**	**	**	***
Elongation	•	•	**	**	***	***	***
Moisture resistance	••	*	**	**	**	*	**
Impact resistance	•	*	*	*	*	**	***
•• bad, • medium, * good, ** very good, *** excellent							

The Textiles

Textiles provide strength for both tensioning and load handling in the belt. They add to the belt rigidity and the mechanical fastener retention is good (Global Belting Technologies, 2015). Conveyor belt textiles are usually synthetic: nylon or polyester. Natural fibres such as wool and cotton are also used at times, each type of fibre has its own set of characteristics which makes it more suitable for certain applications (Global Belting Technologies, 2015).

Several different types of weave construction, as shown in Figure 2-5 exist; some of them include: twill, satin and plain weaves. Some belts have non-interwoven parallel cords, and some are without any elastomeric impregnate (Global Belting Technologies, 2015).

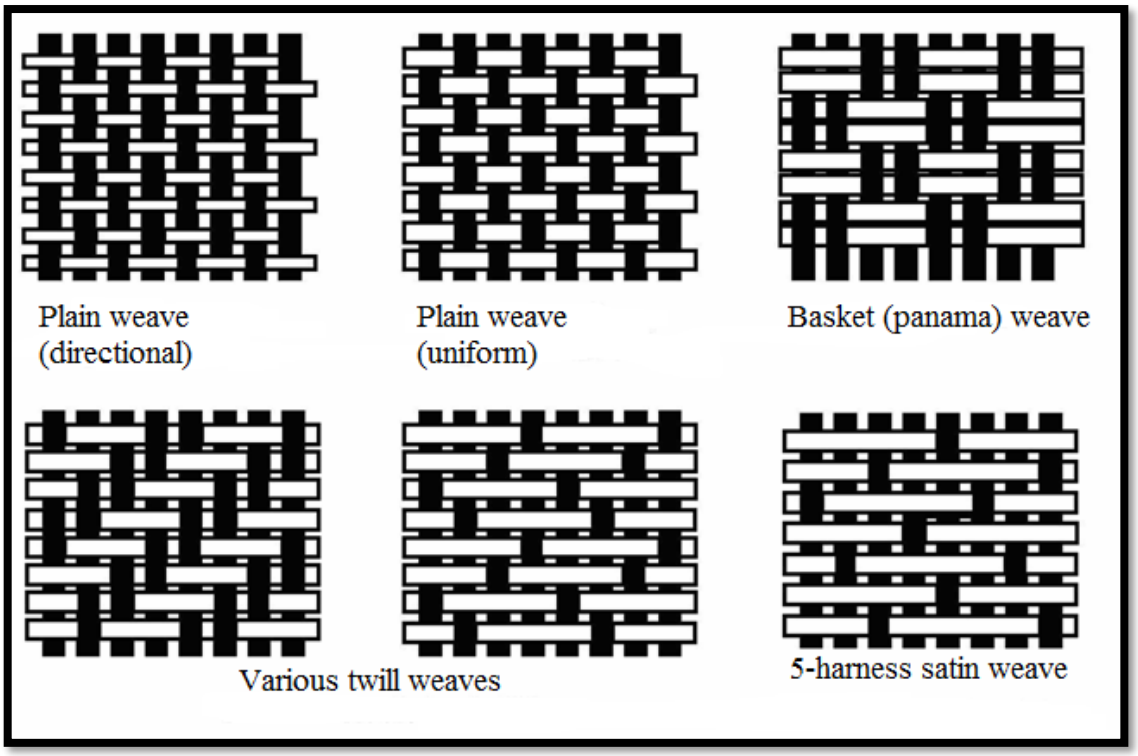


Figure 2-5: Different weave constructions (Kevra, 2016).

The Elastomers or Compounds (Rubber or Plastic)

The plastic or rubber components in the carcass serve to bind together the textiles. An adhesion promoting chemical is applied to most textile structures before the elastomer is applied. The rubber used could be natural or synthetic, the plastics are usually thermoplastic and could be either urethane or PVC (Global Belting Technologies, 2015). Conveyor belt compounds protect the textile layers from abrasion and wear as they operate. They also function as an adhesive for the interplies (Global Belting Technologies, 2015).

2.2.2 Covers

Conveyor belt covers add a cushion to reduce product impact, provide a sacrificial wear surface and protect the carcass from the abusive materials being conveyed. Covers may not be included on belts where a low coefficient of friction is needed (Global Belting Technologies, 2015).

A variety of rubber compounds are available, designed for specific service conditions and materials to be conveyed. These include wear resistance, elevated temperatures, oil resistance and fire resistance. Some rubber compounds made specifically for resistance to oils, for example NBR (Nitrile Butadiene Rubber) come in varying degrees of oil resistance. Common compounds found in conveyor belting include natural rubber, SBR, Buna-N, Neoprene and Butyl (Global Belting Technologies, 2015).

The carcass is protected against external elements by the covers that are manufactured from PVC or rubber. The ratio of carrying side cover to running side cover should not exceed 3:1. Certain cover types with their properties are listed in Table 2-3. Cover specifications can include special features such as flame resistance, heat resistance, chemical resistance and anti-static properties.

The characteristics of the carrying side cover will be dictated by the load and the conveyor inclination (Satyendra, 2013). Based on these conditions the carrying side cover thickness can range from 2 mm to 12 mm and on the running side from 2 mm to 5 mm (Satyendra, 2013).

Table 2-3: Types of cover defined in SANS conveyor belting standards (Pitcher, 2012).

Cover Type	Tensile Strength (MPa)	Elongation at Break (%)	Abrasion Loss (mm3)	Remarks
A	20	400	70	Rubber cover suitable for use on conveyors subjecting the belting to a high amount of sliding abrasion. Typically conveyors handling high density materials loaded at a point of steep incline (>8º)
C	20	400	150	General purpose rubber cover suited to conveying small to large lumps of average density and abrasiveness.
F	14	400	180	Special purpose rubber cover for use in fiery mines or applications where risk from fire or explosion is high.
M	25	450	120	High grade rubber cover suited to conveying large lumps of sharp, high density material likely to cause cuts or tears. Standard cover type applied on steel cord carcass construction conveyor belting.
N	17	400	150	General purpose rubber cover suited to conveying small to large rounded edge lumps of average density and abrasiveness.
NBR	14	350	250	Special purpose rubber cover, applied to conveyor belting of solid woven carcass construction, for use in fiery mines or applications where risk from fire or explosion is high.
PVC	9	250	250	Special purpose cover, applied to conveyor belting of solid woven carcass construction, for use in fiery mines or applications where risk from fire or explosion is high.

2.3 Belt Tension Determination

Belt tension under steady state conditions is usually calculated to overcome all the resistances to motion. The main resistances are classified into five groups: main resistances, secondary resistances, special main resistances, special secondary resistances and slope resistance. Equation 2-1 can be used to calculate F_U (Wheeler, 2012).

$$F_U = F_H + F_{st} + F_N + F_{s1} + F_{s2} \quad \textbf{2-1}$$

Where

F_U = Force required to convey a bulk material (N)

F_H = Main resistances (N)

F_{st} = Slope resistances (N)

F_N = Secondary resistances (N)

F_{s1} = Special main resistances (N)

F_{s2} = Special secondary resistances (N)

The main resistances comprise the indentation rolling resistance, belt flexure resistance, material flexure resistance and the rotational resistance of the idler bearings and seals. Secondary resistances are made up of wrapping resistance of the belt around the pulleys (Wheeler, 2012).

Figure 2-6 illustrates the conventional method for determining the tension distribution of a simple conveyor with a slope and a take-up. From Figure 2-6 it is clear what contributes to the tension variations along the length of the conveyor belt. It is important to note is that these calculations do not describe the tension variation across the width of the belt.

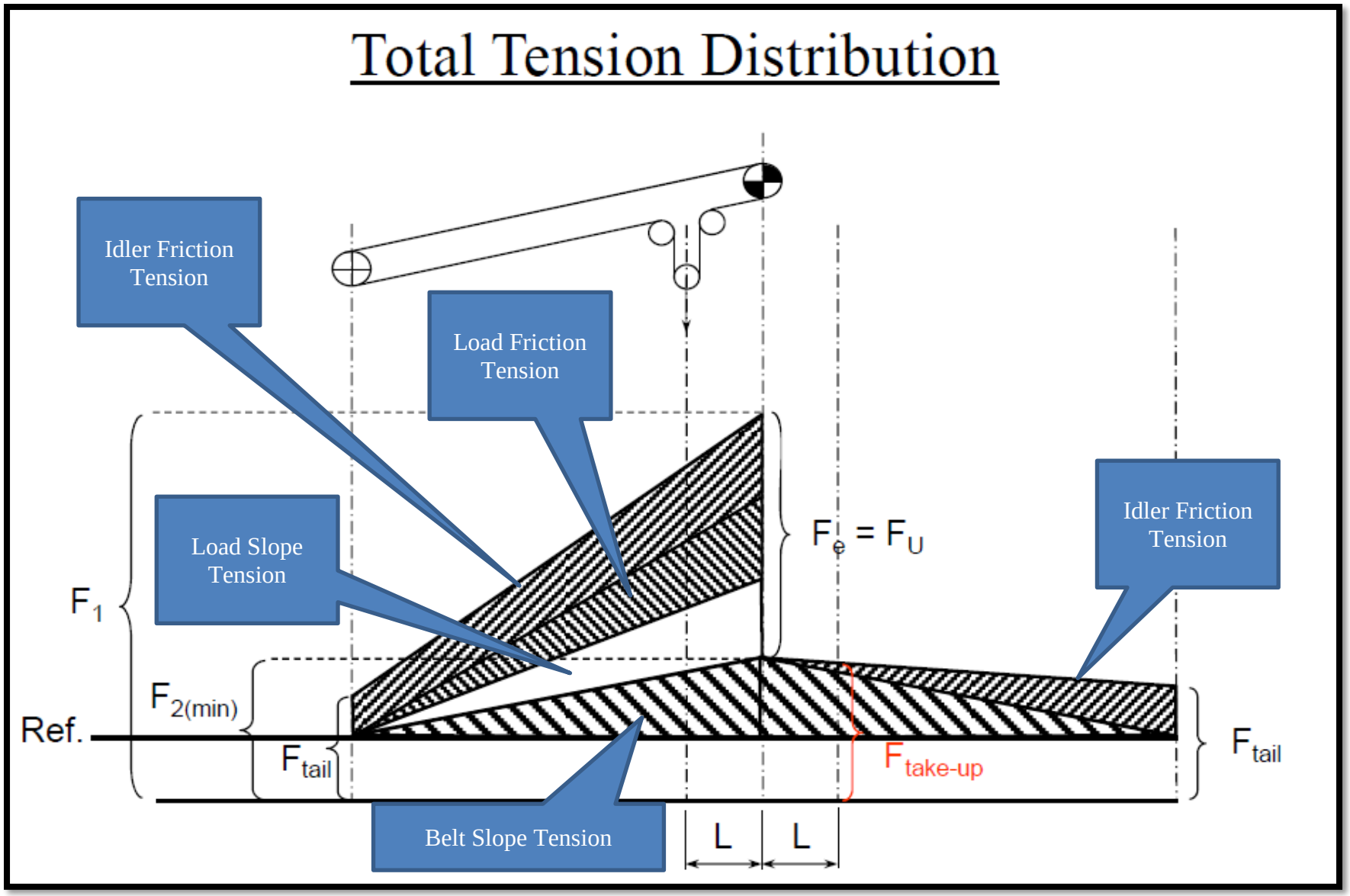


Figure 2-6: Tension distribution for steady state conditions (Wheeler, 2012).

2.4 Idler Junction Failure

The small amount of published research on idler junction failure seems to be limited to inline idlers and steel cord belting. This section discusses the factors that contribute to idler junction failure and the information found on idler junction failure was confined to inline rollers with steel cord belt. No documented research was found on the combinations of fabric belting and the offset idlers commonly in use.

2.4.1 Belt Tension and Load Support

The belt tension is the summation of the force required to straighten a flexible belt and to overcome resistance to movement. These factors depend on the conveyor path and the required load carrying capacity. The belt classification and the idler arrangements are directly governed by the anticipated belt tension. Conveyor belt configurations may be either in the form of a concave or convex curve. A convex curve conveyor is shown in Figure 2-7. Convex curves present a particular problem with regard to idler junction failure.

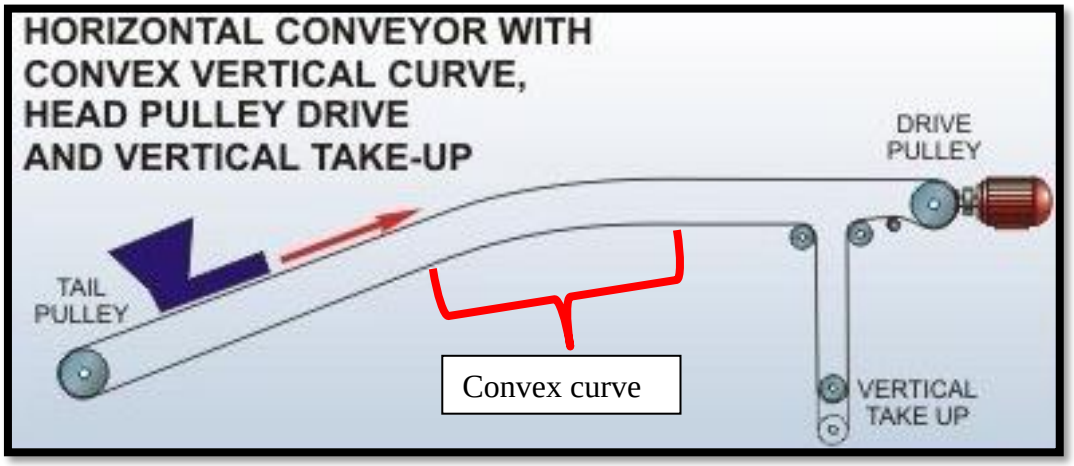


Figure 2-7: A convex curve belt (Ckit, 2017).

The tension in a short radius convex curve will cause the belt to be pulled into the gap between the idlers as shown in Figure 2-8.

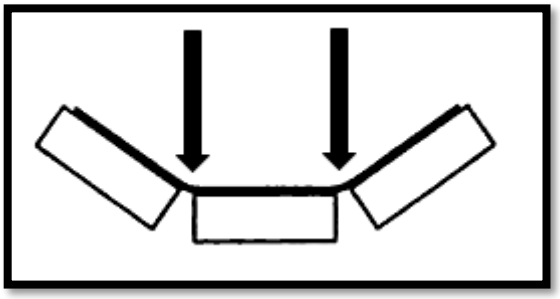


Figure 2-8: The tension on a convex curve will force the unsupported belt area into the gap between the idlers as indicated by the arrows (Fayed & Skocir, 1997).

The trough angle creates a curve along which the belt is constantly bent. On a loaded belt, a portion of the load will be concentrated directly over the unsupported length between the idlers. The load pushes down at that location, causing a smaller radius of belt at that section than when the belt is not loaded.

A heavier load would then result in a smaller radius. The small radius, coupled with the added force in the absence of support causes pinching of the belt between the idler rolls (Fayed & Skocir, 1997). Insufficient belt tension also poses some problems. If the belt tension is concentrated on the belt edges, this could cause buckling at the belt centre and a subsequent problem will be belt flexure. Excessive belt flexure coupled with cycling will cause the belt to harden and delamination to occur (Fenner, 2016).

2.4.2 Belt Rigidity

In order for the belt to have lateral stiffness, it is produced with plies of woven fabric for transverse reinforcement. When the load is substantial and the tension high, the plies of woven fabric overlay the steel cords in steel cord belts (De & White, 1996). The lateral reinforcements, when applied close to the belt surface, are employed to give the belt other desirable properties, such as flame or cut resistance. Some combinations of heavy fabrics and warp sheets are quite complex and are separated by interply rubber.

The interply thickness dictates the amount of shear generated by the reinforcing layers. In order to achieve a minimal amount of difference in force between plies, the thickness of the interply should equal that of the fabric ply (Harandi, et al., 1992). Troughability is defined as the belt property that permits it to conform to the shape of the troughing idlers.

2.4.3 Trough Angle

In the three roll trough shown in Figure 2-9, the trough angle is the angle the wing rolls make relative to the centre roll. The extent to which the belt will rest on the three idler rollers depends on the idler junction gap (between two adjacent roll ends) and the belt stiffness.

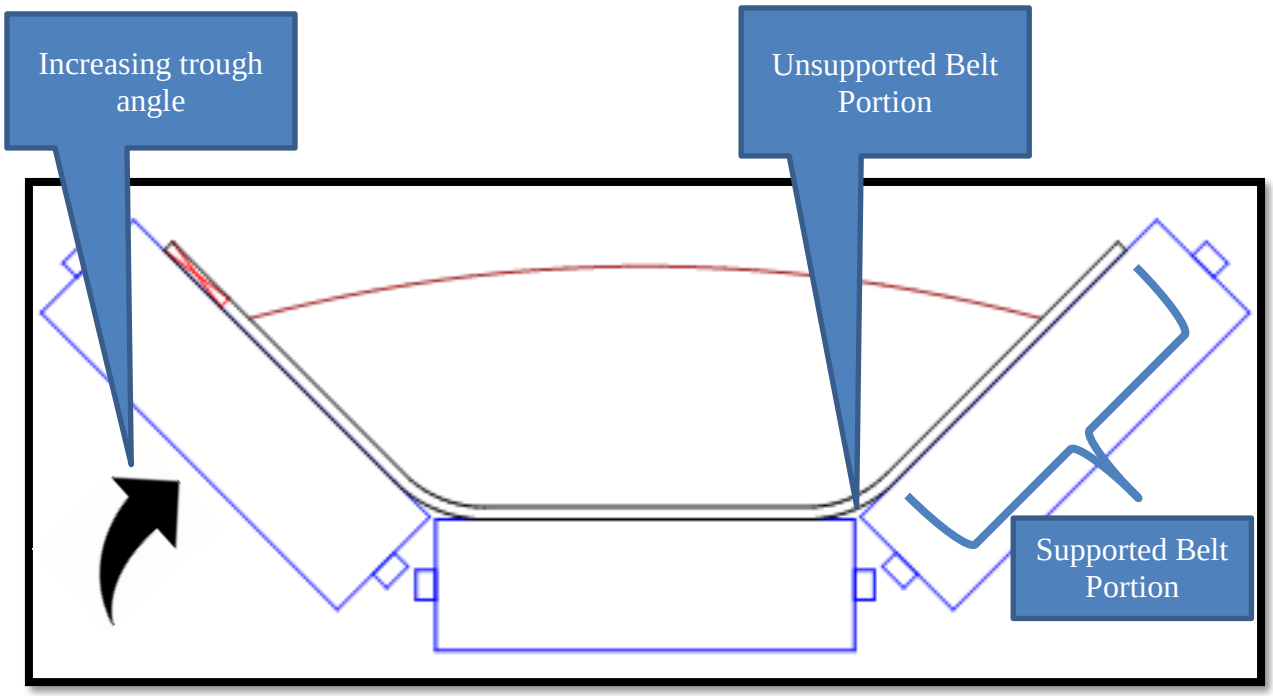


Figure 2-9: Three-roll trough illustrating the supported and unsupported belt trough (AC-Tek, 2017).

As the trough angle increases, more load is exerted onto the unsupported portion of belt, that portion of belt which is not resting on the idler roller. Figure 2-10 and Figure 2-11 show the forces from the wing idlers. It shows that the force on the unsupported length increases as the trough angle increases. The increased force will cause the radius to decrease and pinching is more likely to occur at the idler junction gap.

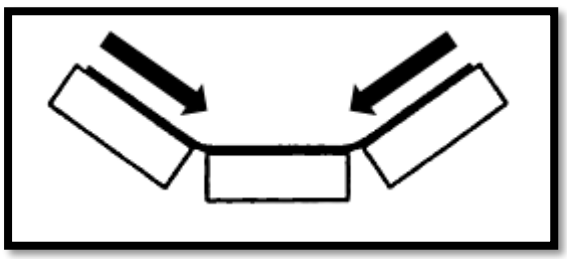


Figure 2-10: Wing idlers at 30^0.

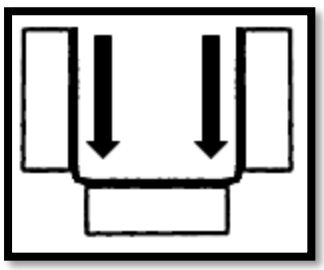


Figure 2-11: Wing idlers at 90^0.

2.4.4 Transition Distance

In order to increase the load carrying capacity, belts are troughed. The belt is shaped from flat to troughed, or vice versa, over a certain length, this length is called the transition length and is depicted in Figure 2-12.

A textile belt should not be tensioned to more than 130% of its allowable working tension in order to prevent permanent elongation along the edges of the belt. Permanent elongation at the edges would place a greater force onto the unsupported belt section at the idler junction, forcing the belt into the gap between the idlers (MHEA, 1986).

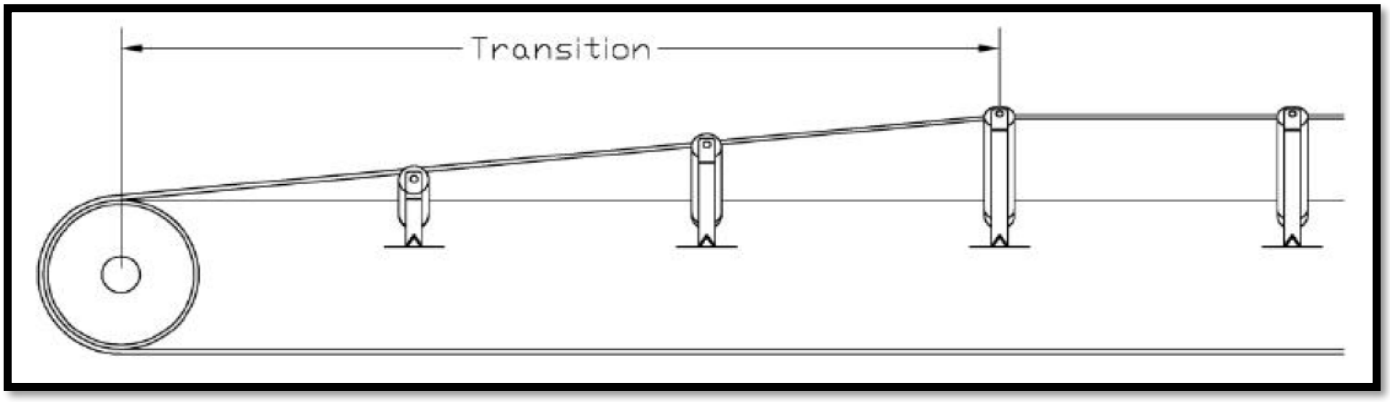


Figure 2-12: In-line or full trough transition (Lemmon, 2015)

2.4.5 Idler junction failure in Inline idlers with Steel Cord Belts

Bending of the belt due to the toughing angles causes tension on the underside. Bending is the dominant factor that contributes to idler junction deformation and ultimately failure. This deformation is dependent on certain factors (Zhang, 2015):

1. Trough Angle: steeper trough angles increase bending.
2. Belt Thickness: thicker belts have a tendency to be more stiff.
3. Material cross sectional loading and idler spacing: A higher loading on the idlers would force the belt into the idler junction point, thus increasing the bending stress.
4. Vertical Curves: convex curves add a component of tension.
5. Idler Gap: increasing the gap between adjacent rolls would increase the likelihood that the belt would be forced into this gap.

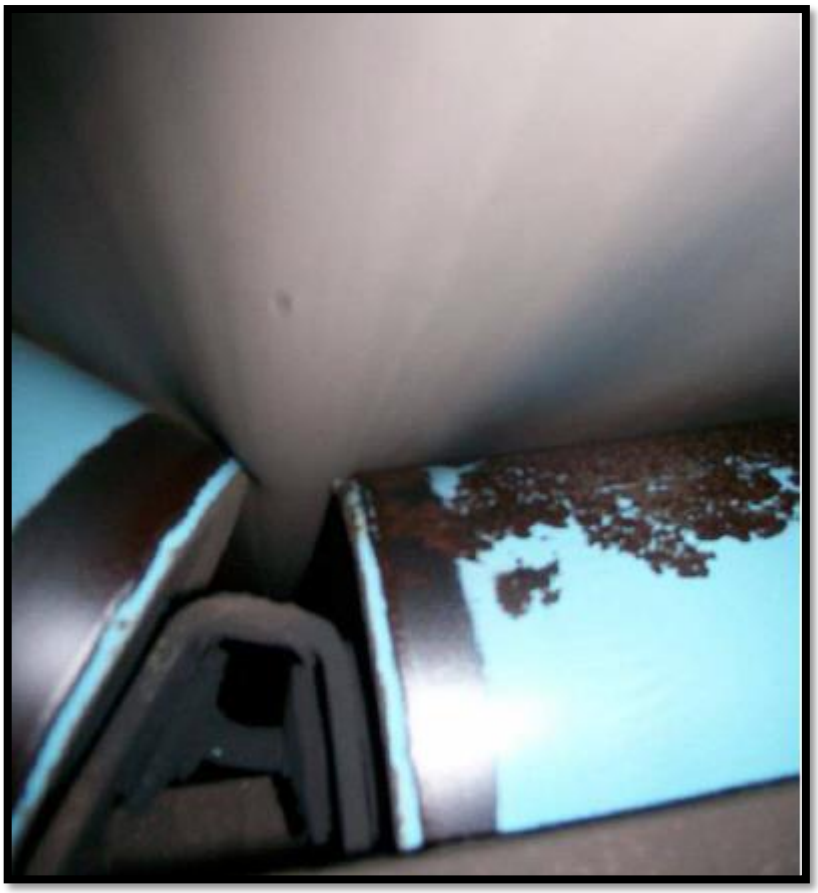


Figure 2-13: Belt contacting idler edge, which can act like a knife edge and damage the belt (Zhang, 2015).

6. Increase idler diameter: this would increase the contact area and reduce the bending at the idler junction zone.
7. Increase from a three-roll trough to a five-roll trough: although the overall trough angles remain the same the bending strain at each idler junction point is reduced.

The contact stress between the belt and idler is comprised of a shear stress which is due to the indentation idler rolling resistance and the normal stress from the load pressing down onto the idler. If it the conveyor belt passes over a convex curve there will be an additional load applied onto the idler while the opposite is true with a concave curve (Zhang, 2015).

To more fully understand the indentation idler rolling resistance, Figure 2-14 helps to visualise what is happening. *Indentation idler rolling resistance arises due to an asymmetric pressure distribution as a viscoelastic belt cover is indented by a rigid idler roll. This causes a retarding moment on the idler roll, dependent on the load, speed, idler diameter and the properties of the conveyor belt cover* (Robinson, 2016).

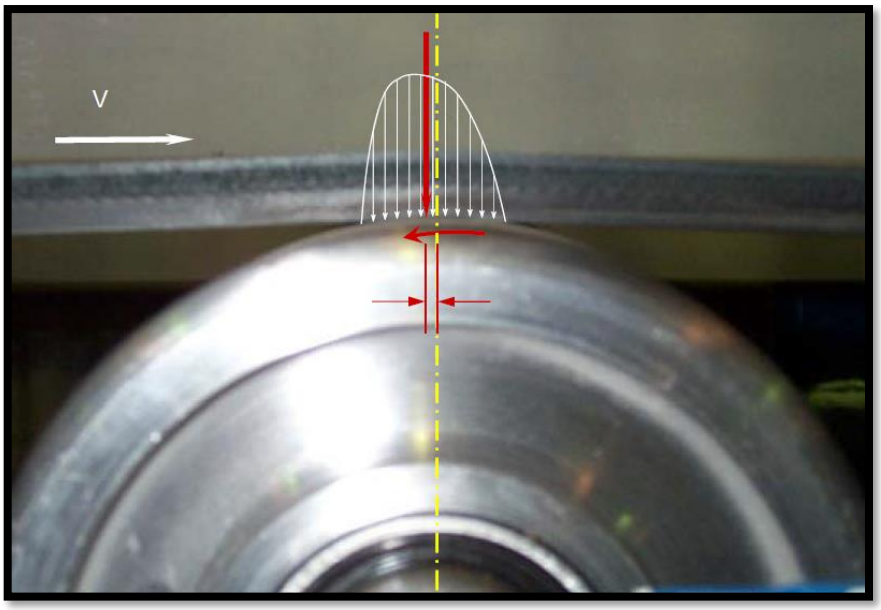


Figure 2-14: Illustration of the asymmetric pressure distribution, that results in the indentation rolling resistance (Wheeler, 2012).

Figure 2-15 shows the effects of high contact pressure, the effect is further highlighted underneath the steel cords.

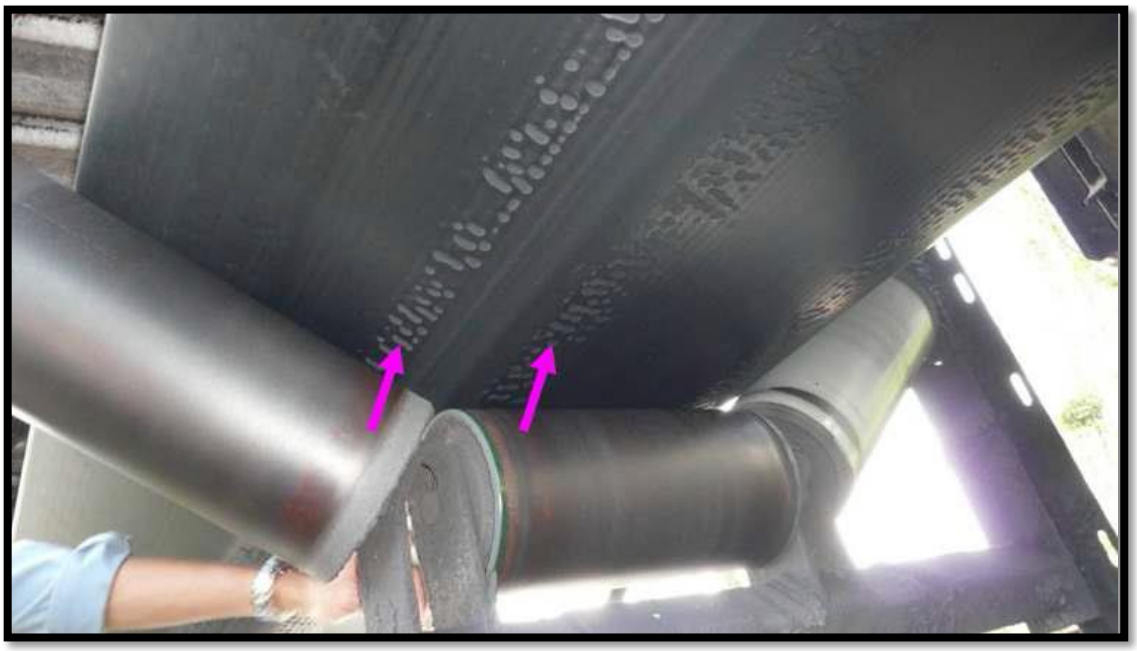


Figure 2-15:Damage on bottom cover due to high contact pressure (Zhang, 2015).

Figure 2-16 illustrates the wear effects in the bottom cover when the wing rolls are tilted forward. The steel cords have worn through the bottom cover, with the highest wear occurring at the idler junction region.



Figure 2-16: Wear on bottom cover caused by the forward tilt of the wing rolls (Zhang, 2015).

Zhang (2015) proposes that the offset idler configuration is an improved design over the inline configuration but no detail is provided as to what the ideal offset distance should be. Figure 2-18 and Figure 2-19 illustrate the damaging effects of "belt friendly" idlers on a on newly installed steel cord belt.

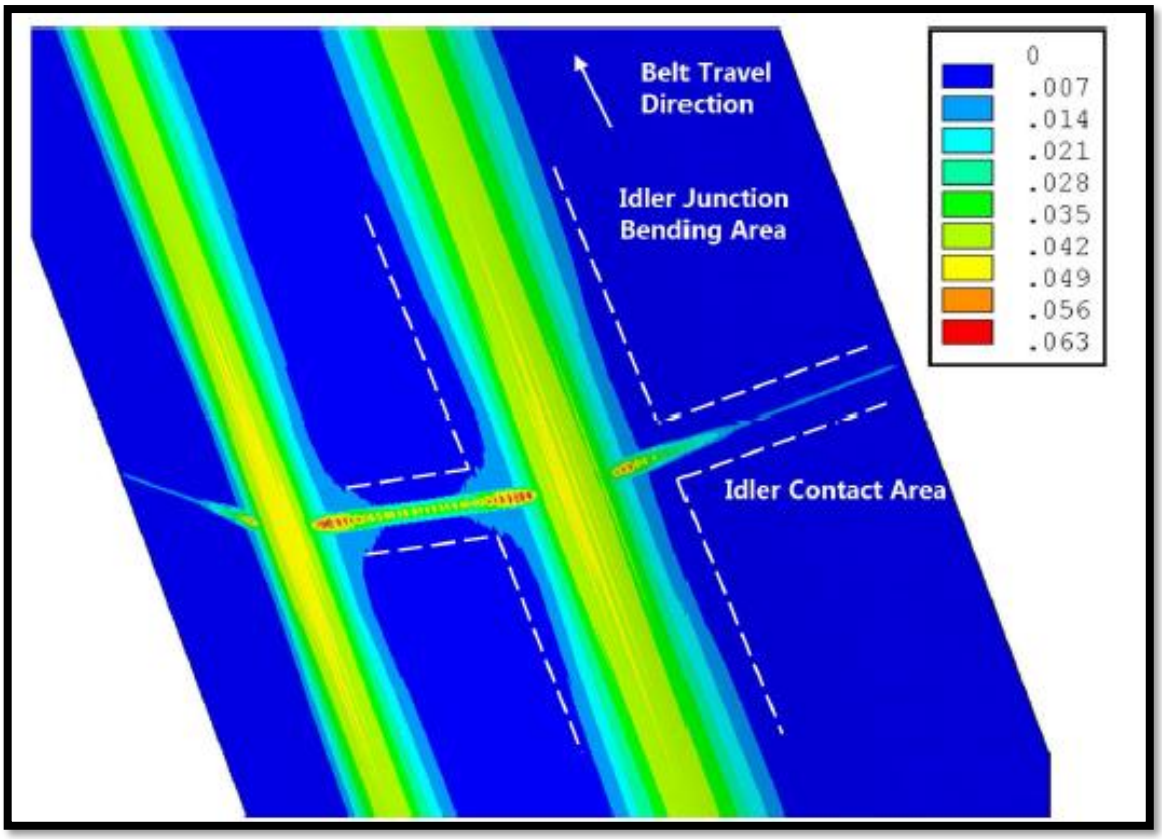


Figure 2-17: Equivalent (von Mises) Strain in the belt cover of a steel cord belt from finite element modelling (Zhang, 2015).

Figure 2-17 depicts a plot of the stress distribution that a steel cord belt experiences on an inline configuration. The high stress areas occur where the steel cables are present in the belt.

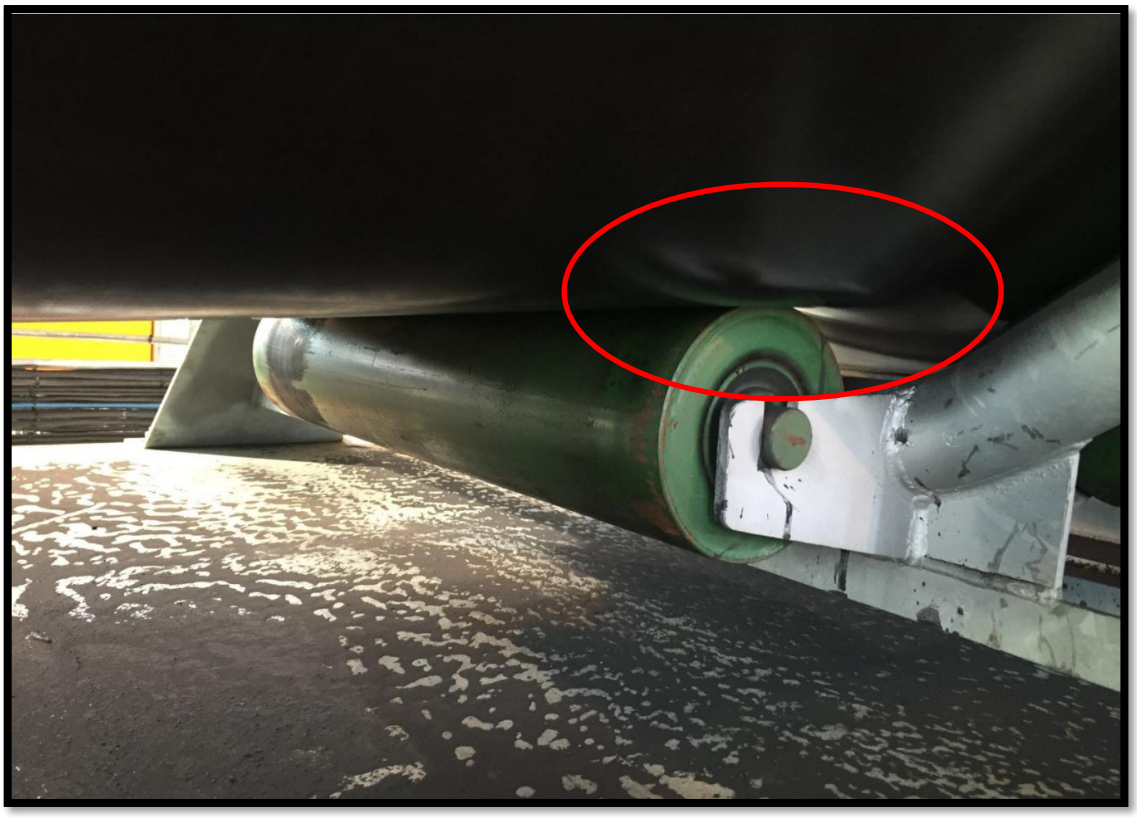


Figure 2-18: Idler junction damage occurring on a belt friendly idler configuration, side view.

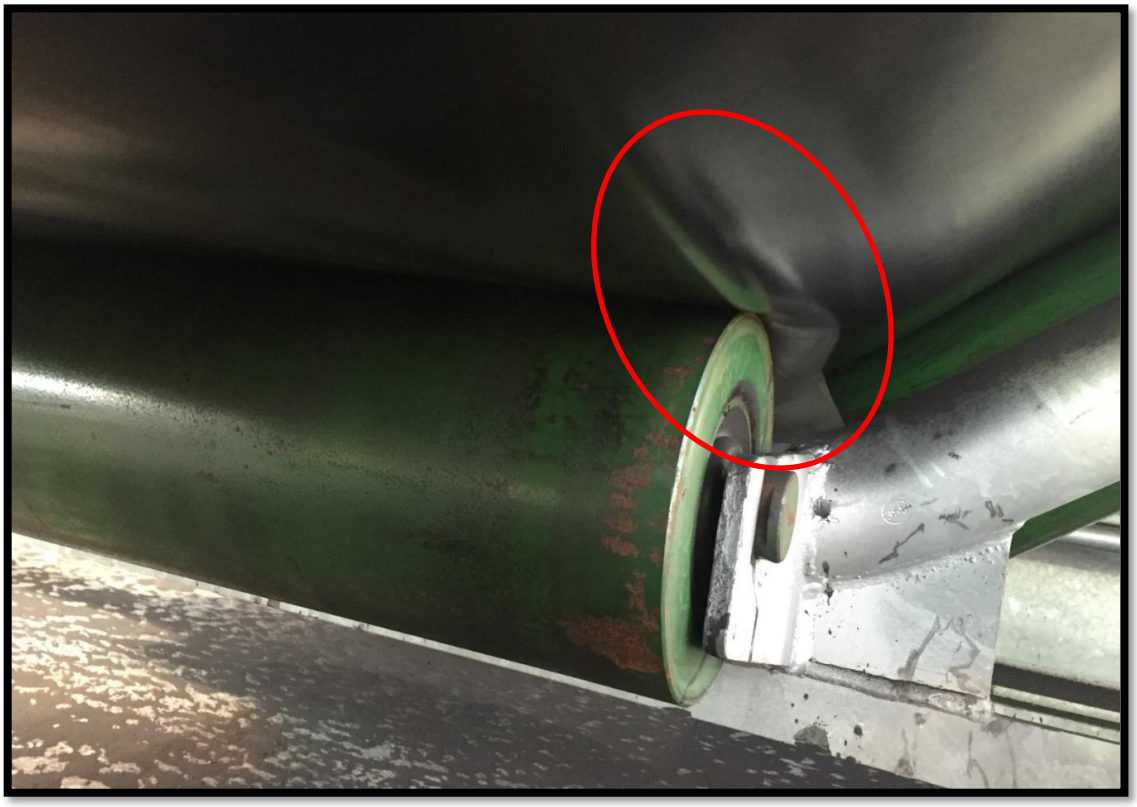


Figure 2-19: Idler junction damage occurring on a belt friendly idler configuration, front view.

2.5 Strain Gauges Applied to Belts

Strain gauges attached to a belt was seen as a possible way of practically measuring the strain that the belt experiences. There were challenges in ensuring that the values obtained were repeatable and could be used for a basis of evaluation of the magnitude and variation of the belt stress.

The way that the belt manufacturers define elongation is to use the crosshead distance between the stationary platen and the moving platen and use the displacement to calculate the elongation.

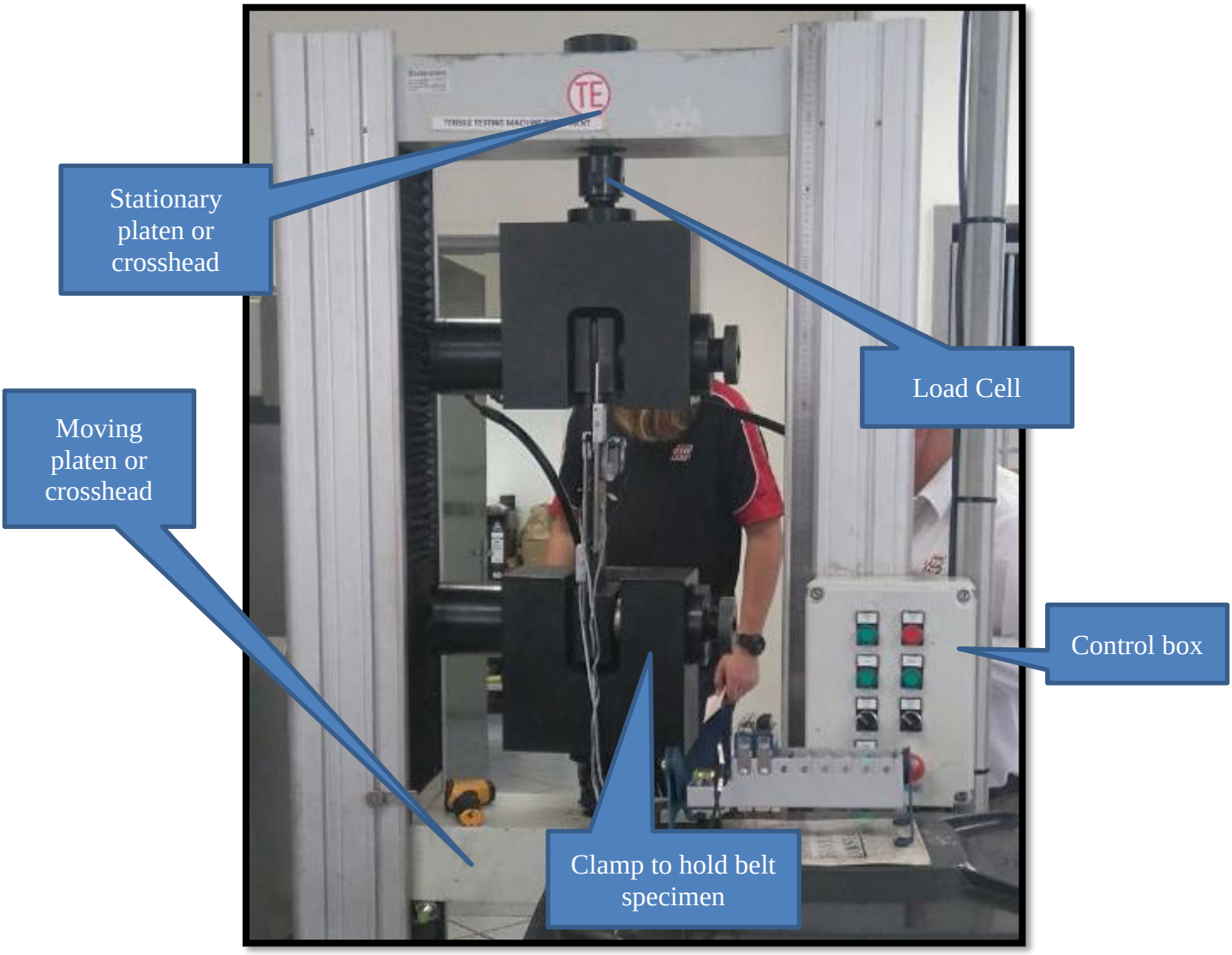


Figure 2-20: illustration of method used to determine the belt elongation.

This is not a very accurate means of determining the elongation but rather an extensor should be used on the specimen. This conventional method could not be used as a means to compare elongation values to those of the strain gauges.

There are some limitations with the application of strain gauges on conveyor belts. The Young's Modulus of the covers of the conveyor belt is much lower than that of the strain gauge (Egger M, 2002). The consequence of this is that the area under the gauge was stiffer than the surroundings. Another concern is in essence the strain transmission which is described as follows: "Shear stress in the bonding adhesive is greatest at the ends and very low in the middle" (Hannah R.L., 1992). Egger (2002) does provide an equation to account for this, which is Equation 2-2 shown below:

$$\varepsilon_{belt} = \kappa_{corr}\varepsilon_{measurement} \qquad \textbf{2-2}$$

Where:

ε_{belt} = Strain that the belt is experiencing

κ_{corr} = Corrective value for the measured strain

$\varepsilon_{measurement}$ = Strain that is being measured on the belt

Using the equation above and comparing it to the calculated strain there was a high degree of correspondence between the two, this is illustrated in Figure 2-21.

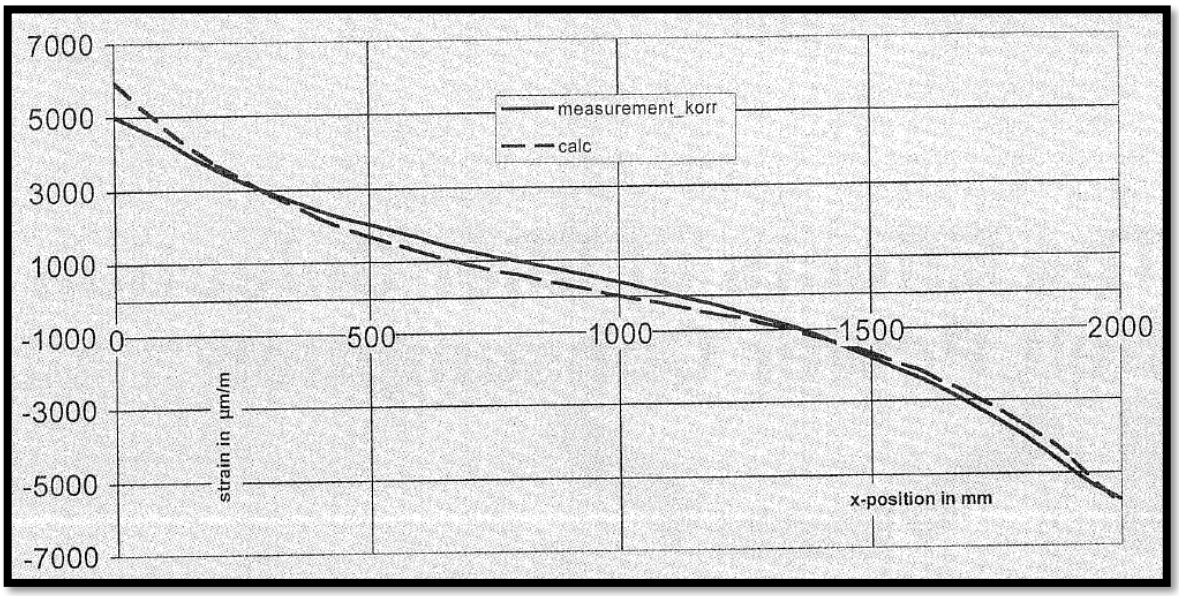


Figure 2-21: Bending Strain of the top strand due to a conical pulley, 125mm belt width, measured by strain gauges compared with the calculated distortion (Egger M, 2002).

3 DESIGN AND DEVELOPMENT OF THE EXPERIMENTAL TEST FACILITY

In order to achieve the objectives of this project a test facility had to be constructed that could meet certain requirements. An important requirement was to develop a test facility that can measure stress in the belt, particularly in the idler junction region. It is fair to state that historical data reveals that the highest levels of failure occur on convex curves (Pitcher, 2015). With this mind, the test facility developed for this study is in the form of a convex curve. It is important to note that regardless of the relative loading on a belt, the idler junction pressure is accentuated on a convex curve.

The test facility should allow for repeatable test measurements, and the various test parameters should be easily adjustable. Important test parameters would be to test various trough angles; the test facility should be designed so that the facility is modular so that testing beyond the scope of this project can be evaluated. The test facility should be designed so that it can handle the design loads and operate safely.

The above should be achieved while considering certain constraints. The first and foremost was cost, this would shape which test instrumentation could be selected and the overall design of the test facility. There were also the limitations of the sponsors, in terms of their technical capabilities and what they could provide in a certain time frame. Another major factor having a bearing on the design was the space available for the construction of the test facility and the resources needed to erect it.

3.1 Concepts Generation

An experimental facility was required to replicate the stress situation that would be present on a working conveyor. To do this various design ideas were generated and the most effective was chosen.

Concept 1

The initial idea was to have a continuously running conveyor that would be tensioned by the pulleys and loaded with material. The stress would then need to be measured as it went over idlers and around pulleys. The major concern with this design is that handling the material on the belt would be a problem.

Concept 2

A more elaborate test facility would need to be constructed to avoid the problem of handling the material discharging off the end. This could be accomplished by having an inverted idler frame that would press the belt down into the troughed shape. There would be no need to load the belt with material but the question remains as to how representative the loading profile would be, particularly on the wing rolls and how that would translate into the stress developed in the idler junction region.

Concept 3

A double conveyor system could be employed that discharges material onto the tail of one conveyor through a chute arrangement and then collects the material into a bin. The bin will allow for a controlled feed onto the initial conveyor. A convex curve could be added to allow for additional downward force, see Figure 3-1.

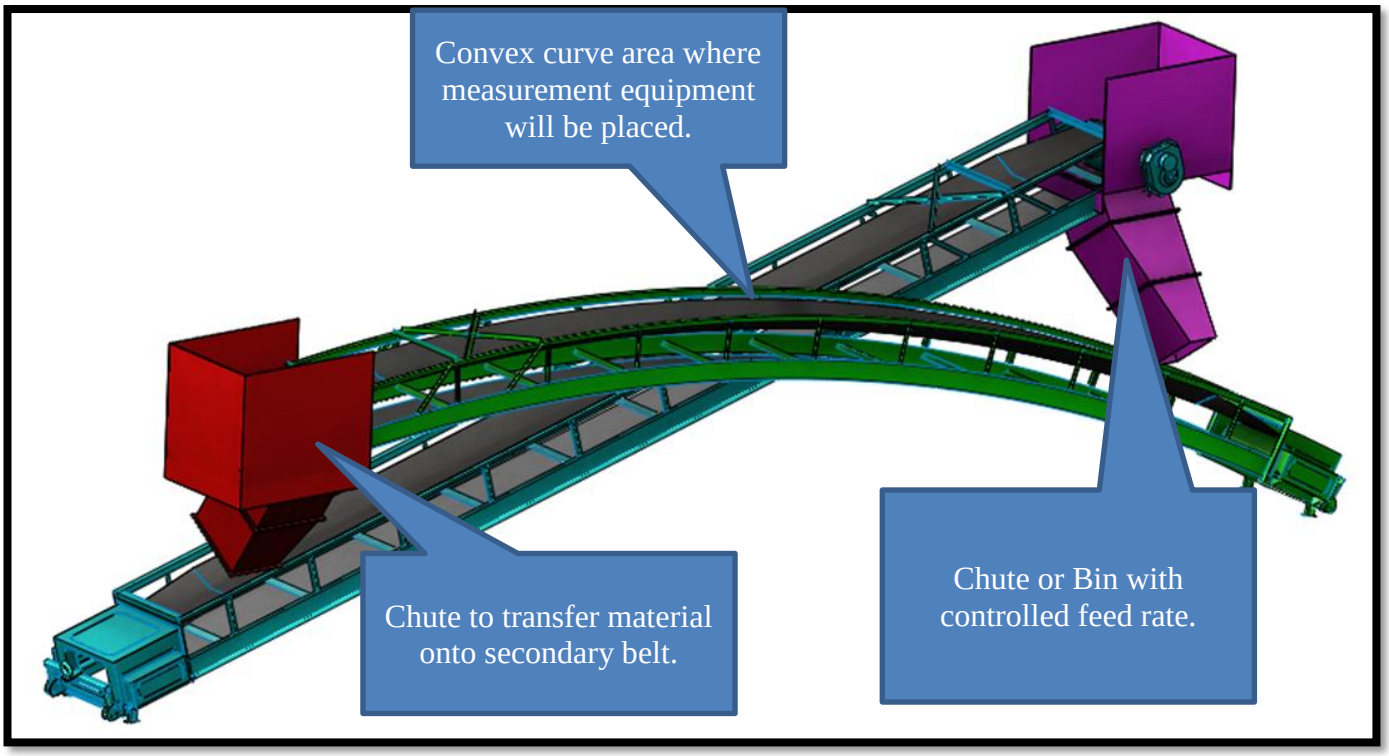


Figure 3-1: Possible concept for a test facility.

The difficulties associated with this idea are first, the cost, and second, how to have stress measuring equipment that is attached to the belt to go over idlers and around a pulley.

In order to measure the stress certain challenges arise. Strain gauges attached to a moving belt that has to go around a pulley would almost certainly be destroyed or at least damaged to the point where they could only be used once.

This then leads to the possibility of measuring stress by using a non-contact instrument. Digital Image Correlation (DIC) was seen as a prime candidate for a solution. It involves spraying the body with a certain speckled pattern and then measuring the strain of that body by comparing the difference between successive photographs of how the pattern varies (Dantec Dynamics, 2015). This is illustrated in the graphic below, Figure 3-2.

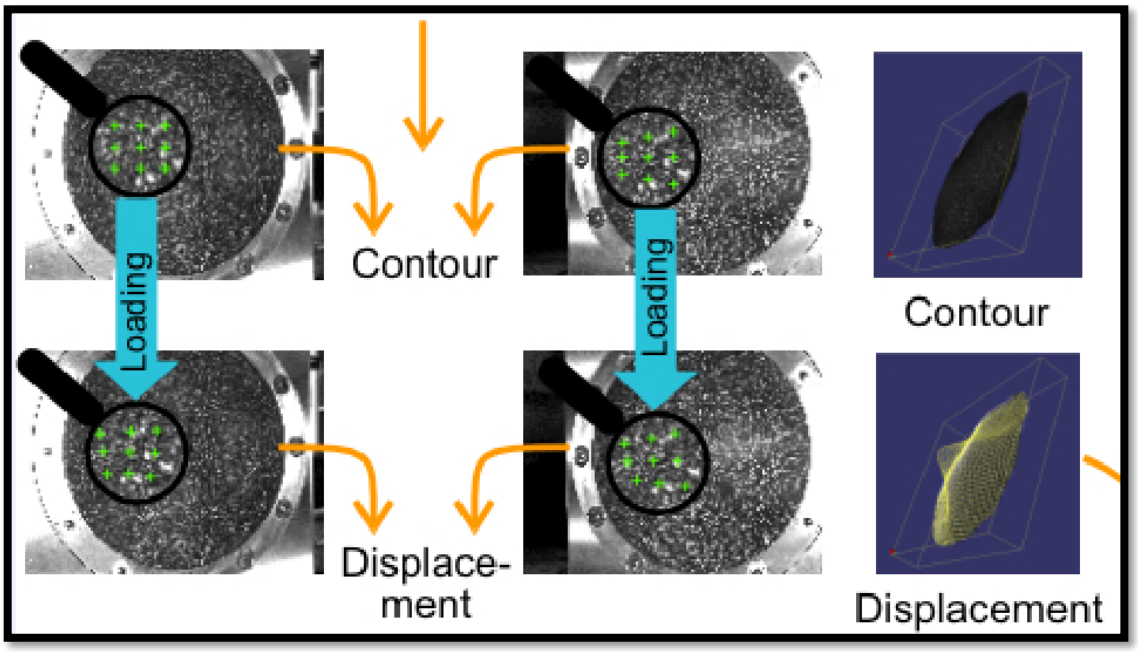


Figure 3-2: Illustration of how the Digital Image Correlation (DIC) technique works (Dantec Dynamics, 2015).

Photographic equipment was investigated but the equipment was very expensive and still had limitations. The major issue that was encountered was that the quality of the results would be compromised at the speeds the belt would be expected to be run. The test was to be designed to run at 250, 500, 750 rpm on a 127 mm diameter roller. A high speed DIC camera system would need to be purchased and that was outside the cost capability of the research project. This then led to a redefined approach which is outlined in the fourth concept.

Concept 4

The final concept for the experimental facility was to have a convex curve configuration, which will create additional loading to exacerbate the stress in the idler junction region, while retaining its applicability to a real application. The endless belt configuration was deemed unobtainable given the cost limitation. Instead a quasi-static application was chosen, whereby the belt could move a certain distance but not continuously run around pulleys. This design also allowed for material to be loaded onto the belt and could merely be reset by moving the belt back to its initial position.

3.2 The Final Design of the Experimental Facility

The various components that make up the test facility are now described. The labels “a” to “n” describe the major components of the test facility, shown in Figure 3-3.

The belt is tensioned via the hydraulic puller (a) which runs on rails (l). The rails allow for the belt to move a distance of up to 1.5 m. An important feature is to create movement over the extent of the area of interest- the measurement equipment is located to coincide with this area of interest which is at the centre of the structure.

It is necessary to have the belt move through the area of interest while data is collected as it moves. The region of interest is the area preceding the junction, through the idler junction, to after the idler junction.

The tension is transmitted through the steel wire cable (j) and around the sheave wheels (d). The sheave structure (d) houses two sheaves, the larger sheave is the load-bearing element while the smaller sheave is there to direct the cable tension. (See Appendices Section 8.2.3, Figure 8-14 and Figure 8-15).

The cables carry a maximum load of 20 tons therefore the sheave frame holder (m) needs to be able to withstand a load of the order of 40 tons. The sheave frame holder was embedded into a cube of concrete with the dimension of 1200 mm length per side. The soil conditions were found to be soft and unstable, so to accommodate the soil condition a larger area was excavated. The concrete was reinforced and braced with steel members (see Appendices Section 8.2.3, Figure 8-14).

The cable is connected to a shackle of the belt attachment (k). The adjustable belt attachment will allow for the belt to be troughed from zero to 90 degrees. This design reduces time for the various setups as the trough angle is increased from 0 degrees.

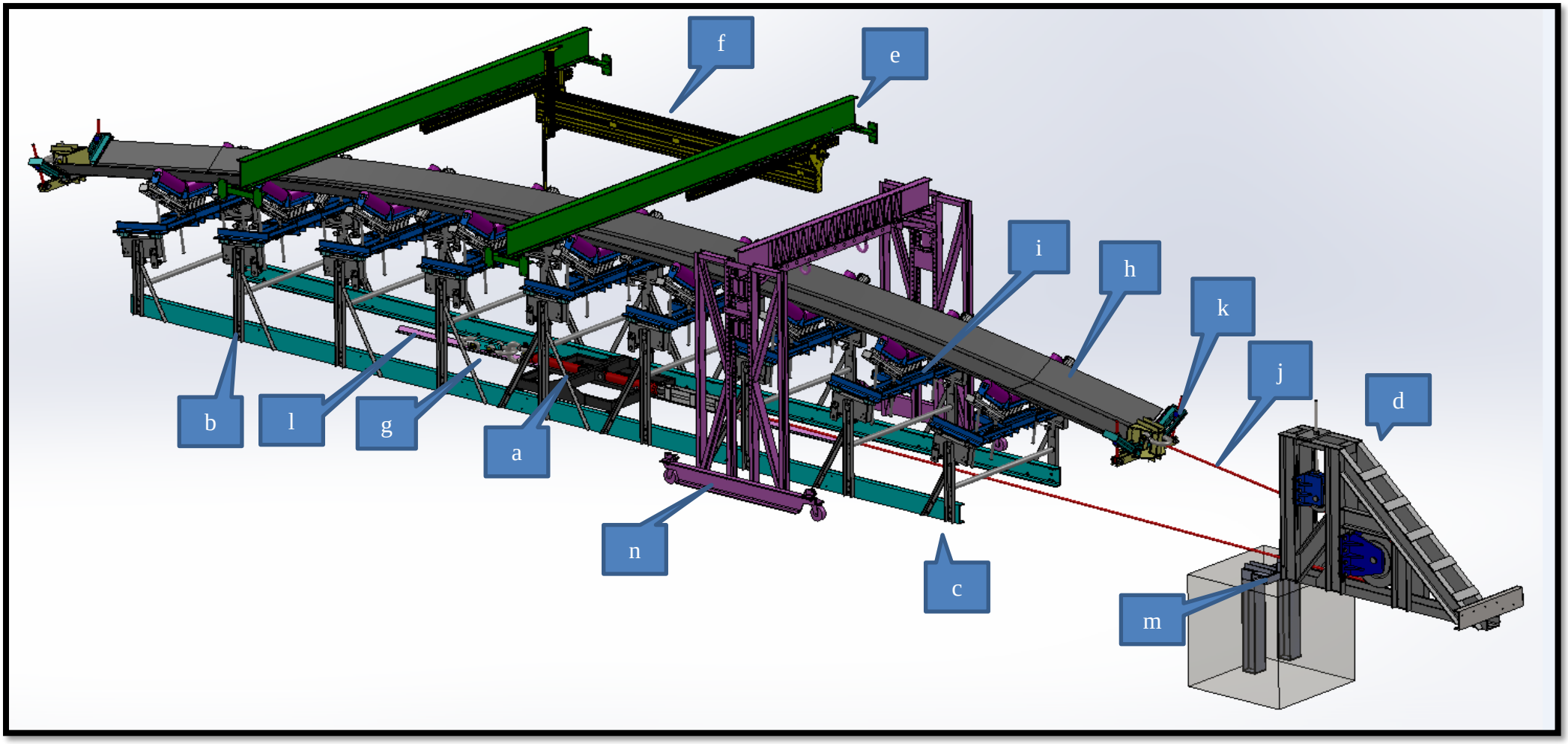


Figure 3-3: Components of the test facility.

In the initial design concepts, a pulley was proposed. Therefore, the belt would be carried on the idlers and then be pulled around the pulleys and the two belt ends would be tensioned after that. This idea posed two major challenges

1. The strain gauges could not undergo the strain of going around the pulleys in a continuous cycle. This may exceed the maximum strain limit of the gauges and each successive cycle of the belt would yield a different strain value for the same load.
2. The second hurdle is to accommodate the transition distance to normalise the stress (change of the trough shape from a flat belt to having a trough angle of up to 90 degrees). This would increase the length of the test facility dramatically. All of the equipment should be built under cover due to the sensitive electric equipment.

Thus, the belt attachment and sheaves were designed to overcome these challenges. As shown in Figure 3-4 and Figure 3-5 the steel wire rope is threaded around the pulleys which is also connected to the belt attachment. Figure 3-5 shows a close-up view of the belt attachment which is set at 35 degree.



Figure 3-4: Image of the Sheave structure and belt attachment.

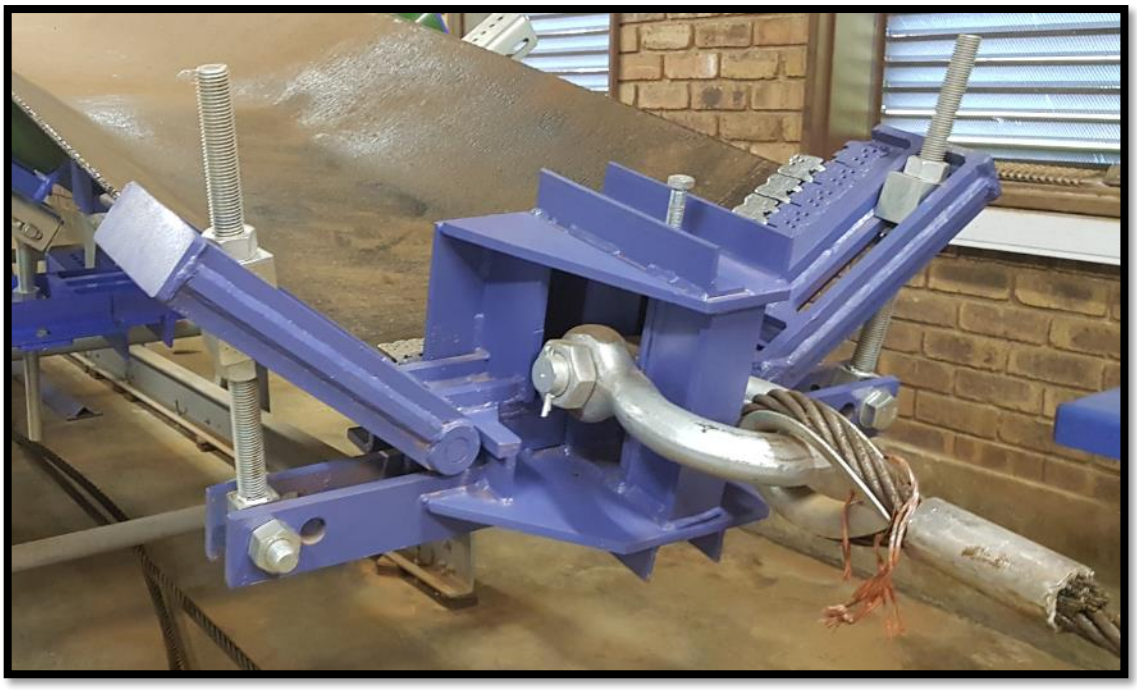


Figure 3-5: Belt attachment in operation.

The belt attachment allows for the tension from the wire rope to be distributed into the belt (h). The belt is set at a radius of 35m on a convex curve (see Appendices Section 8.1.1 and 8.2.5 for the process to determine and set the radius). The belt is connected to the belt attachment via a mechanical splice.

The length of the testing facility and the maintenance of the troughed shape was viewed with the utmost importance so as to eliminate the stress effects of the transition distance, as discussed in Section 2.4.4. The transition does induce additional stress and so the added length of the three idlers on each side of the three centre ones, where all the measurement will take place, was included to circumvent this issue or to lessen its effects.

The belt is supported by the universal idler frames (i), which rest on the column supports and support base (b). The column supports bolt directly into the base frame and allow for easy repeatable and accurate assembly (see Appendices Section 8.2.5, Figure 8-18 and Figure 8-19).

The universal idler frames are versatile in their design. The trough angle can be varied from zero to ninety degrees with a simple jacking bolt arrangement. The offset distance can reach a maximum of 450 mm while the wing rolls can be set at up to 5 degrees of forward tilt. The universal idlers are designed to be very strong and rigid structures to minimise deflection and accommodate large moment loads generated by the offset.

The overhead structure (e) provides the mounting for the belt profiler (f) The overhead frame needs to have negligible deflection and as such a deep I beam section was chosen.

As the name suggests the belt profiler will move in three orthogonal directions and be able to map the profile of the belt. There are three magnetic encoders used for the linear measurement along each axis, see Figure 3-6. The probe of the belt profiler will come into contact with the belt and will be moved across the weft direction of the belt a predefined distance so that a comparison of the different types of belts can be obtained (see Appendices Section 8.2.6, Figure 8-20 and Section 8.3.1).

The belt profiler uses magnetic encoders which provide precise repeatable results without any calibration required. The belt profiler needs to cater for the variation from the highest point in the belt trough to the lowest point.

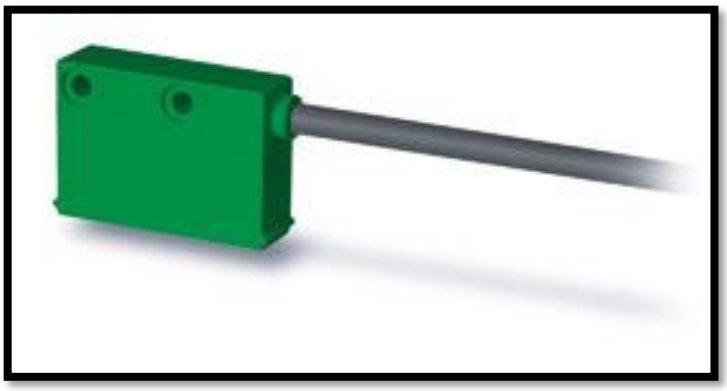


Figure 3-6: Magnetic encoder used on the testing facility.

There are various load cells placed on the testing facility to capture the necessary data. A tensile load cell (g) will measure the tension applied into the steel wire cable. Under the frames of the idlers, compression load cells will be placed to measure the force being applied from the belt, the convex curve and material that is loaded onto the belt (see Appendices Section 8.2.5, Figure 8-19).

The stress within the belt will be measured by means of strain gauges applied directly to the belt. The provision for the belt to move over the idlers is essential as it allows for the belt to move from a stress zone prior to the idler junction, past the idler junction zone, to the zone after the idler junction. It is important to see if there is a stress change from before, to after the idler junction and the distance that it takes to normalise the stress in the belt after the idler junction, this is depicted in Figure 3-7. The RTDs (Resistance Temperature Detectors) (PT100) will measure the temperature on the top and bottom belt cover and that of the ambient temperature of the test facility.

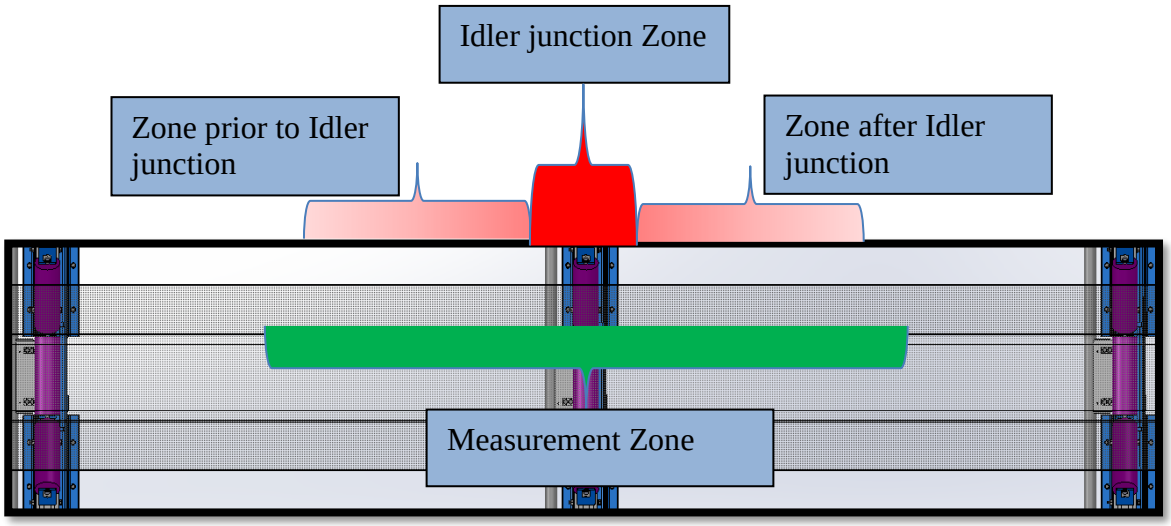


Figure 3-7: Illustration of important zones in the test setup, top view.

There are two distinct setup options available, these each have their specific purpose. Figure 3-8 illustrates the straight setup option in dimetric view while Figure 3-9 shows a front view of the setup. This shows that there will be five rows of idlers, this can also be varied to four rows of idlers. The value of varying the number of idler supports is to determine the effect of sag tension on the idler junction.

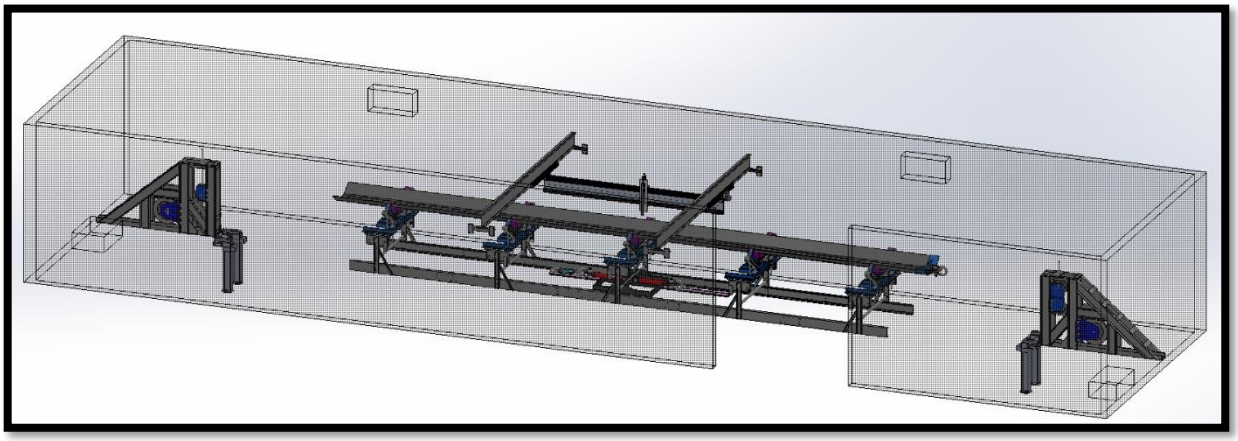


Figure 3-8: Experimental facility depicting the straight setup, dimetric view.

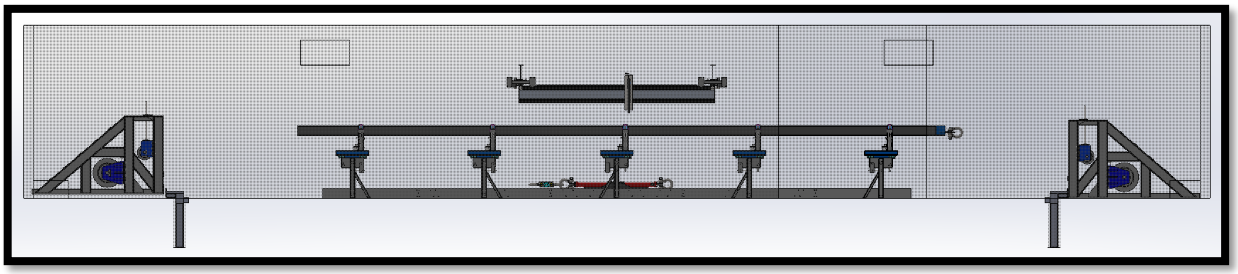


Figure 3-9: Experimental facility depicting the straight setup, front view.

Figure 3-10 and Figure 3-11 illustrate the convex setup. The convex setup will exacerbate the stress in the junction region. This is due to the additional loading that will be experienced by the idlers due to the curvature of the belt.

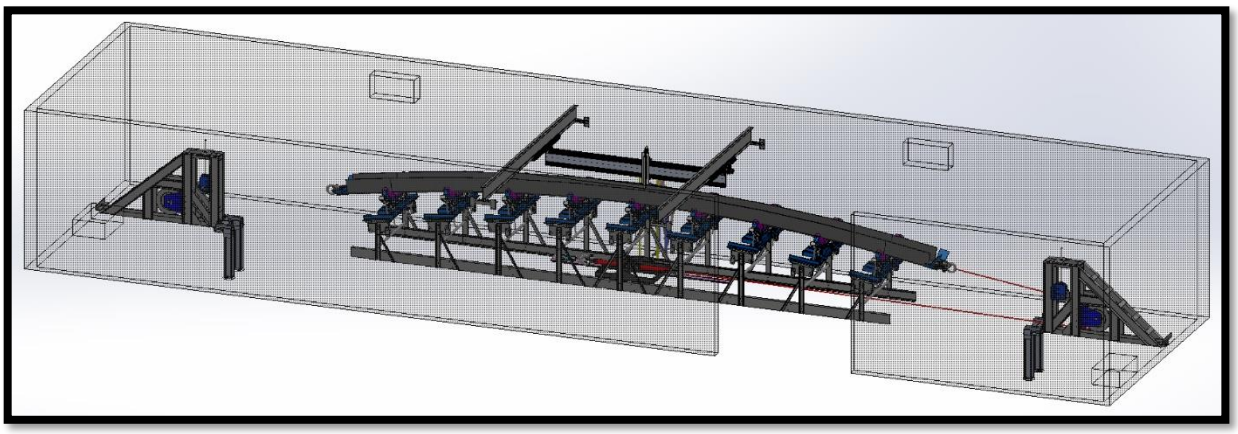


Figure 3-10: Experimental facility depicting the convex setup, dimetric view.

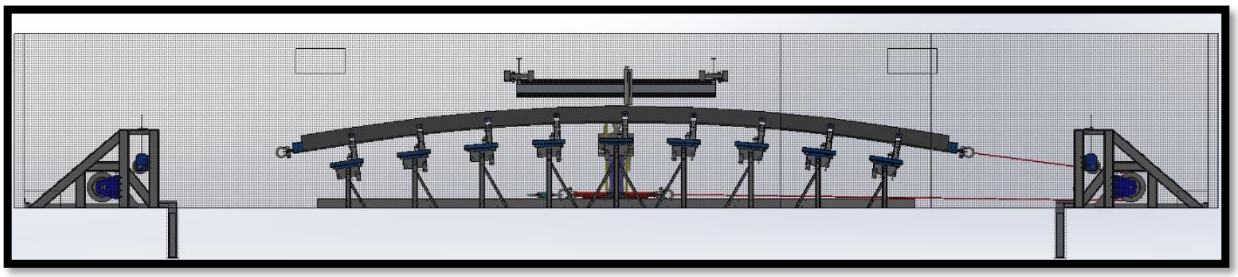


Figure 3-11: Experimental facility depicting the convex setup, front view.

The support structure was designed to hold the idlers (idler rolls and idler base), the load due to the convex curve, the mass of the belt and the material (if present). The belt will be maintained in the trough configuration to reduce the stresses that are induced as a result of the transition distance which is from where the belt changes from its troughed state to the flat state as it goes around a pulley.

The trough state will be maintained by means of a section of steel, the belt attachment, that has its geometry adjusted to conform to the trough of the belt. The belt attachment will then be connected to a steel rope to which the load will be applied (see Appendices Section 8.2.3, Figure 8-14).

The belt gantry lifter (n) (see Appendices Section 8.2.4, Figure 8-16 and Figure 8-17) will be used to lift the belt under tension. This will allow the universal idlers' trough angle and forward tilt to be adjusted without removing the tension; the reasons for this are discussed in Sections 4.4 and 0.

3.3 Experimental programme

Due to the large number of testing parameters, as tabulated in Table 3-1 a systematic procedure needs to be conducted to expedite the process. This program will commence after this research project has proved that the test facility is capable of performing the tests as outlined below.

Each type of belt being tested, PVC and Ply, will have the trough angle varied in increments of 15 degrees starting at zero and ending at 90 degrees. For every trough angle the offset distance of the centre roll will be varied in 25 mm steps to a maximum of 450 mm. The forward tilt of the wing rollers can also be varied in discrete values of 0, 2 or 5 degrees. The loading on the belt, through the hydraulic puller, can also be varied but may not exceed the strain limit of the strain gauge.

The stress will be measured at key points along the conveyor, see Figure 3-12. These will be at the belt edge (1) and the centre of the belt (5). This will allow a comparison of the calculated stresses at these points to measured stresses. Other areas of interest will be at the centre of the wing roller (2) so that the stress distribution can be more accurately quantified, and then just before (3), just after (4) and in the idler junction (6). Location (7) would represent a string of strain gauges so that the maximum or peak stress can be accurately located.

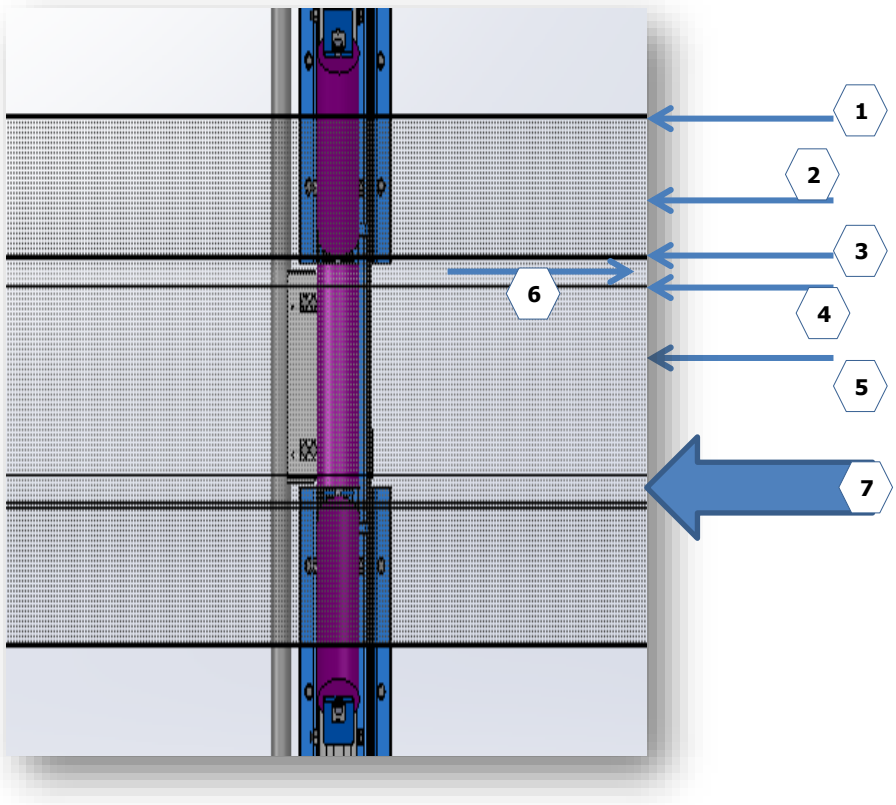


Figure 3-12: Location for stress measurement, top view.

Table 3-1 below illustrates the presentation of data that would be expected from the test facility.

Table 3-1: Layout of Data to be collected from Test Facility.

Belt	Forward Tilt	Trough Angle	Offset	Load %	Stress 1...n	Load Cell 1…k	Encoder 1..3
Belt 1…4	0-5 Deg	0-90 Deg	0-450 mm	80-100%	xxx	xxx	xxx

3.4 Calibration

The calibration process is of utmost importance to ensure reliable and accurate output of results. Calibration and validation work were undertaken to ensure that the results that are obtained are accurate and repeatable.

The NI DAQ equipment, see Section 8.3.1, was utilised during the calibration process, so that it would be easy to apply the correct scaling of the live readings during testing.

The major pieces of equipment to be calibrated were:

1. The load cells. The load cells were calibrated from an initial state to the maximum state. Details are provided in Section 4.2.
    a. 2 ton load cells
    b. 20 ton load cells
2. Strain gauges on belting. Details are provided in Section 4.1.
    a. Strain gauges were attached to the belting in the warp and weft directions. Tests will be conducted to determine if stress on the surface of the belt is similar to that in the carcass (validation of the assumption that the stress does not vary through the thickness of the belt, i.e. the carcass and covers see the same stress and strain).
3. The magnetic encoders are a digital system and as such do not require any form of calibration.

4 COMMISSIONING, TESTING AND VERIFICATION OF THE TEST FACILITY

This chapter describes the commissioning of all the equipment and how it was validated to ensure that it was fit for use.

4.1 Strain Gauge Calibration

4.1.1 Obtaining a Useable Calibration Factor

The requirement is to relate the voltage output of the strain gauge to the actual strain that the belt is experiencing. One could relate the voltage output to other parameters applied during testing. A useful parameter is the stress, in force per unit of width of belt (kN/m or N/mm). When obtaining strain values on a strain gauge, a certain load for a given width of belt sample is applied. This is a kN/m value, then the strain gauge reading can be linked to this value. If the readings on gauges are consistent on the top or bottom cover over the range of testing, this would provide confidence that this method is suitable for determination of the stress within the belt.

Due to the nature and construction of belting all the various belts need to be calibrated individually with their unique calibration factor for each belt. Equation 4-1 provides a means for converting the voltage to the tension in the belt.

$$T = \kappa v \qquad \textbf{4-1}$$

Where:

T = Tension (kN/m)

κ = Calibration Factor ($^{\mathrm{kN}}/_{\mathrm{mV}}$)

v = Strain Gauge Voltage Output (V)

Due to the time constraints and the difficulty associated with the belting companies to conduct these tests and then provide data from the testing, only one of the belts was tested to validate that this method can be used. The details are described in the following section.

4.1.2 Calibration Method and Procedure

It was very important to have confidence in the results of the strain gauges. In order to determine if the results from the gauges were factual and consistent, a series of tests was drawn up with the ultimate goal of comparing the output of the strain gauges to known values.

A. Sample Pre-Preparation

The belt sample shape for tensile testing is of particular importance as the conventional sample, as per (SANS 1173, 2013) has a cross sectional area that is continuously varying, shown in Figure 4-1. This creates problems as the elongation that is obtained is not a linear value.

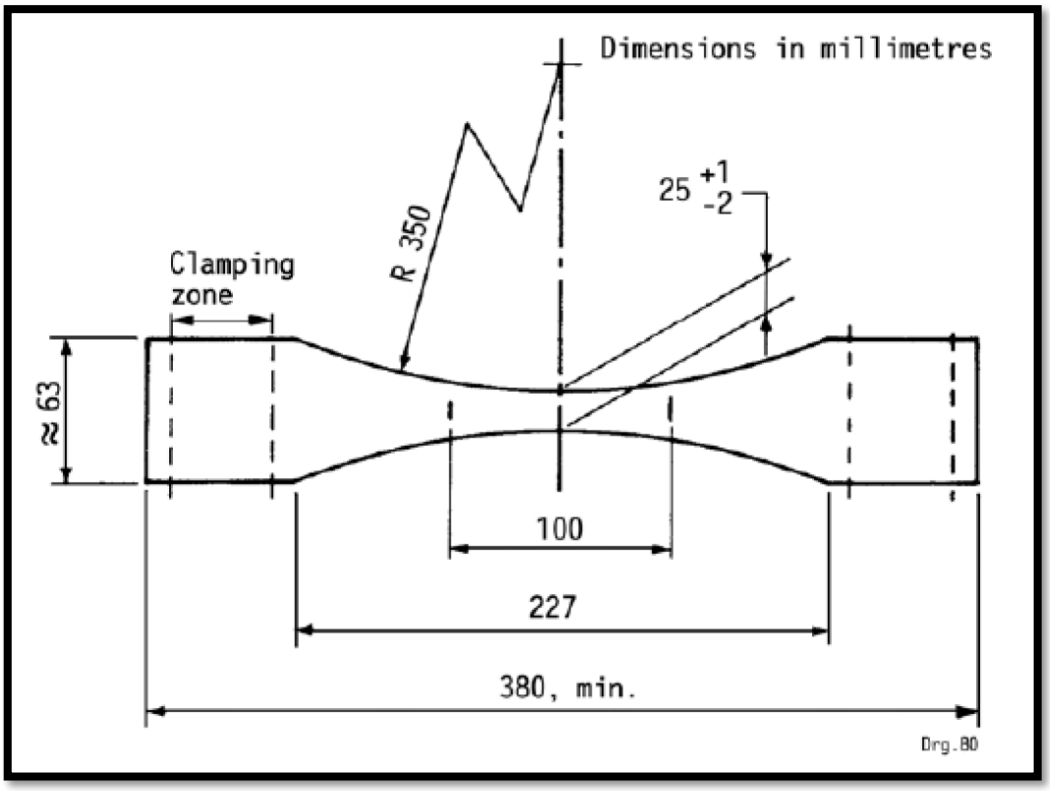


Figure 4-1: Conventional Sample with continuously varying cross sectional area.

Therefore, a sample with the gauge region that had parallel sides was preferred, as shown in Figure 4-2.

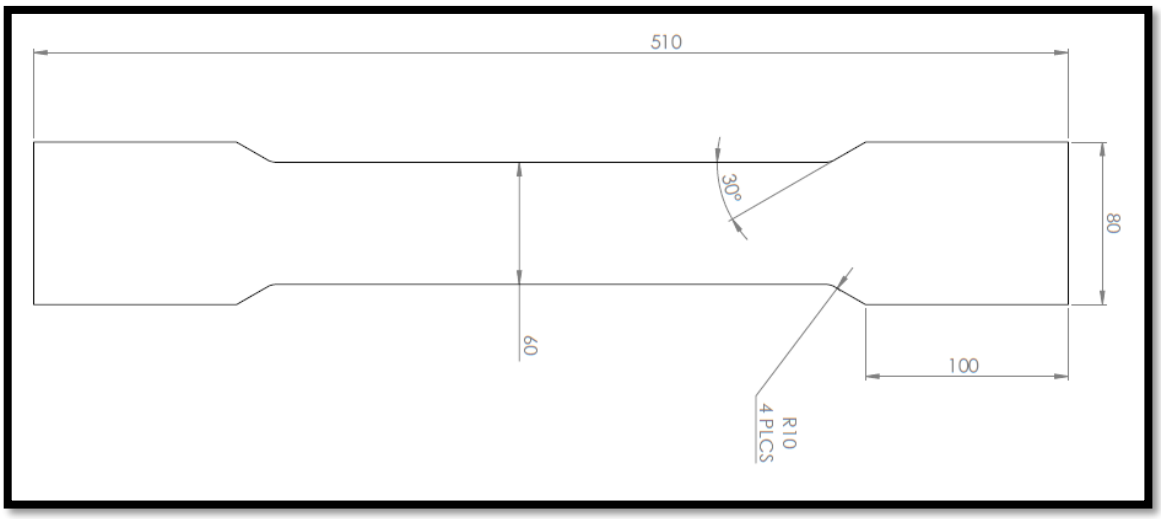


Figure 4-2: Sample with modified gauge length to have parallel sides.

The next issue was that the method used to cut the belt samples also introduced uncertainty. The samples are conventionally cut with a die or manually; both of these introduce a taper on the edges which makes it difficult to quantify the exact thickness of belt that is present. The pressure exerted on the rubber causes it to deform creating a non-uniform edge. The solution to this was to have the belt samples waterjet cut so that the taper becomes negligible and the cut is very smooth.

The belts were cycled at least 200 times in accordance with specification ISO 9856. The load was varied from 2 to 10 percent of the belt breaking strength. This is to remove the permanent stretch of the belts; once this has been completed the elongation will become very similar as in Figure 4-3.

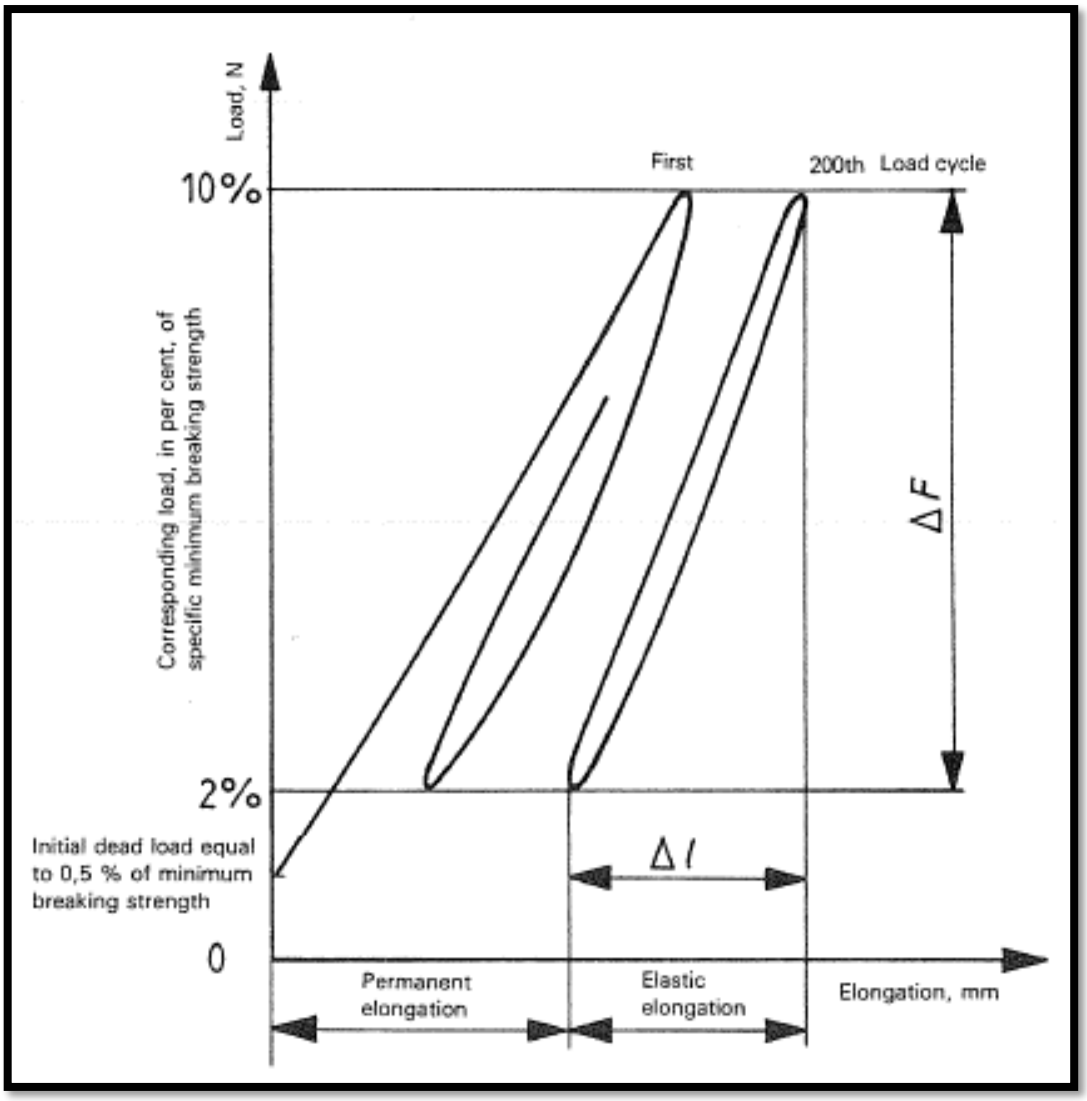


Figure 4-3: Graph of variation of amplitude of the load as a function of elongation (ISO 9856, 1989).

After cycling the samples up to 300 times it was seen that not all the permanent stretch was removed (if it were to be accepted from general conveyor manufacturers' data that most belts have about 1% permanent stretch); in fact, it was slightly more than a quarter of a percent. The dynamic cycling is an important sample pre-calibration step and it is necessary to increase the load to say 10 % and 40 % to reduce the number of cycles (so as not to become a time constraint) but remove more of the permanent stretch.

The samples were cycled in the tensile tester as shown in Figure 4-4, an extensometer was attached to the belt sample as it underwent dynamic cycling.



Figure 4-4: Belt sample in tensile tester with extensometer attached.

Once the belt samples were prepared and conditioned they were ready to be applied with the strain gauges and other measuring instruments.

B. Instrument Application Preparation

There were several instruments that were required in order to check various parameters on the samples.

1. Vernier calipers to measure the top and bottom cover elongation and compare it to the strain gauge readings.
2. Micrometer to measure the thickness change as the sample is tensioned and then relaxed to an initial load.
3. Heat sensor to measure the temperature change that the belt sample will experience.
4. Strain gauges, to measure the variation in strain across the sample, as shown in Figure 4-7.

Figure 4-5 depicts the arrangement of the various pieces of measuring equipment that were used on a conveyor belt sample. A vernier was attached to each side of the belt sample. The purpose of this was to ensure that the elongation on both the top and bottom covers was identified. Generally, belts have a thicker top cover than bottom cover. So

it needed to be determined if in a purely axial tensile test there is a variation in the strain of the top and bottom covers.

In Figure 4-5 the sample arrangement in the tensile tester is shown with the verniers attached on either side of the belt sample. The distance between the jaws of the vernier is 150 mm. Initial tests were done at 50 mm and it was seen that the elongation was small with regard to the resolution of the instrument. Therefore, by trebling the distance between the jaws it trebled the sensitivity of the measurements.

A third vernier was used to measure the decrease in width of the belt as a tensile force was applied to the sample. The resolution of the vernier was inadequate for measuring the width, therefore a more sensitive instrument was needed to get a more accurate reading and hence a micrometer was used.

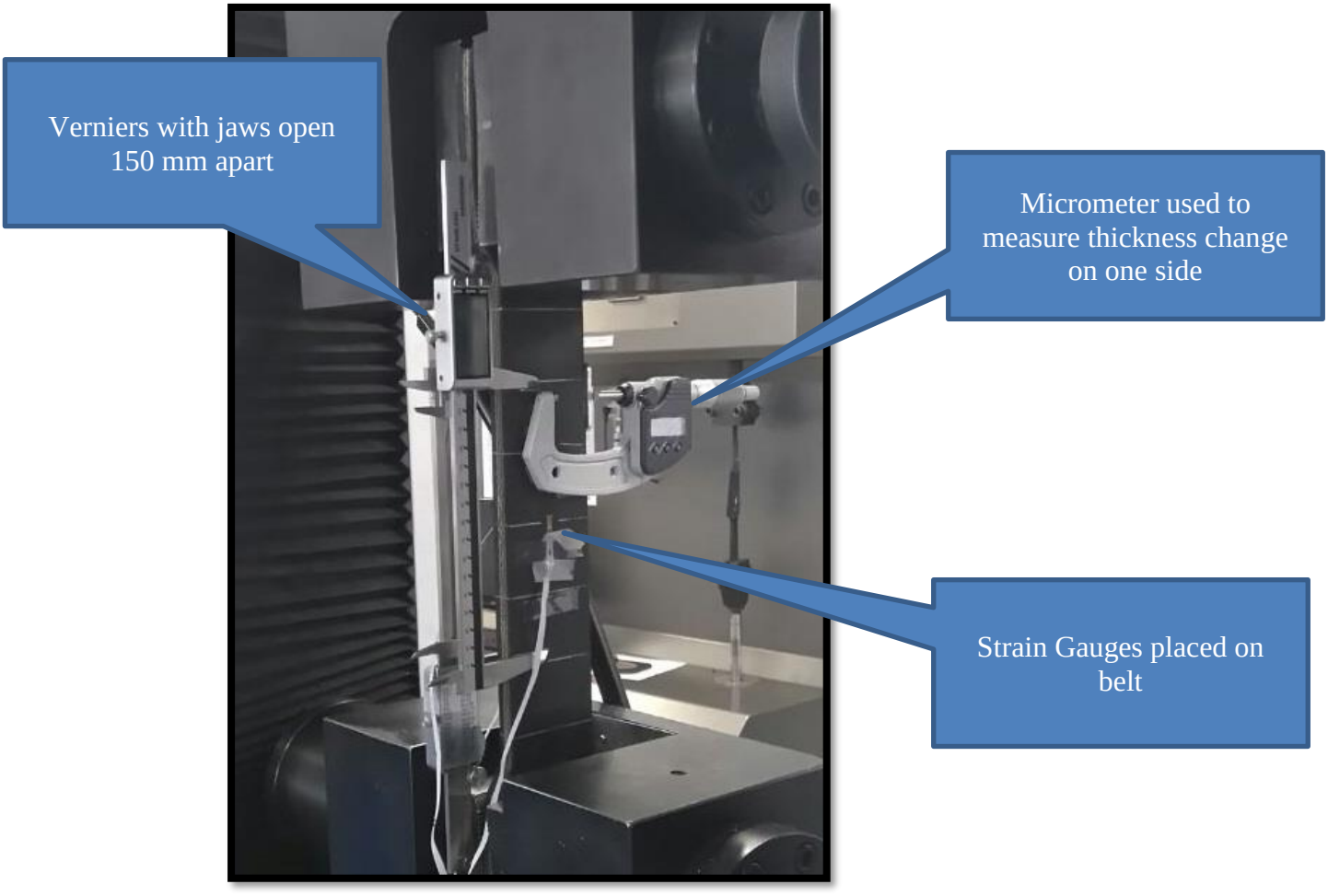


Figure 4-5: Setup of belt sample with in a tensile testing machine.

The gauges were bonded in a quarter bridge fashion (as shown in Figure 4-6) on each side. This quarter bridge configuration will have temperature compensation and will be sensitive to the combined effect of the bending moment and normal force that the belt experiences during loading.

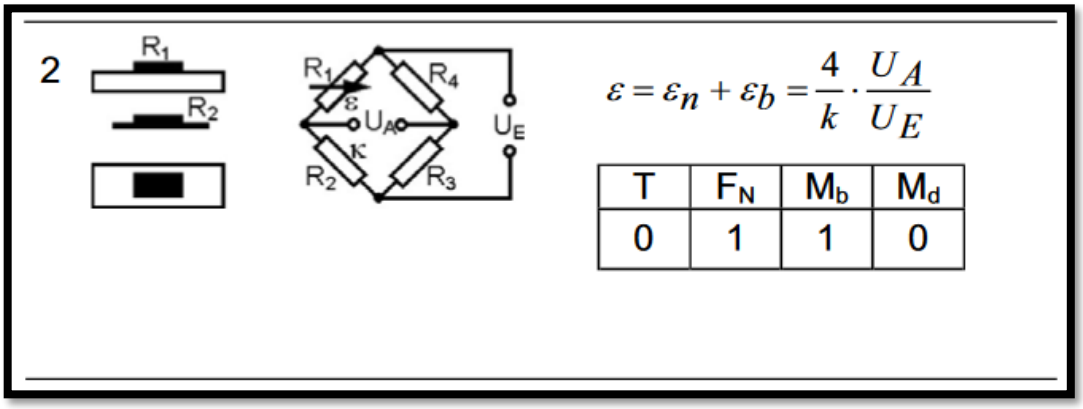


Figure 4-6: Quarter bridge configuration sensitive to both the normal force and bending moments, with temperature compensation (Hoffmann, 2015).

The gauge arrangement is shown Figure 4-7, with the belt sample having the strain gauges attached to the surface of the belt. The objective of the test is to determine whether there were strain variations in the vertical (ADG, BEH, CFI) and horizontal (ABC,DEF,GHI) lines, which was done with 10 mm gauges and 5 mm gauges. This was done to mitigate the effects discussed above in Section 0 with regard to the stiffening effects of gluing the gauges at the edges. Further to that, two types of adhesive were used, a polymer (SC2000) and a cyanoacrylate (super glue) type.

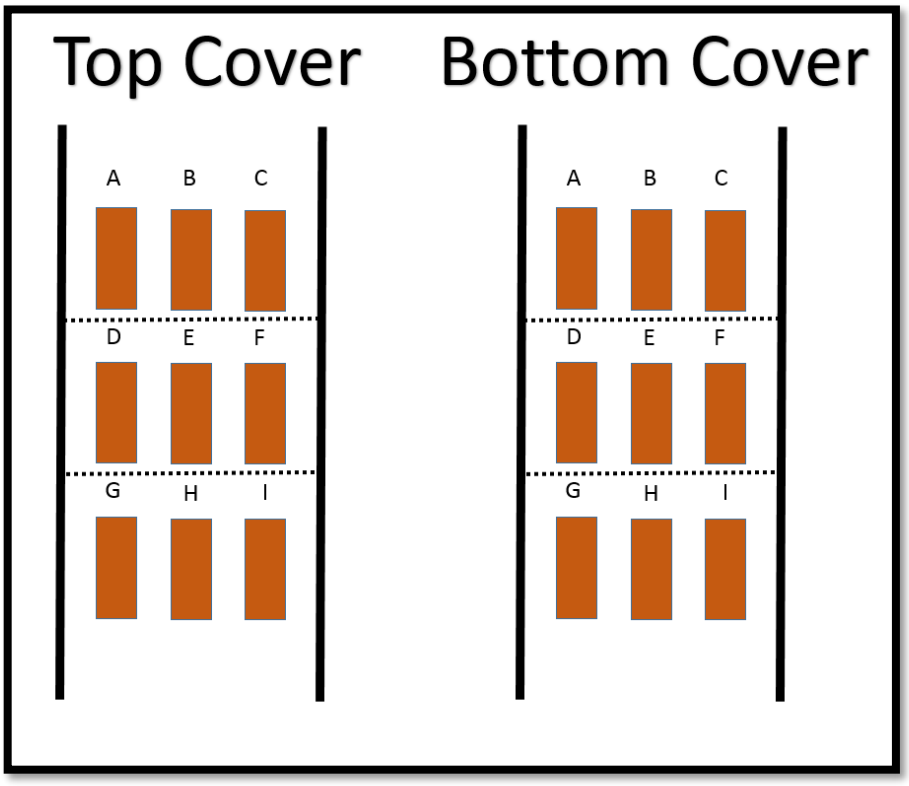


Figure 4-7: Top and Bottom covers of the belt sample, illustrating gauge location.

A dumbbell sample with parallel sides, as shown in Figure 4-8, was chosen over a conventional curved sample, as maintaining a constant cross sectional area is very important in determining an accurate strain value. The alignment of the gauges on the belt was of particular importance so that the peak strains could be pinpointed in the orthogonal directions.



Figure 4-8: Belt sample with gauges attached.

C. Testing Procedure

The loads were applied to the belt samples via a tensile tester so that the elongation and subsequently strain that the samples experienced was accurately known, this was then compared to the strain that was measured by the gauges on the belt samples and a corrective value was obtained. This was repeated multiple times to ensure a confidence level in the repeatability of the results, the procedure being as follows:

1. Insert the samples into the tensile tester as shown in Figure 4-5. The samples are placed into the tensile tester after the strain gauges are applied. The samples were then prestressed up to 1 kN.
2. The samples were then cycled ten times up to 5 kN and back down to 1 kN. This is similar to 2 and 10.5% of belt breaking strength.
3. Measurements of the elongations, temperature and strain were recorded at each increment of load variation. The increment of load variation was set at 0.5 kN and increased up to 5 kN and then brought back down again to 1 kN.

Several aspects of the research that this calibration test was designed to look at were:

1. Was the strain measured on the surface of the top and bottom covers similar?
    a. This could mean that the stretch/strain in the thicker cover would be greater as it would be a greater distance from the carcass. (Option 1 in Figure 4-9.)
    b. Or as depicted in option 2 in Figure 4-9 that the strain levels are reasonably equivalent.

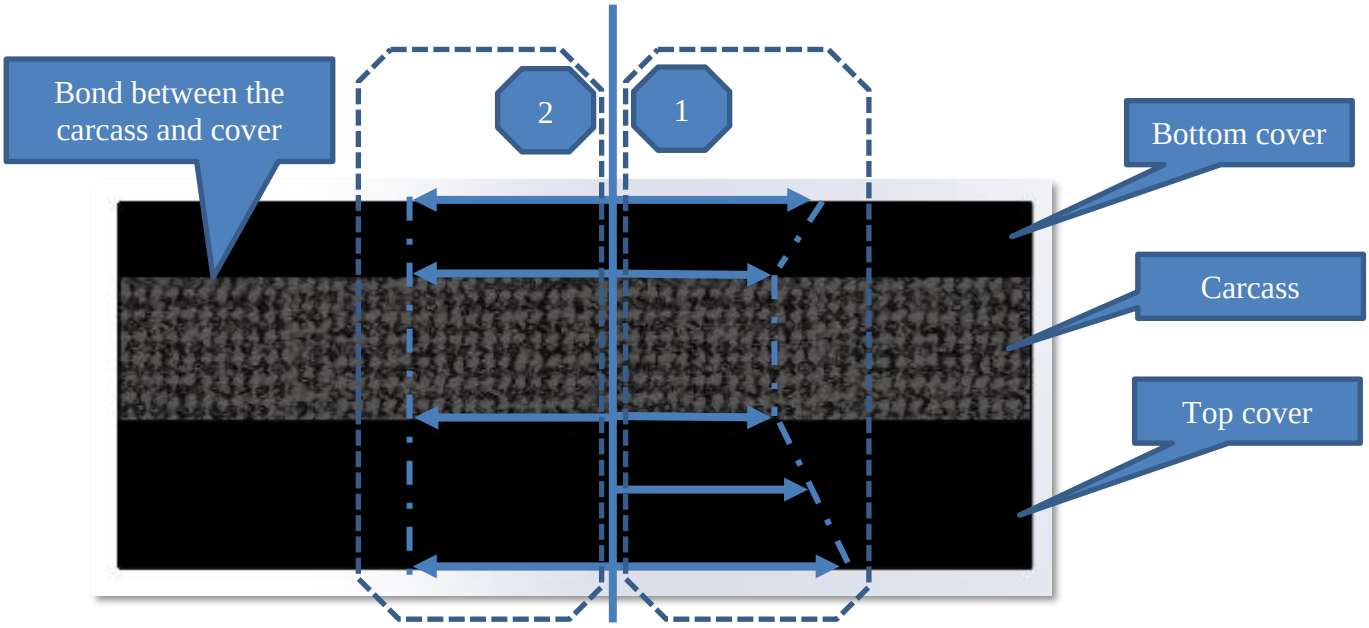


Figure 4-9: Illustration of possible outcomes of the testing, with regard to the cover elongation.

2. Due to the fact that a belt carcass is a woven fabric construction, could there be tension variations across and along the belt? It needs to be quantified what a reasonable variation along the length and width of the belt would be.
    a. To do this strain gauges were arranged on the surface of the belt samples as shown in Figure 4-10.
    b. The strain gauges were arranged in a predefined grid pattern at about 50mm apart.
3. It may be necessary that each belt would have its unique corrective value.

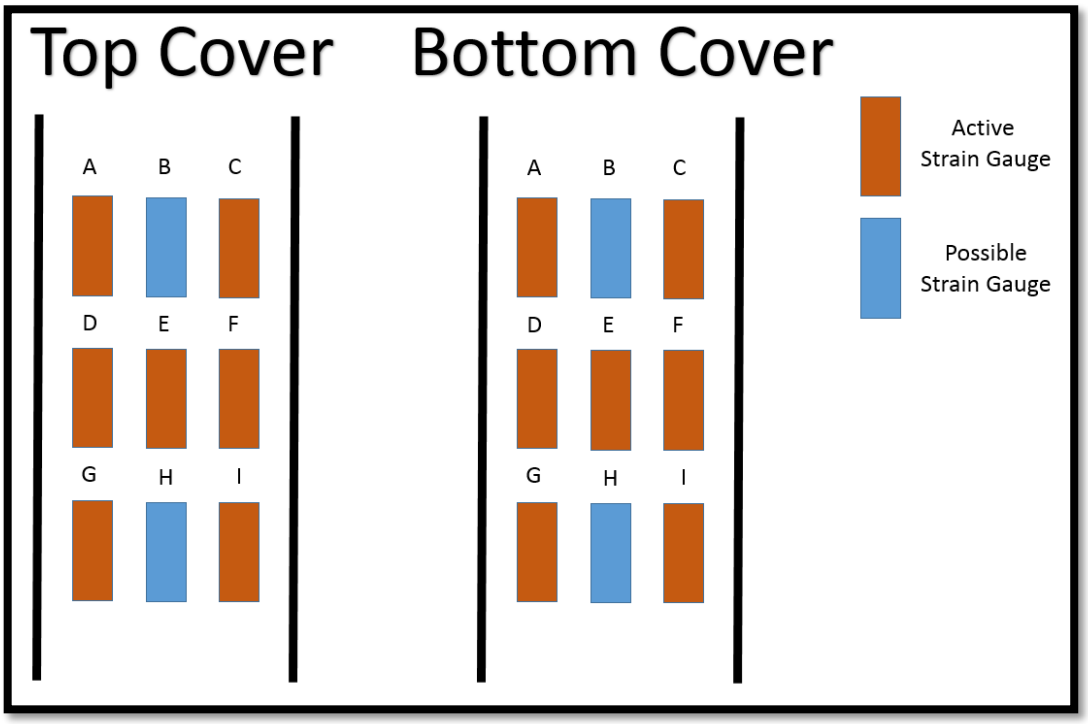


Figure 4-10: Strain gauge arrangement patterns.

4.1.3 Strain Gauge Calibration Results

The most important results of the tests conducted on a class 800 3 ply 5 mm top and 3 mm bottom cover belt concern the following:

1. Comparison of the verniers with readings and some of the anomalies that were observed in the data.
2. The force versus the strain gauge output is probably the most important set of data. With this relationship, the strain gauge output on a full scale experiment can be interpreted so we can understand when the belt is being overstressed.

When plotting the force versus cumulative elongation using the verniers on the top and bottom covers over several experiments, it is clear that the top cover consistently experiences a greater elongation than the bottom cover. Another interesting result is that there was residual elongation left, as illustrated in Figure 4-11, once the belt was returned back to its starting position of 1 kN.

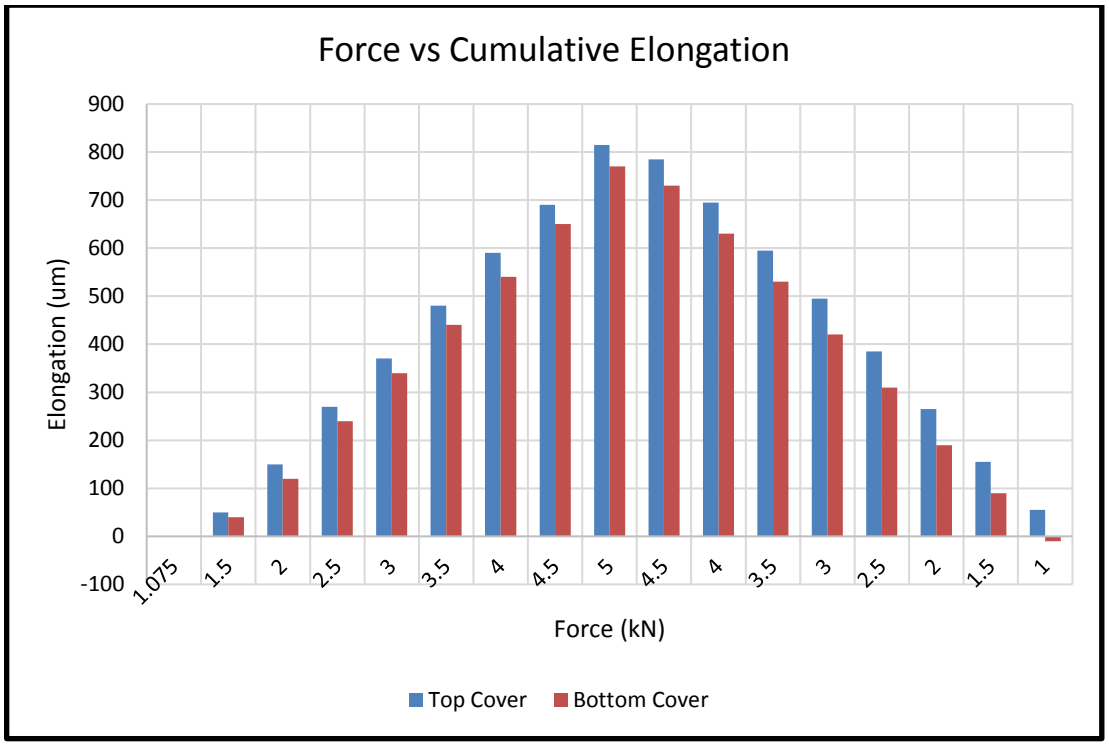


Figure 4-11: Bar Graph of Force vs Cumulative length.

It can be seen in Figure 4-12 that there is hysteresis in the belting and that the graph takes on a definite loading and unloading profile for both the top and bottom covers.

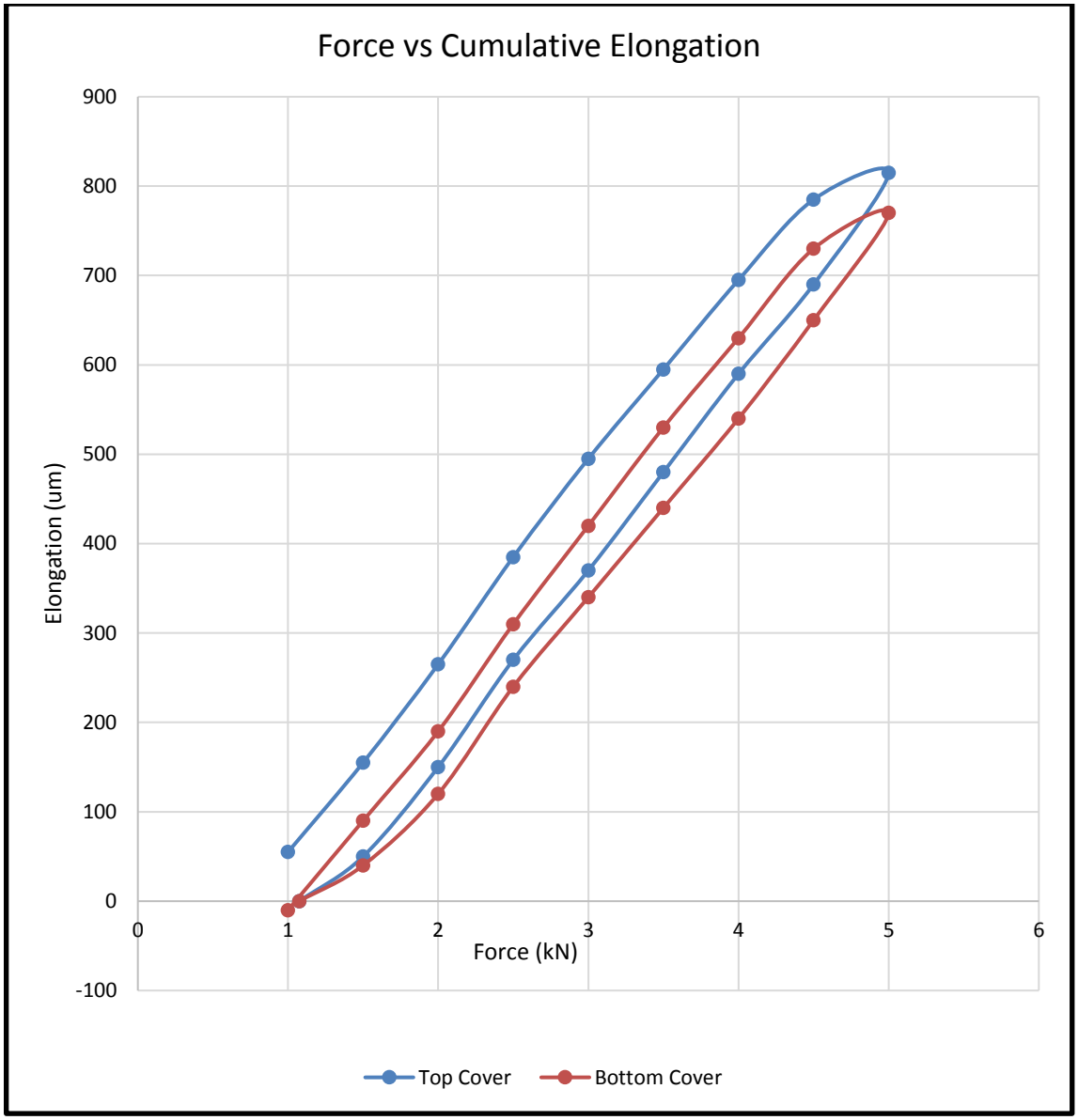


Figure 4-12: Scatter Graph of force vs cumulative length.

If the loading (Figure 4-13) and unloading (Figure 4-14) cycles are broken up into their respective segments then the graph approximates a straight line with a high degree of certainty. If we consider the coefficient of determination (R^2), this value approaches unity, indicating that there is a high degree of correlation between the straight line trendline and the experimental data.

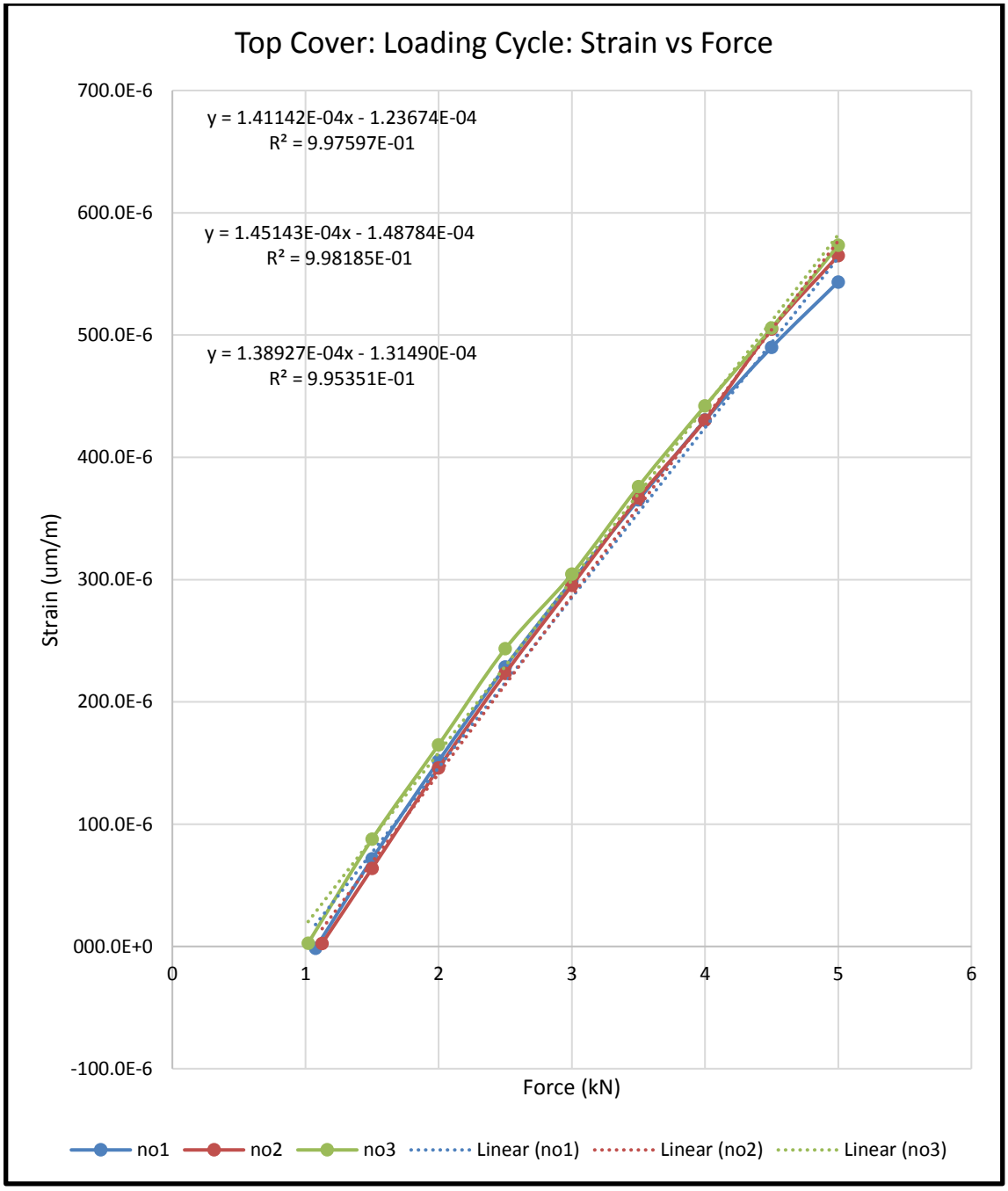


Figure 4-13: Strain versus cumulative length for the loading cycle for the top cover.

Another useful aspect to consider is what the spread of the results would be across the experiments. From Table 4-1 we can see that the uncertainty diminishes with an increase in loading. This is important as the 3.5-5 kN loading is close to where the full scale testing will be expected to take place, which is roughly 6.5 to 10 % of the belt breaking strength or belt class.

Table 4-1: Variance between the readings for strain for a given load.

				Average	Variance
Strain	576.9E-6	582.0E-6	563.1E-6	**574.0E-6**	**3.29%**
Load	5	5	5		
Strain	431.8E-6	440.9E-6	424.2E-6	**432.3E-6**	**3.86%**
Load	4	4	4		
Strain	286.6E-6	299.8E-6	285.3E-6	**290.6E-6**	**4.98%**
Load	3	3	3		
Strain	214.1E-6	229.2E-6	215.8E-6	**219.7E-6**	**6.88%**
Load	2.5	2.5	2.5		

There is a similar trend with the unloading cycle. Again the experimental data and the coefficient of determination (R^2) show a high degree of correlation, with a decreasing spread in the values as the values tend towards 5 kN.

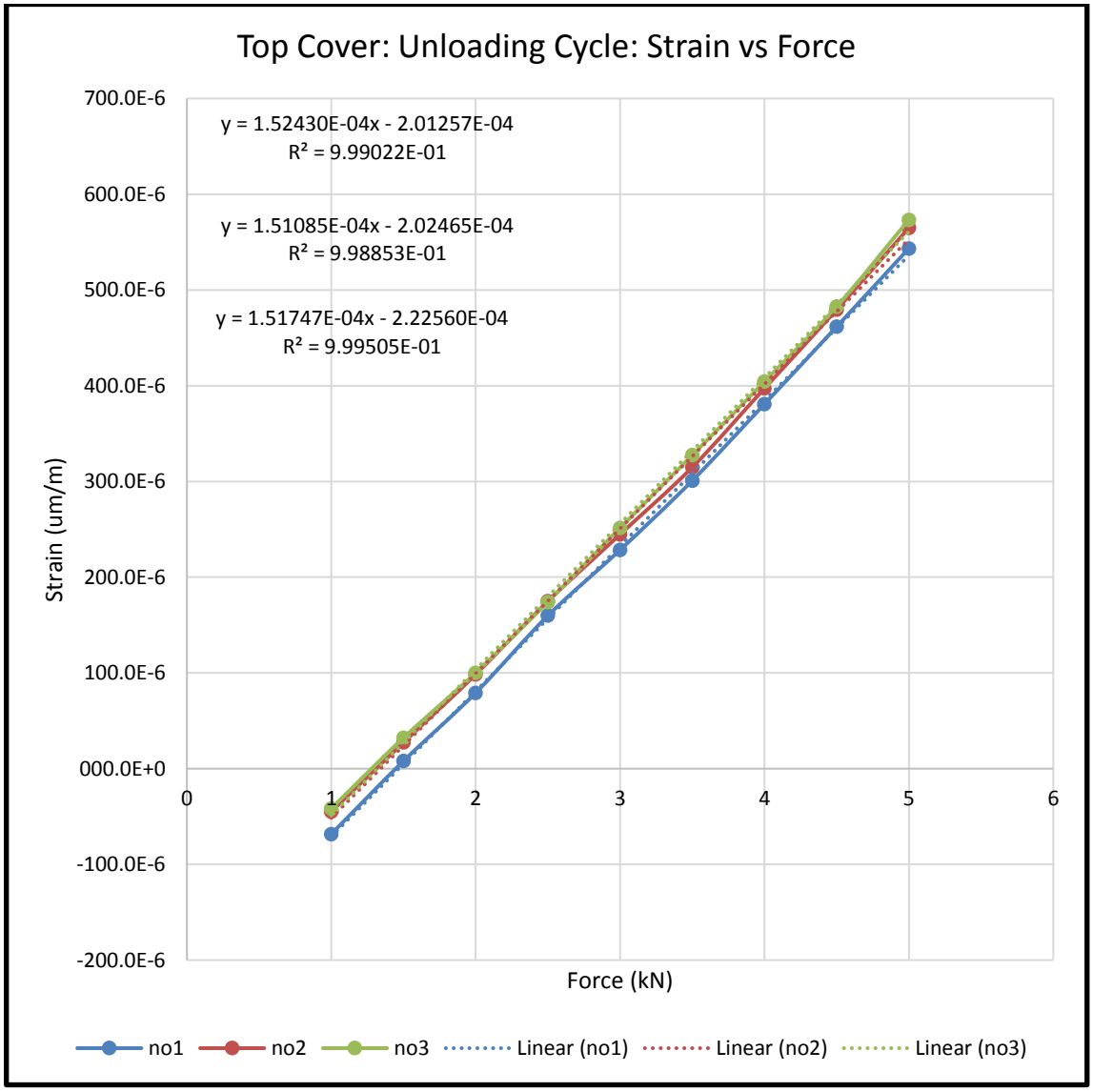


Figure 4-14: Strain versus cumulative length for the unloading cycle for the top cover.

These tests indicated that the following questions would need to be looked at more closely:

1. Does the proximity of the vernier influence the readings on the gauges?
2. Does the orientation of the tensile tester and sample affect the readings?
3. Does it matter how far down the clamping area the sample is clamped?
4. Does the type of adhesive affect the readings?
5. How do the adhesives perform physically?
6. When using SC2000 adhesive does the number of adhesive layers affect the readings?

4.2 Load cell calibration

2 Ton Load Cells

The load cells were calibrated with a tensile tester. Each of the eighteen two-ton load cells were calibrated individually. The tensile tester that was utilised in the calibration process was a MTS Criterion C45, see Appendices Section 8.3.2, Figure 8-21. This unit had an uncertainty value of 0.3 % of the reading value, as seen in Appendices Section 8.3.2, Figure 8-22. Therefore, on the 2000 kg output the uncertainty was within 7.2 kg.

The test arrangement included the flat plate onto which the shear beam load cells were bolted, a swivel foot mount so that the load could be applied uniformly and the two platens of the tensile tester, which provided the compressive force required. The tensile tester had a load capacity of 100 kN. A schematic arrangement is shown in Figure 4-15.

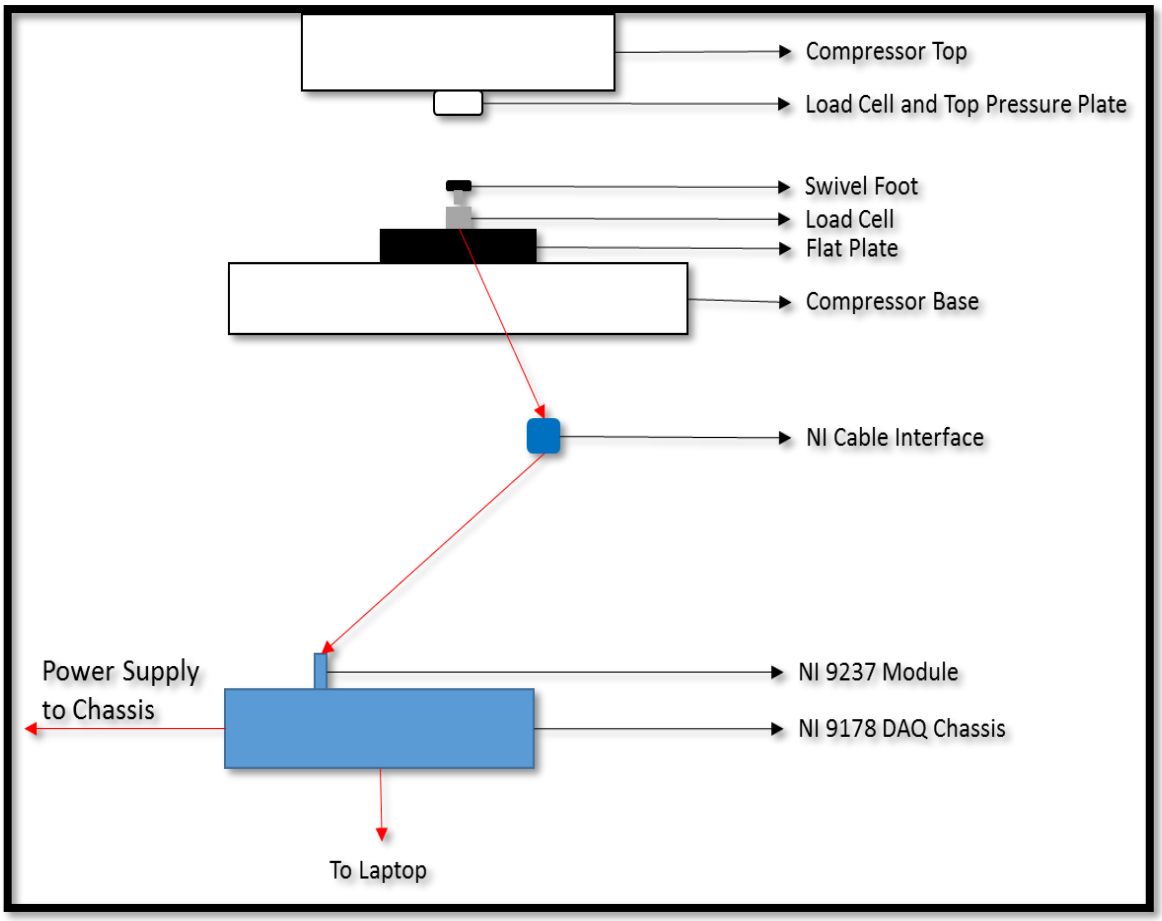


Figure 4-15: Schematic illustration of the 2 ton load cell calibration process.

The calibration process included obtaining values for loading and unloading cycles for each load cell. For each load cell seventeen measurements were taken, from 0 N up to 20 000 N in 2 500 N increments. All of this data was automatically stored using an NI 9237 Module connected to a NI 9178 DAQ Chassis. The physical setup is shown in Figure 4-16.

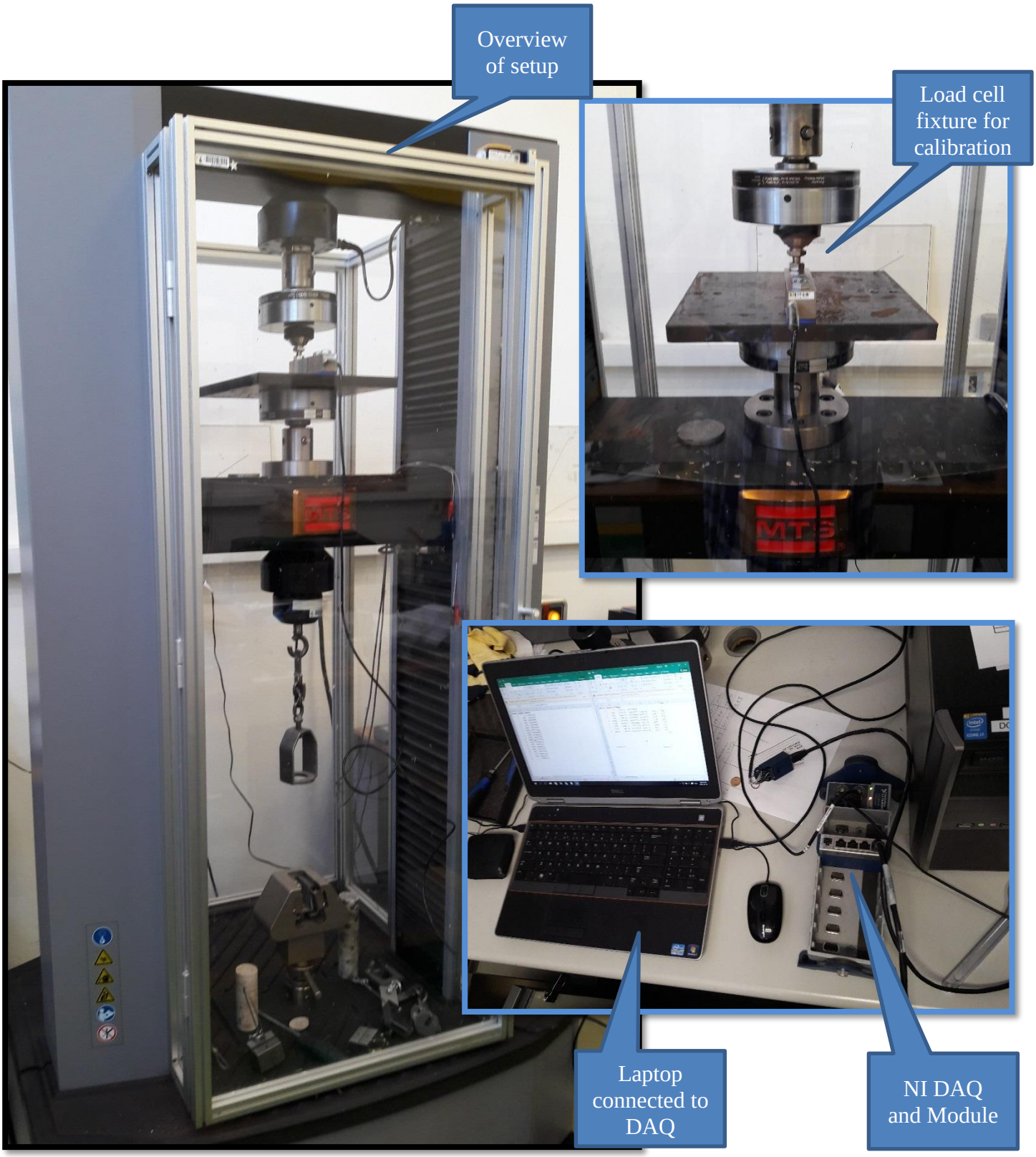


Figure 4-16: Illustration of the setup, used for the calibration of the load cells.

The results of each of the load cells were collected and combined into a single master sheet of data, the individual results for each of the 2 ton loadcells is available in Appendices Section 8.4, Table 8-10. The data was then analysed and graphed. From Figure 4-17 we can see the results of calibration process of the load cells. They have a very high degree of linearity in the loading and unloading cycles. Note, that the 18 graphs lie so close together that it appears to only be a single line.

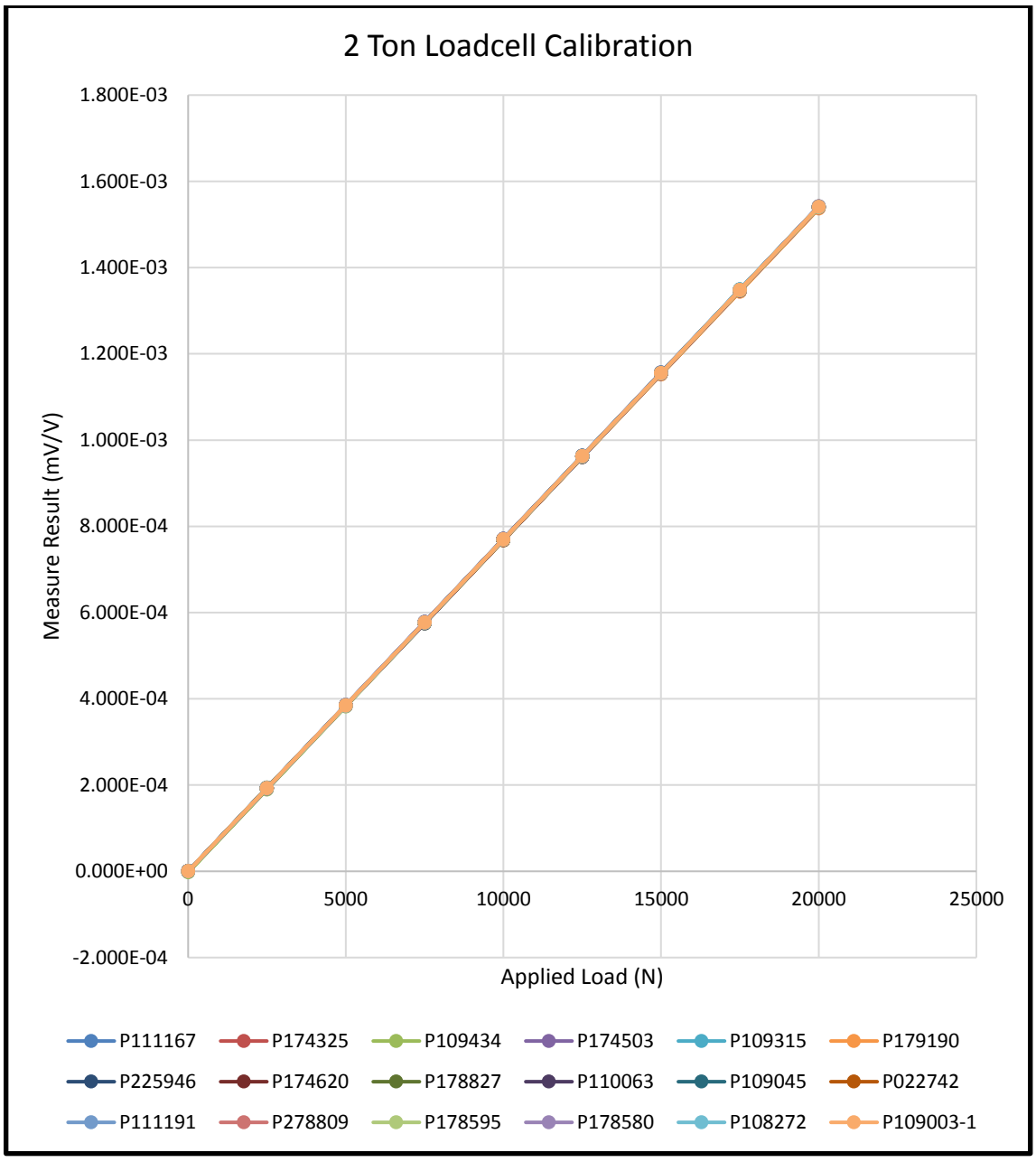


Figure 4-17: 2 Ton loadcell calibration results.

The maximum absolute uncertainty at each of the loads for which the load cells were calibrated are shown in Table 4-2.

Table 4-2: Uncertainty at each load tested for the load cell calibration.

Force (N)	Uncertainty (N)
0	-6.09
2500	43.70
5000	50.81
7500	51.55
10000	47.60
12500	43.71
15000	55.65
17500	65.99
20000	70.89

20 Ton Load Cell

The calibration procedure for the 20 ton tension link load cell was different from that of the 2 ton load cells. In Figure 4-19 the major pieces of equipment for the process are labelled. The testing unit had a resolution of 0.01 volts and a corresponding uncertainty of 26 kg. Figure 4-18 graphs the results of the calibration for the 20 ton loadcell; similar to the 2 ton loadcells a high degree of linearity is seen. The data for the calibration of the 20 Ton loadcell is seen in Appendices Section 8.4, Table 8-11.

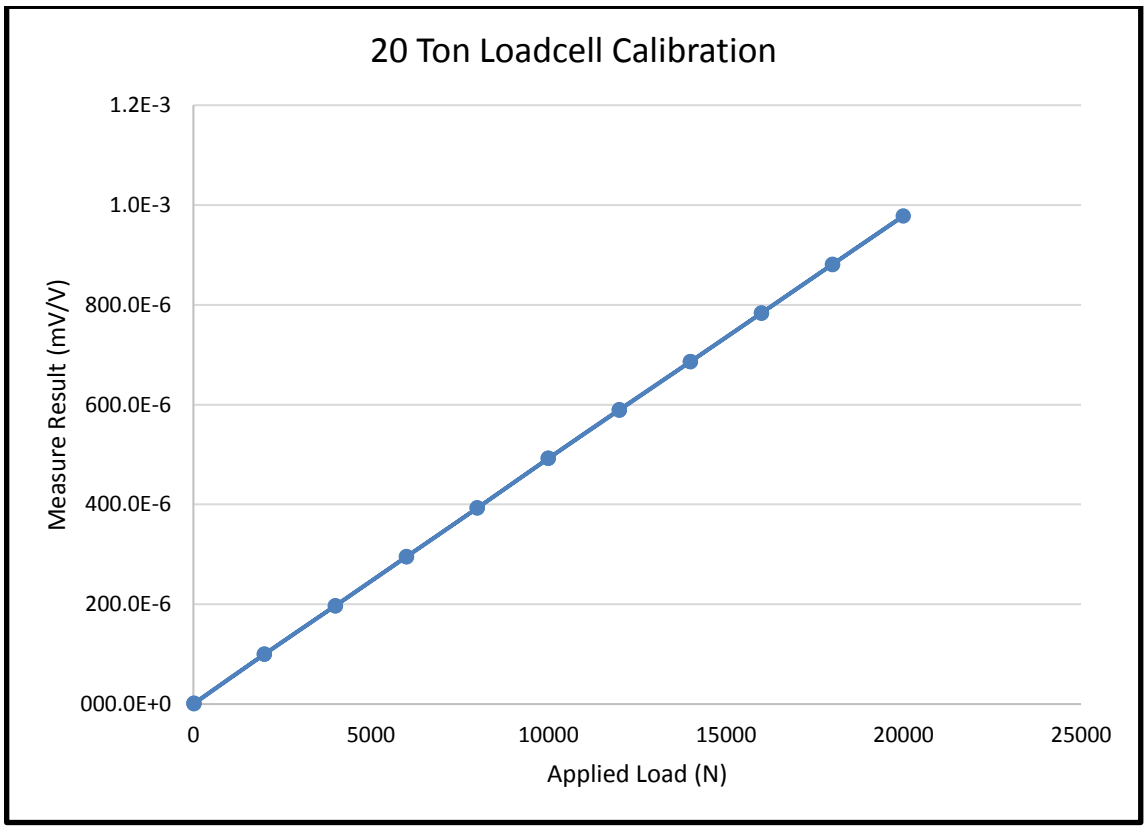


Figure 4-18: 20 Ton loadcell calibration results.

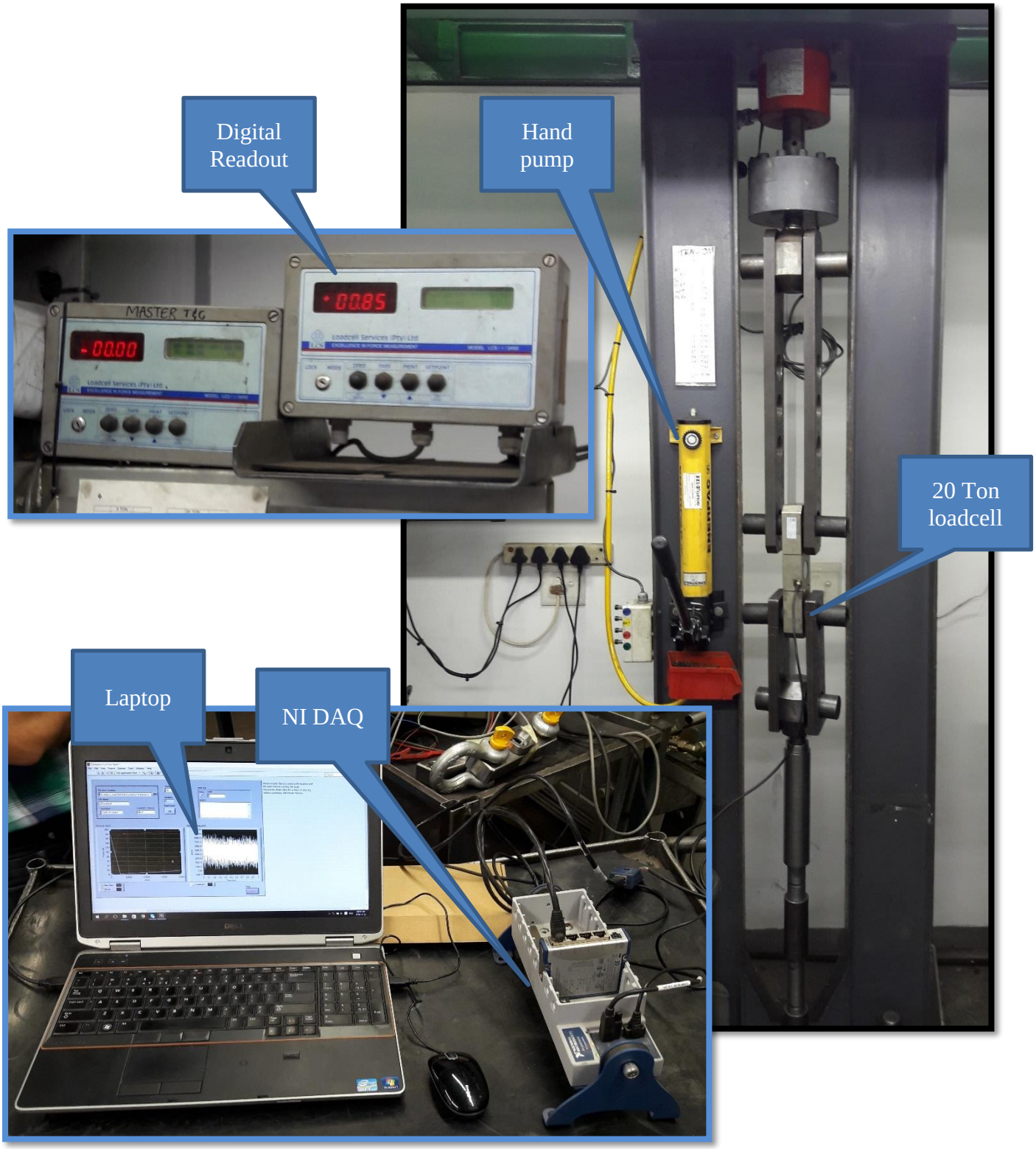


Figure 4-19: Overview of the setup for the calibration process for the 20 ton load cell.

4.3 Test Facility Commissioning

The commissioning of test facility had many challenges that needed to be overcome. Some of the major items are discussed here along with their solution and result.

There are several categories:

1. The structure
2. The belt profiler design
3. The belt profiler assembly accuracy

4.3.1 The Structure

The accurate and true alignment of the structure was of paramount importance. This was to ensure the high accuracy of the results. Misalignment in the idler frames could contribute to the stress that develops in the idler junction region as the belt would scuff and rotate the idler instead of having pure rotation as would be the case with a perfectly aligned idler. The process that was followed to align the structure was as follows and is depicted graphically in Figure 4-20:

1. The centre line was scribed on the floor and used as a datum reference for the alignment of all the structure.
2. From this the base structure was anchored into the ground which would support the idler frames.
3. The column supports were bolted into the pre-drilled holes of the base structure.
4. The idler frames needed to be square relative to the datum line and were aligned so that each idler frame's centre roll would have a minimal deviation from its corresponding neighbour. The alignment was a tedious process but one that needed to be methodically done to ensure that the accuracy of the results was not compromised.
5. The belt was placed over the idler frames. The overhead structure was also erected.

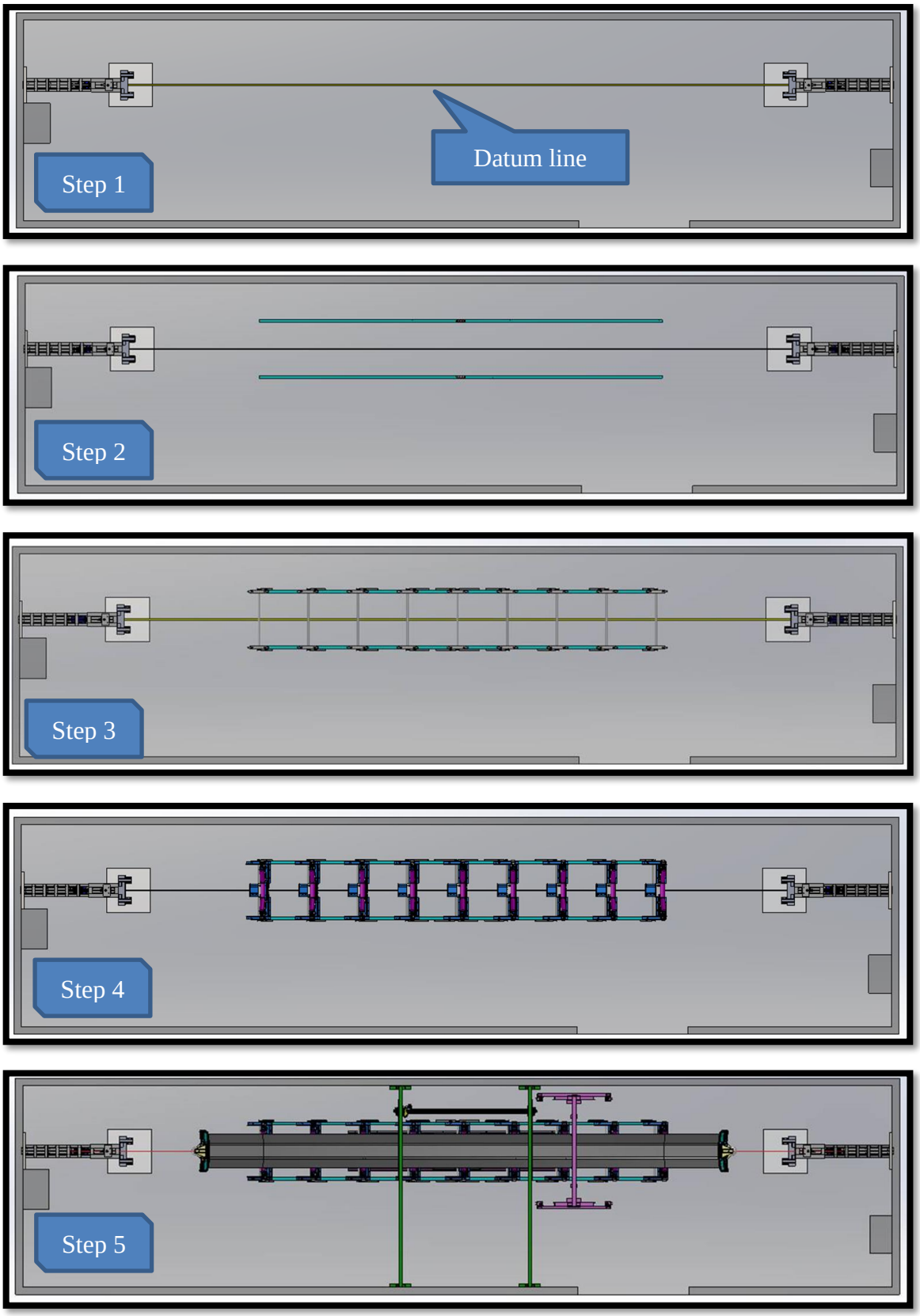


Figure 4-20: Overview steps of how the rig was aligned.

4.3.2 The Belt Profiler Design

An overview of the belt profiler design is shown in Figure 4-21. Some of the major or important pieces of equipment are labelled.

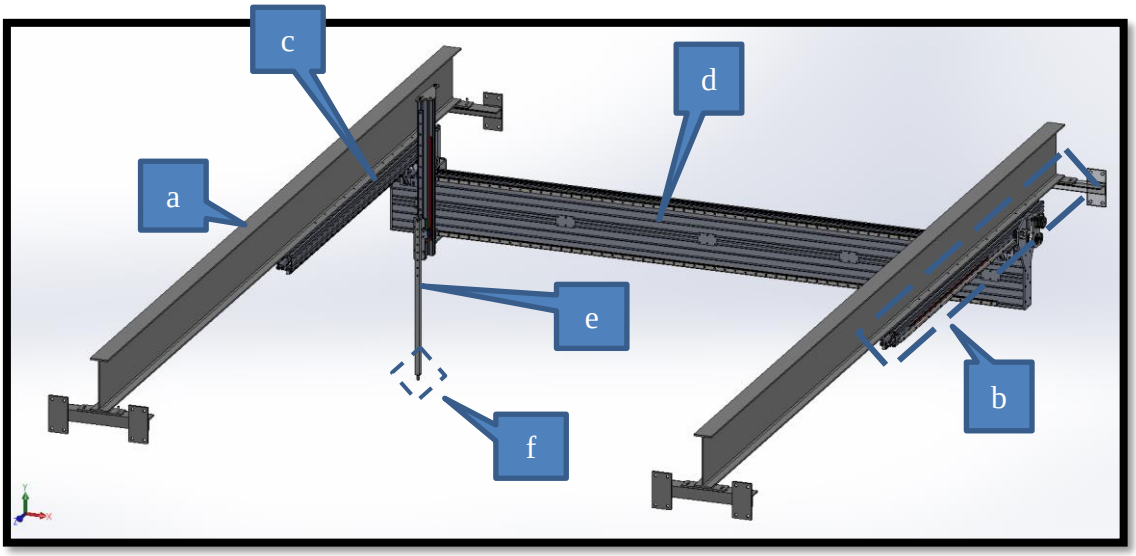


Figure 4-21: Overview of belt profiler design.

The design of the belt profiler overcome three major challenges: deflection, installation accuracy and the probe. The deflection was overcome by utilising deep sections that provided the high moments of area per unit length of mass. The steel I beams (a) are the main structure supports and are bolted through the supporting wall. They span the building to ensure that while items were being moved in and out of the building would not interfere with the structure. There were challenges with the I beams, in that they had a natural camber (see Figure 4-22) that was up to 10mm at certain points.

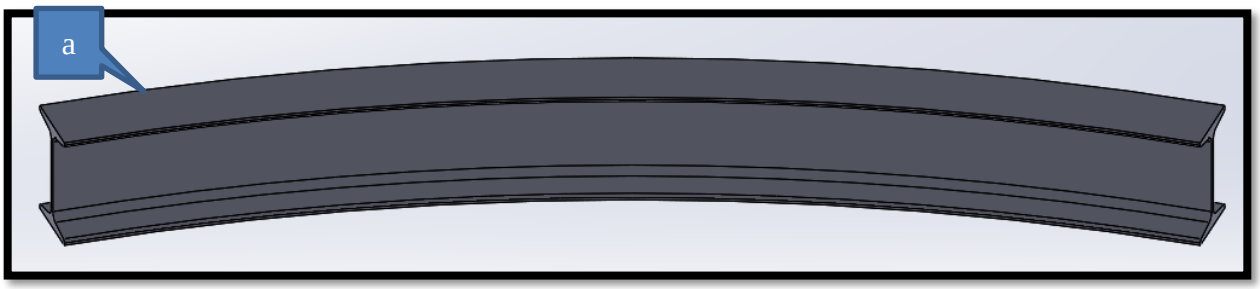


Figure 4-22: Illustration of an I beam with a natural camber (exaggerated) in the length of the unit.

In order to overcome this problem which would bend the 90x90 aluminium beams (c) the slotted rectangular tubes (b) (slotted on both the top and bottom) were incorporated into the design and compensate for the camber of the I beam, as shown in Figure 4-23.

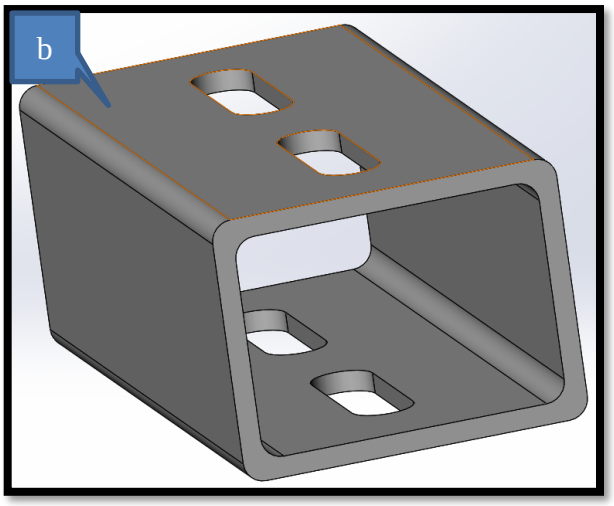


Figure 4-23: Slotted rectangular tubes.

There were 14 rectangular tubes per 90x90 aluminium beam, the relatively high number of rectangular tubes was so that at each point the aluminium beam could to lowered to ensure that it was perfectly straight, this is illustrated in the Figure 4-24. Thus, the natural deflection of the steel I beam and the inaccuracies associated with assembly were all accounted for by the inclusion of the independent adjustment of the aluminium cross beam by 56 bolts and 28 rectangular tubes. Connected to the 90x90 aluminium beams via a linear bearing system (a linear rail and two linear bearings, shown in Figure 4-24) is the very deep double 180x90 aluminium beam section (d). This was selected so that natural deflection due to its own weight was minimal.

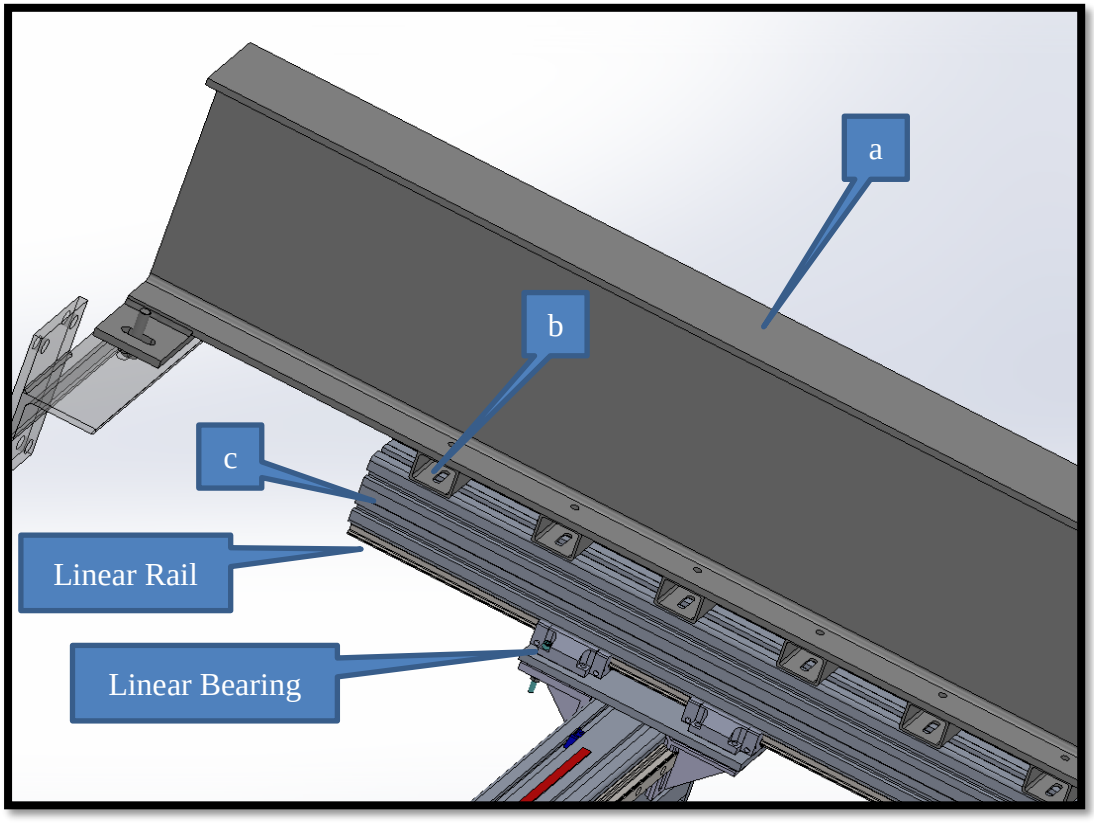


Figure 4-24: Illustration of the rectangular tubes connected to the I-Beams and per 90x90 aluminium beam.

The belt profiler stem (e) and the probe (f) ride along the double 180x90 aluminium beam section (d), by means of a stepper motor with a rack and pinion arrangement shown in Figure 4-25.

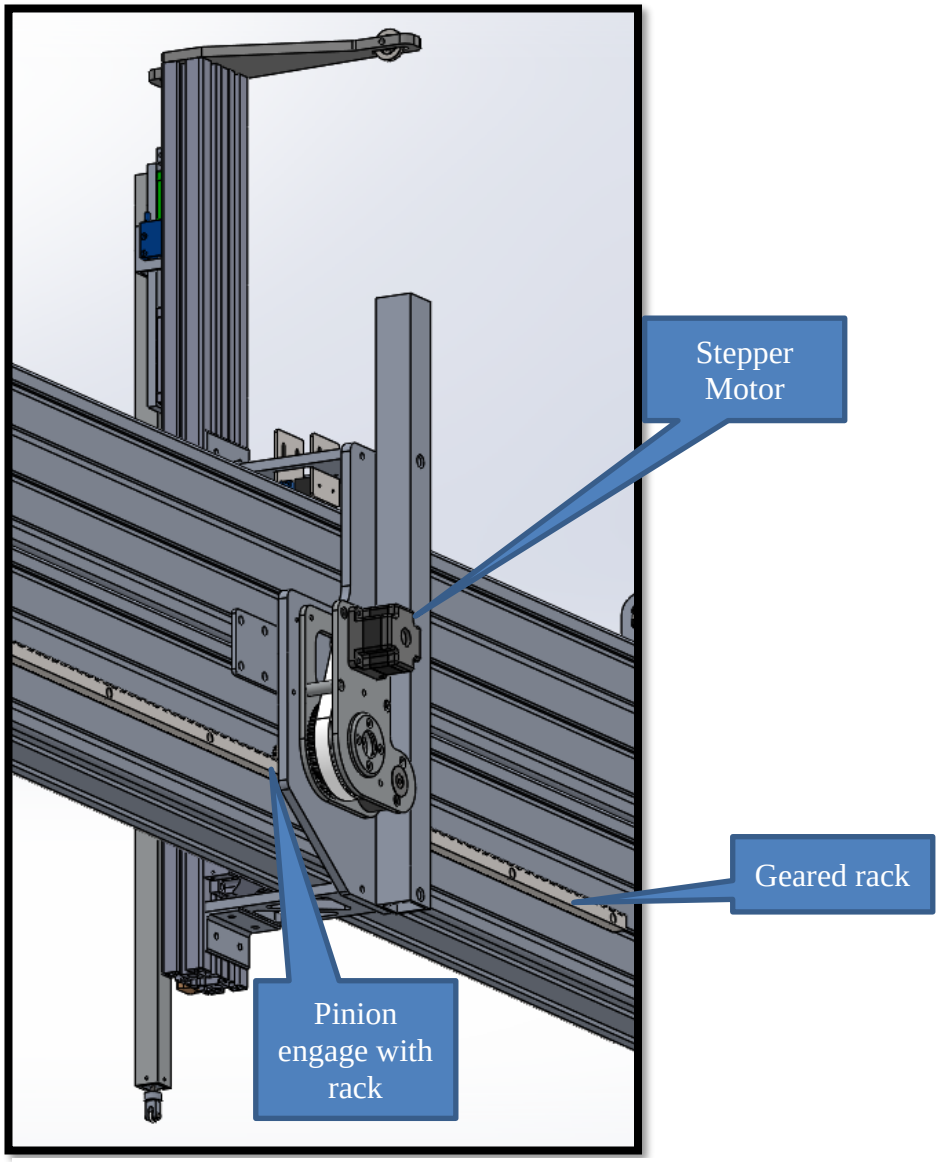


Figure 4-25: Workings of the stepper motor on the belt profiler.

The probe makes contact with the belt and needs to move at 90 degree angles and move down the warp direction of the belt, as shown in Figure 4-27. The design of the probe needs to accommodate this rapid direction change and avoid chatter on the belt as it moves. Figure 4-26 illustrates the simple design that was used in order to overcome these challenges, it is a steel ball bearing resting on a low friction plastic surface that allows for the sudden direction changes.

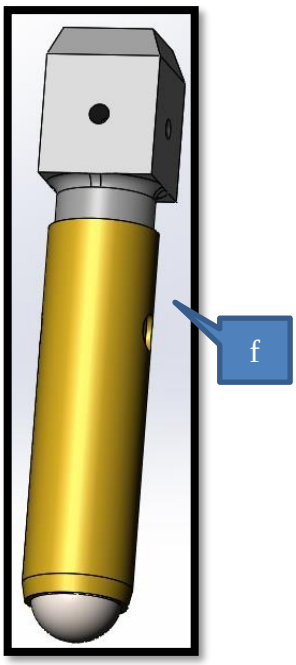


Figure 4-26: Illustration of the belt profiler probe

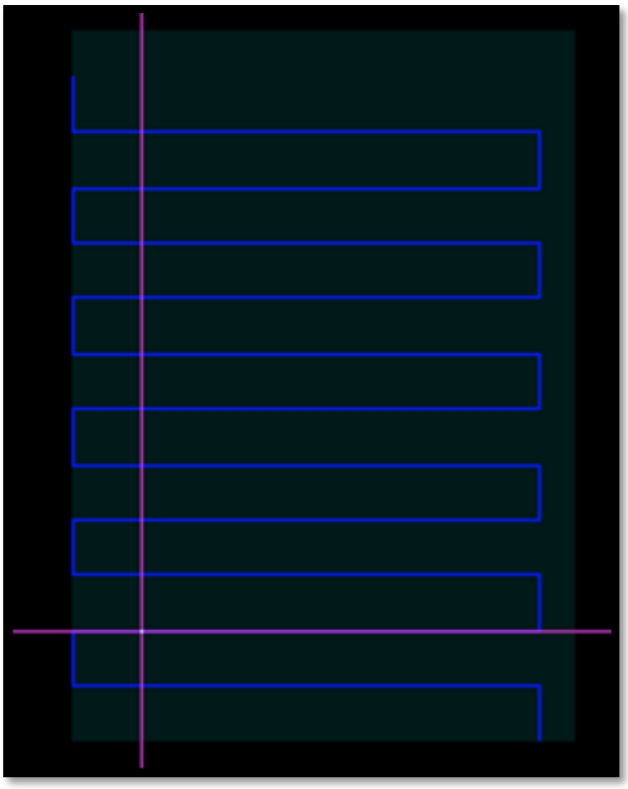


Figure 4-27: Path the probe will follow on each test piece of conveyor belt.

The belt profiler stem (e) transverses the width of the belt and needs to accommodate the shape change of the belt trough. The belt profiler stem moves vertically under gravity and has a counterweight to control the force applied onto the belt. This vertical motion is achieved by means of the cam roller bearing (green) moving along the aluminium rail (brown) shown in Figure 4-28.

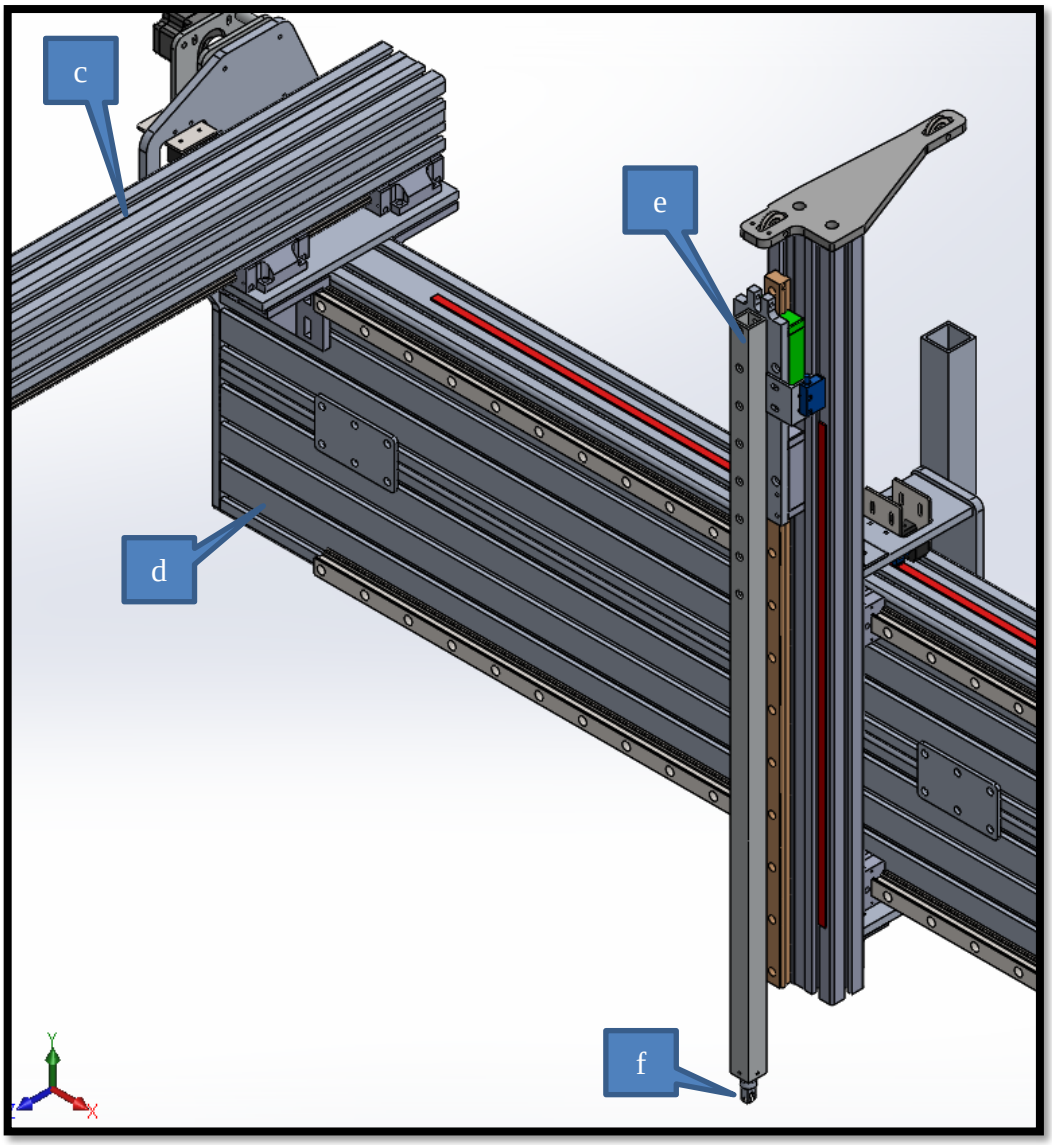


Figure 4-28: Movement of the belt profiler stem by means of the aluminium rail (brown) and cam roller bearing (green).

4.3.3 The Belt Profiler Assembly Accuracy

The belt profiler alignment was particularly challenging for several reasons. Firstly an accuracy of 0.3 mm over the entire system was set as the objective. This represented a considerable challenge as the measuring space was 3 m x 1.2 m x 0.6 m. Various calibration methods were tried and are discussed below.

CMM

Using an accurate CMM (Co-ordinate Measuring Machine) Faro Gage (see Appendices Section 8.3.2, Figure 8-23) and levelling the unit relative to the horizontal. The CMM's reach was a limitation and the uncertainty of measurement was in excess of the objective.

Laser level

The first attempt at levelling the probe movement plane was done by using a laser to determine a position on the square tube of the belt profiler stem, see Figure 4-29, the laser was mounted independently of the structure. A position on the corner of the belt profiler was taken as the datum position Point A1 as shown in Figure 4-30, and the rest of the belt profiler was adjusted until the same position was indicated by the laser on the square tube (for A2 - A14 and B1 - B14).

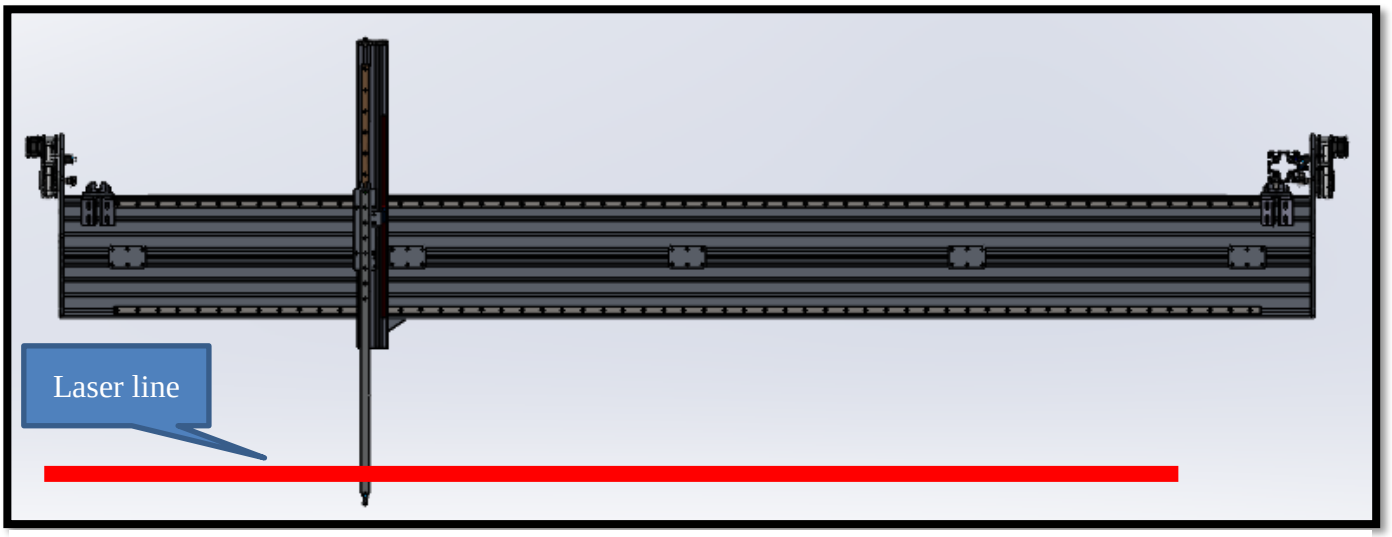


Figure 4-29: Laser line on belt profiler stem.

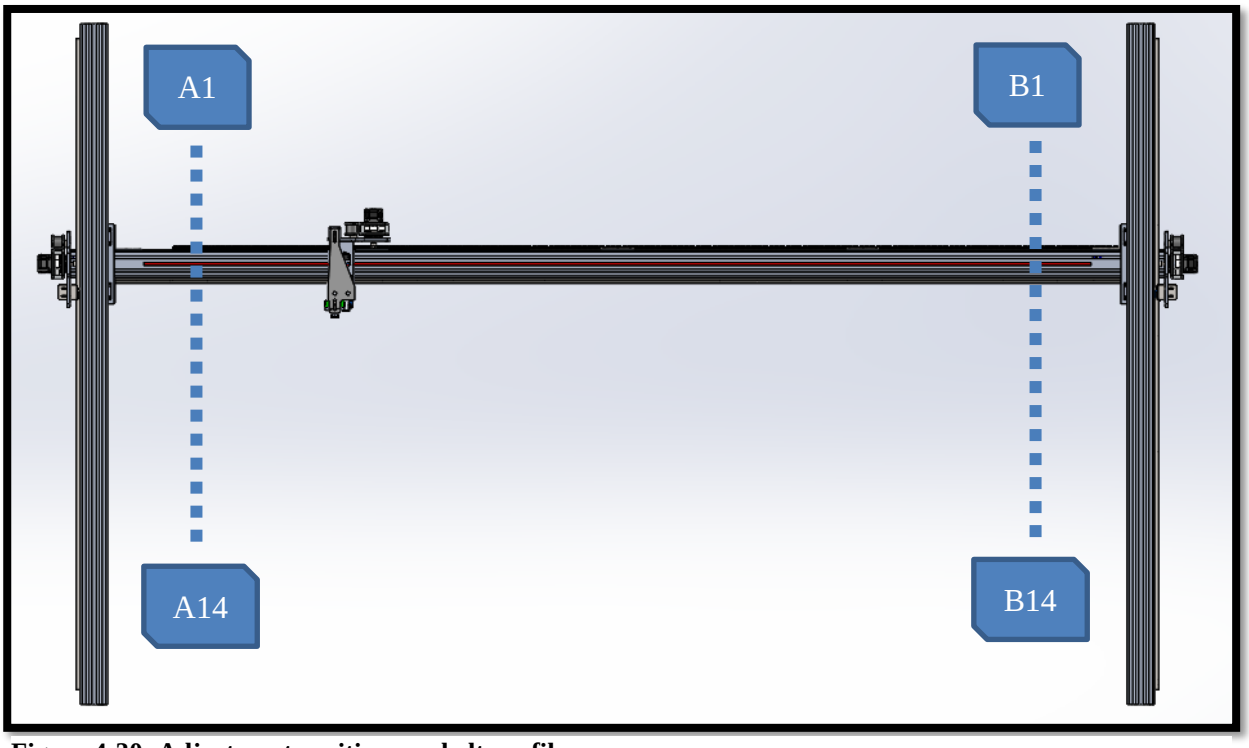


Figure 4-30: Adjustment positions on belt profiler.

This method was inadequate because of the divergence of the horizontal laser beam, as shown in the schematic in Figure 4-31, this meant that the laser had to be placed as close as possible to the profiler probe tube in order to acquire a reading of the required accuracy. This meant that the horizontal range (D) of the laser was then limited.

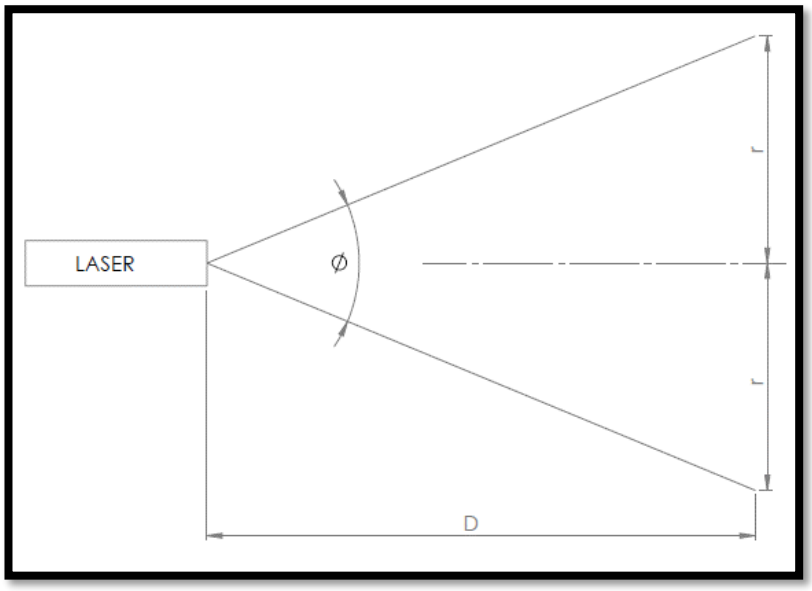


Figure 4-31: A schematic of laser divergence; the laser spreads by an angle of ϕ so over a distance D, the laser spreads to a width of 2r.

In order to circumvent the issue of laser divergence, photographs were taken of each reading. A ruler was attached to the square tube of the belt profiler stem so that a scale could be applied to the readings as shown in Figure 4-32.

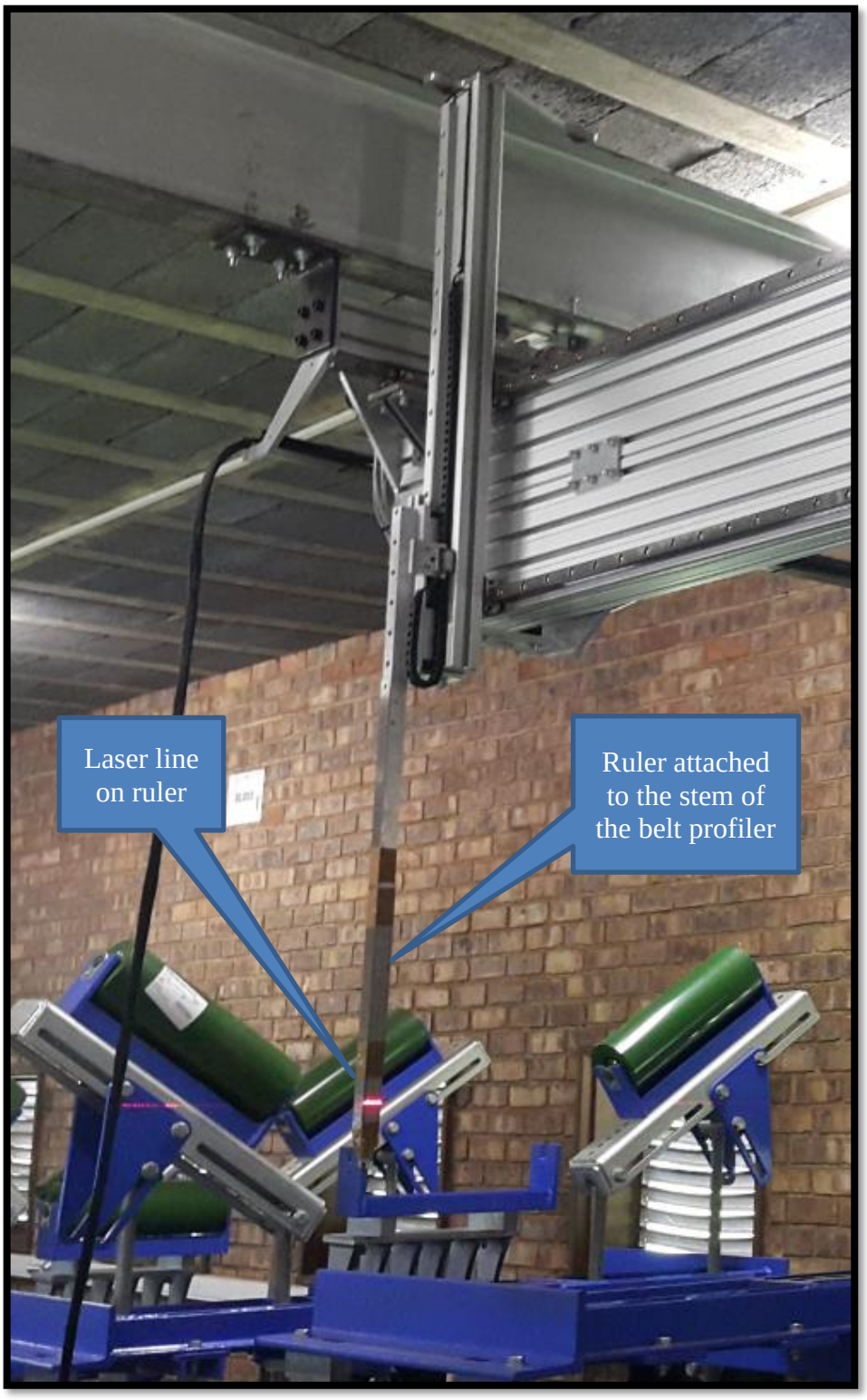
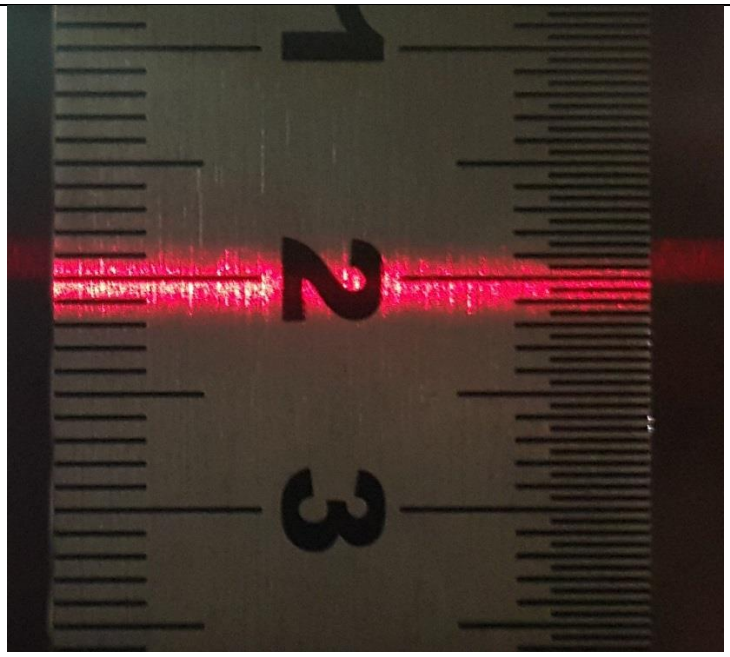
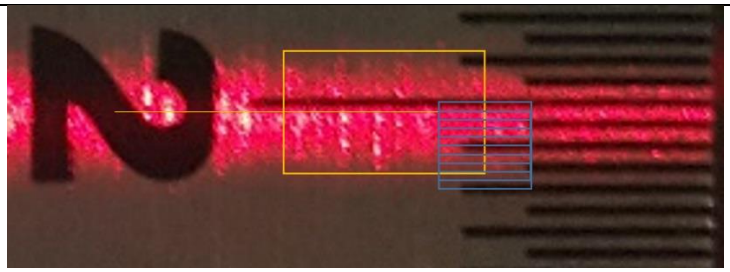
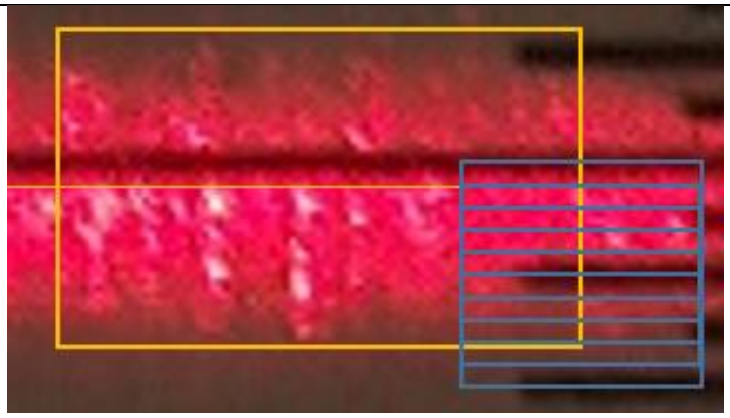


Figure 4-32: Ruler attached to the stem of the belt profiler.

After that, the photograph was enlarged and the units on the ruler were digitally divided in order to provide a more accurate reading; the laser was enclosed so that the middle of the laser beam could be determined. The process is shown in Table 4-3.

Table 4-3: Process of obtaining readings photographically with the laser method.

Step 1: A photograph of the reading was taken and enlarged.	
Step 2: Enclose the laser (yellow rectangle) and then determine the centre of that rectangle, perpendicular to the ruler measuring lines. Then subdivide units on the ruler, (blue rectangle).	
Step 3: Find the reading, each blue line represents 0.2mm. This reading is 2.2mm	

Besides the concern of laser divergence, there was also an issue with the laser level not being level. Two laser levels were placed on the same line and divergence between the two beams was noticeable. More thought had to be given to a levelling method that could deliver the accuracy required. This lead to the inception of the water method as follows.

Water Trough: Coloured Water

The next attempt was to use coloured water to indicate the profiler probe tube on the rule; this would give a clearer indication on where the centre of the reading was, as shown in Figure 4-33.

The water, simply due to gravity, would always be level and a photograph taken from the correct angle would produce a reflection on the water, making it easy to find the reading with the symmetry between the reading and the reflection on the water as shown in Figure 4-34.



Figure 4-33: The coloured water shows exactly where the line on the ruler was.

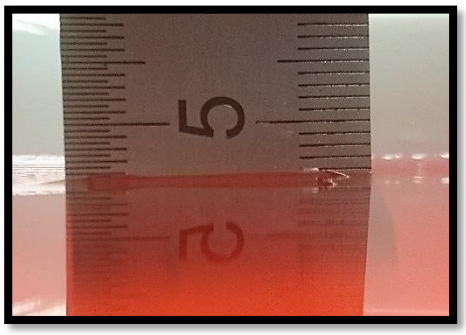


Figure 4-34: A photograph taken from the correct angle provides symmetry, making it easy to find the centre of the reading.

The photographs in Figure 4-33 and Figure 4-34 were taken as an experiment to determine whether the method would be useful in achieving the goal of levelling the profiler probe movement plane. The location where the photographs were taken was well illuminated. In the testing facility the illumination was insufficient and this method could not be employed successfully.

Water Trough: Clear Water and a Lighting Source (Torch)

After the unsuccessful implementation of the first water plan, another method was proposed; a flashlight would be used to illuminate the part of the ruler showing on top of the water. Figure 4-35 illustrates the overview of the water trough setup.



Figure 4-35: Overview of the water trough levelling method

The trough was filled with water and a flashlight was placed inside; shown in Figure 4-36. Photographs of each reading were taken and enlarged. The same method described in the laser levelling method was used to determine the exact position of the illuminated beam on top of the water.

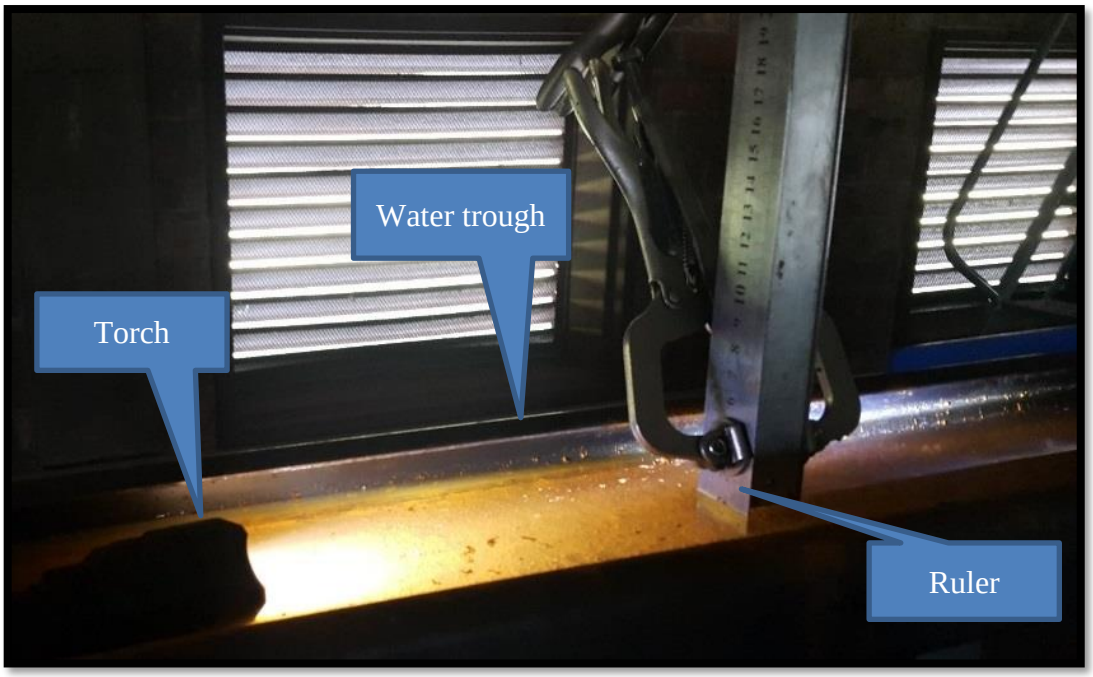
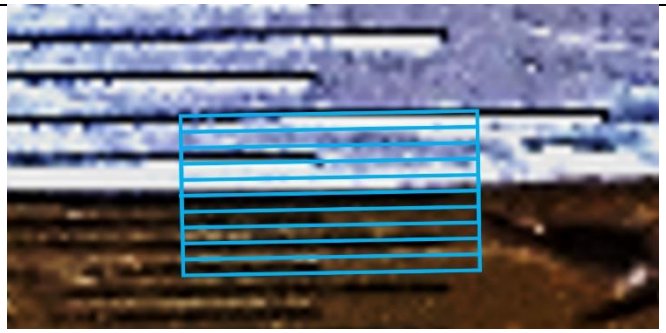
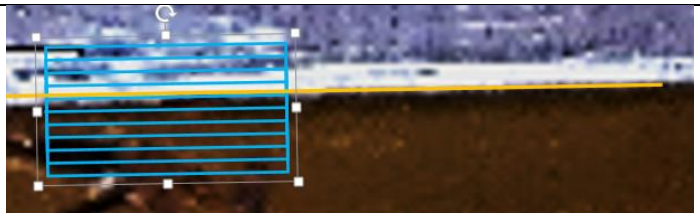


Figure 4-36: The setup of the final water aided probe movement plane calibration.

One challenge with this method was that the water line seemed to bow on the surface of the ruler. In order to ensure consistent results, the ruler was wiped clean and re-submerged into the trough. This ensured a consistent bow and readings were taken from the middle of the ruler as shown in step 3 in the method described in Table 4-4. A similar process as with the laser method was followed in order to get more accurate readings.

Table 4-4: Process of obtaining readings photographically with the water method.

Step 1: Take a photograph of the reading and enlarge the photograph	
Step 2: Subdivide units.	
Step 3: Determine the reading, each blue line represents 0.2mm. This reading is 14.2mm	

The movement plane was calibrated in the following order, see Figure 4-37 for reference:

1. From point 1 to point 3.
2. From point 3 to point 6.
3. From point 6 to point 4.

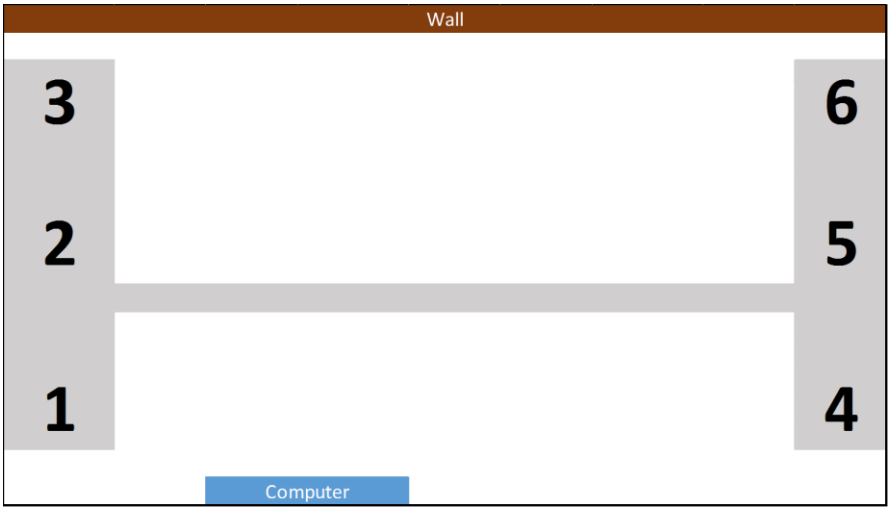


Figure 4-37: Schematic of the profiler probe movement plane.

The picture of each reading was studied after the reading was taken and that position was adjusted using the bolt connection from the I beam to the aluminium extrusion. The results from the calibration are shown in Table 4-5 and Table 4-6.

Table 4-5: Results from the profiler probe movement plane calibration, along the 90x90 aluminium beam.

From 1 to 3			From 6 to 4	
Position	**Value (mm)**		**Position**	**Value (mm)**
1	175.00		1	2.40
2	175.00		2	2.50
3	175.00		3	2.50
4	175.00		4	2.30
Variance	0.00		Variance	0.01
Max-Min	0.00		Max-Min	0.20

Table 4-6: Results from the profiler probe movement plane calibration, across the 90x90 aluminium beam.

From 1 to 4			From 5 to 2			From 3 to 6	
Position	**Value (mm)**		**Position**	**Value (mm)**		**Position**	**Value (mm)**
1	194.20		1	134.25		1	124.25
2	194.20		2	134.00		2	124.00
3	194.40		3	134.25		3	124.00
4	194.40		4	134.00		4	124.20
Variance	0.01		Variance	0.02		Variance	0.02
Max-Min	0.20		Max-Min	0.25		Max-Min	0.25

From Table 4-5 and Table 4-6 the difference for the maximum and minimum results yields that the objective of achieving an accuracy within 0.3 mm was achieved.

4.4 Overall Testing of the Facility

During this phase of the commissioning process all the aspects of the test facility came together and the performance of all the individual pieces of equipment could be checked. Verification for some of the major pieces of equipment during live testing was as follows:

1. Once the belt was placed on the test facility it was connected to the belt attachment and loaded to belt reference load value to ensure that the joint was secure and fit for purpose. It was then discovered that the hydraulics cylinders were only pulling about 5 tons of load, which is inadequate for the system. It was expected that the maximum output of the hydraulic cylinders would be in the region of 32 tons. The hydraulic system needs to re-examined in order to reach the desired capacity. Pressure gauges need to be installed so that the pulling force can be determined. It may be that the power pack is undersized and that a new motor and pump is all that is required to reach the desired output.

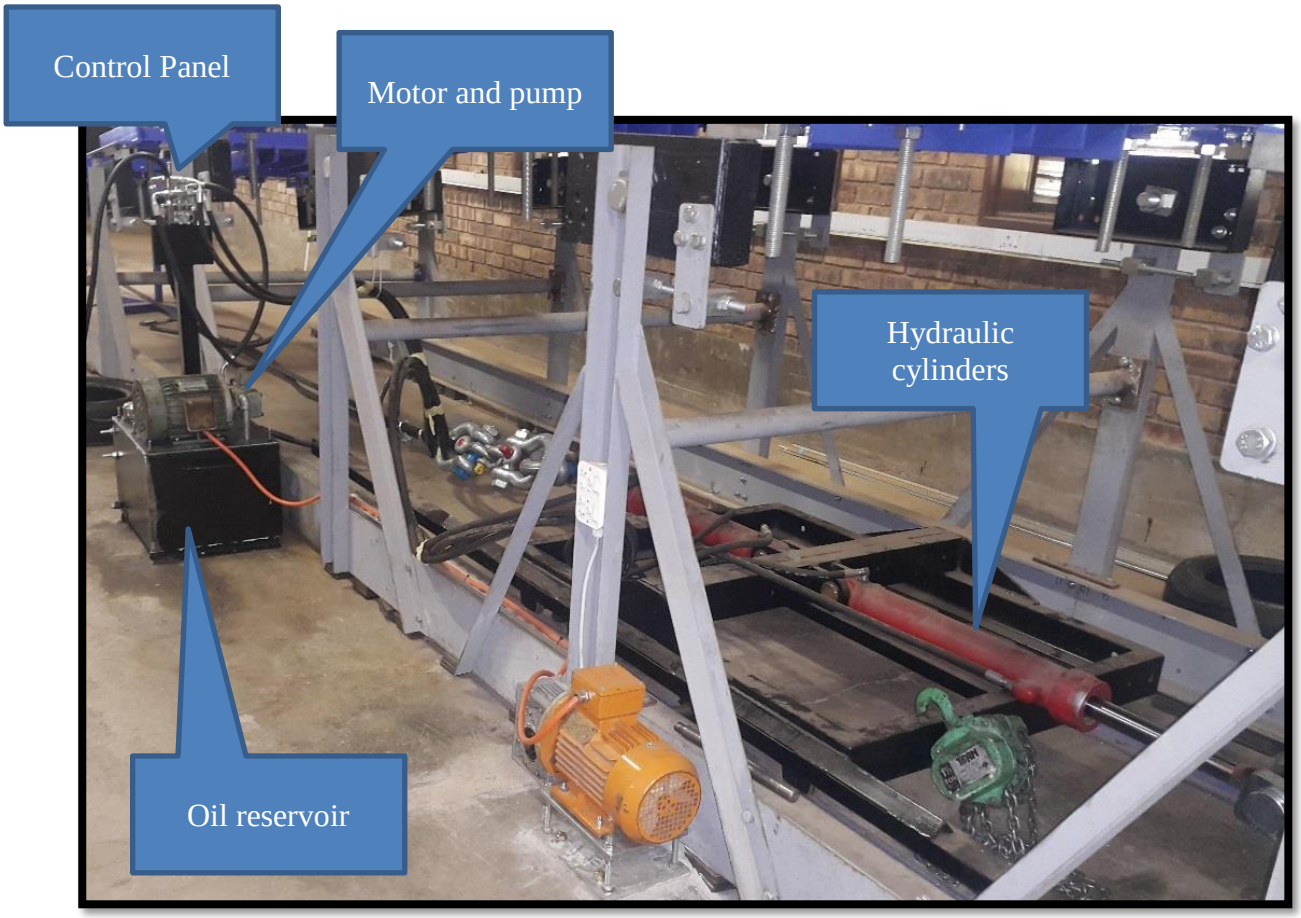


Figure 4-38: Image of the hydraulic cylinders in operation.

2. The gantry lifter was used to lift the belt under load, this load was limited to the 5 ton capacity that the hydraulic cylinders were capable of pulling. Figure 4-39 illustrates the functioning of the gantry lifter. The 20 ton jacks on either side engage and lift the beam which then pulls the belt up; this is to ensure that the universal idlers could be adjusted as necessary and this would be performed safely.

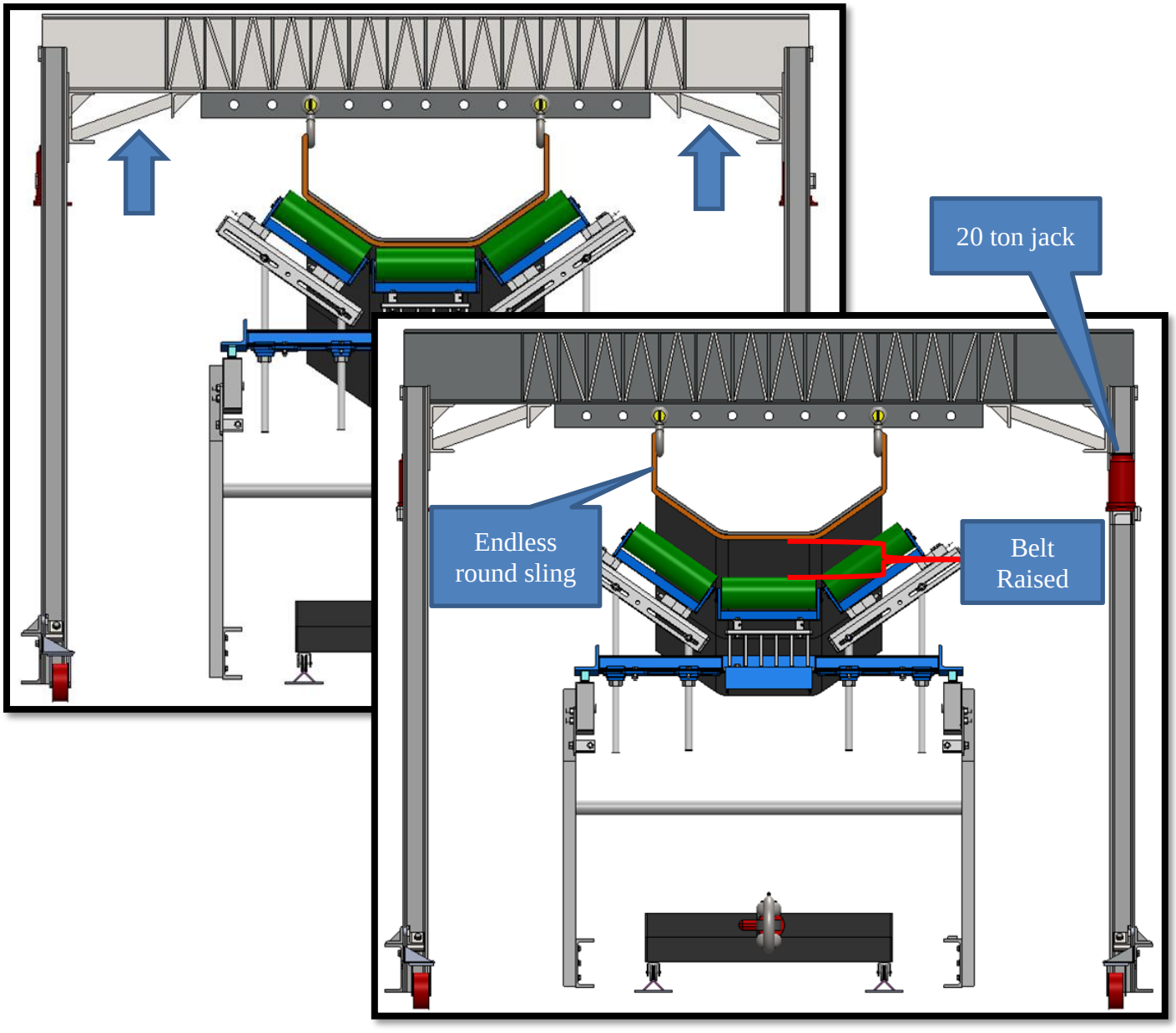


Figure 4-39: Belt gantry lifter depicting the how the belt will be raised off the idlers.

3. The sheaves were adjusted to ensure that the force was pulling through the centroid of the belt trough, shown in Figure 4-40. Figure 4-41 and Figure 4-42 show how adjusting the guiding sheave interacts with the steel wire rope such that it directs it to the desired angle around the main load bearing sheave. This was an important step to ensure that the bending of the belt (at the region just behind where the mechanical joint is inserted into the belt) is kept to minimum.

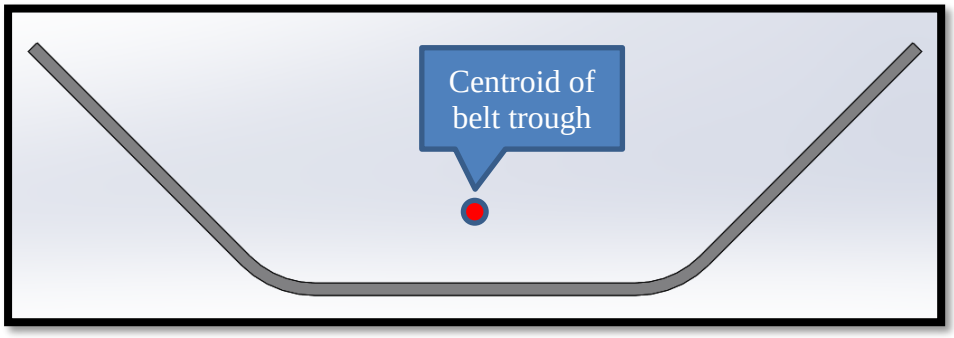


Figure 4-40: Illustration of the belt trough centroid.

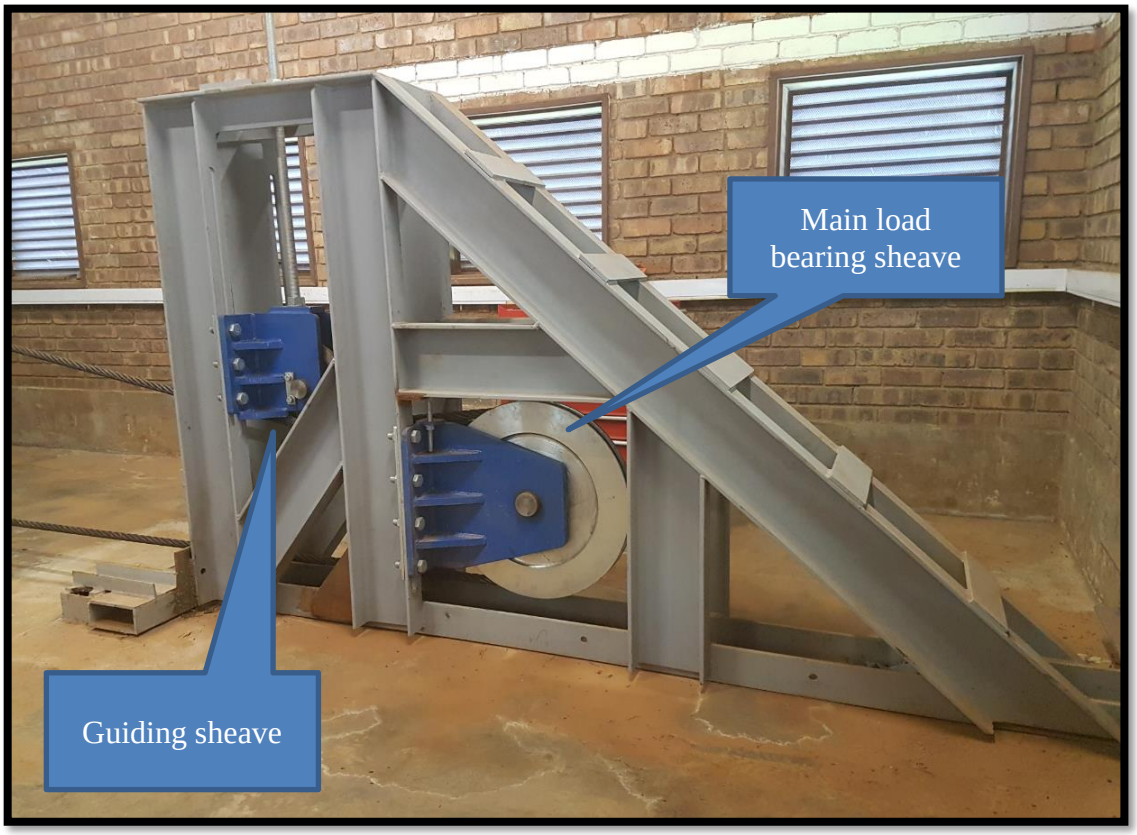


Figure 4-41: Sheave structure will the main sheave and guiding sheave in place.



Figure 4-42: Guiding sheave directing the steel wire rope.

4. The data acquisition system was tested to ensure all the instrument outputs could be read and that the data could be easily manipulated. Figure 4-43 depicts the dashboard setup where live readings will be acquired. A close up of the NI cDAQ 9178 illustrating the modules that are used to acquire load cell readings and strain gauge readings is shown in Figure 4-44. The connection of the instruments to the data acquisition system and the laptop which was used to capture and store the data is shown in Figure 4-45.

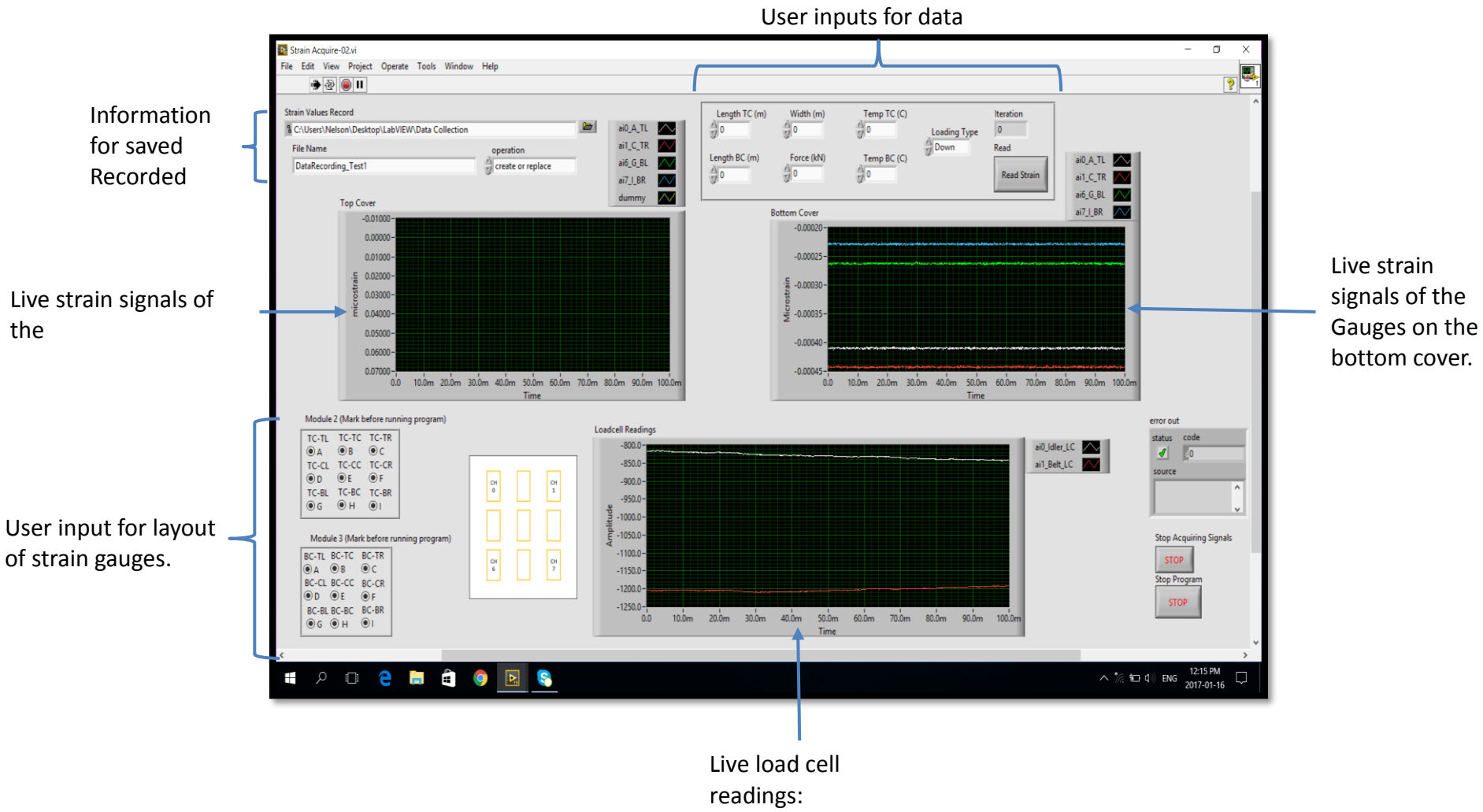


Figure 4-43: Dashboard for Labview data acquisition for the strain gauges.



Figure 4-44: National Instruments hardware

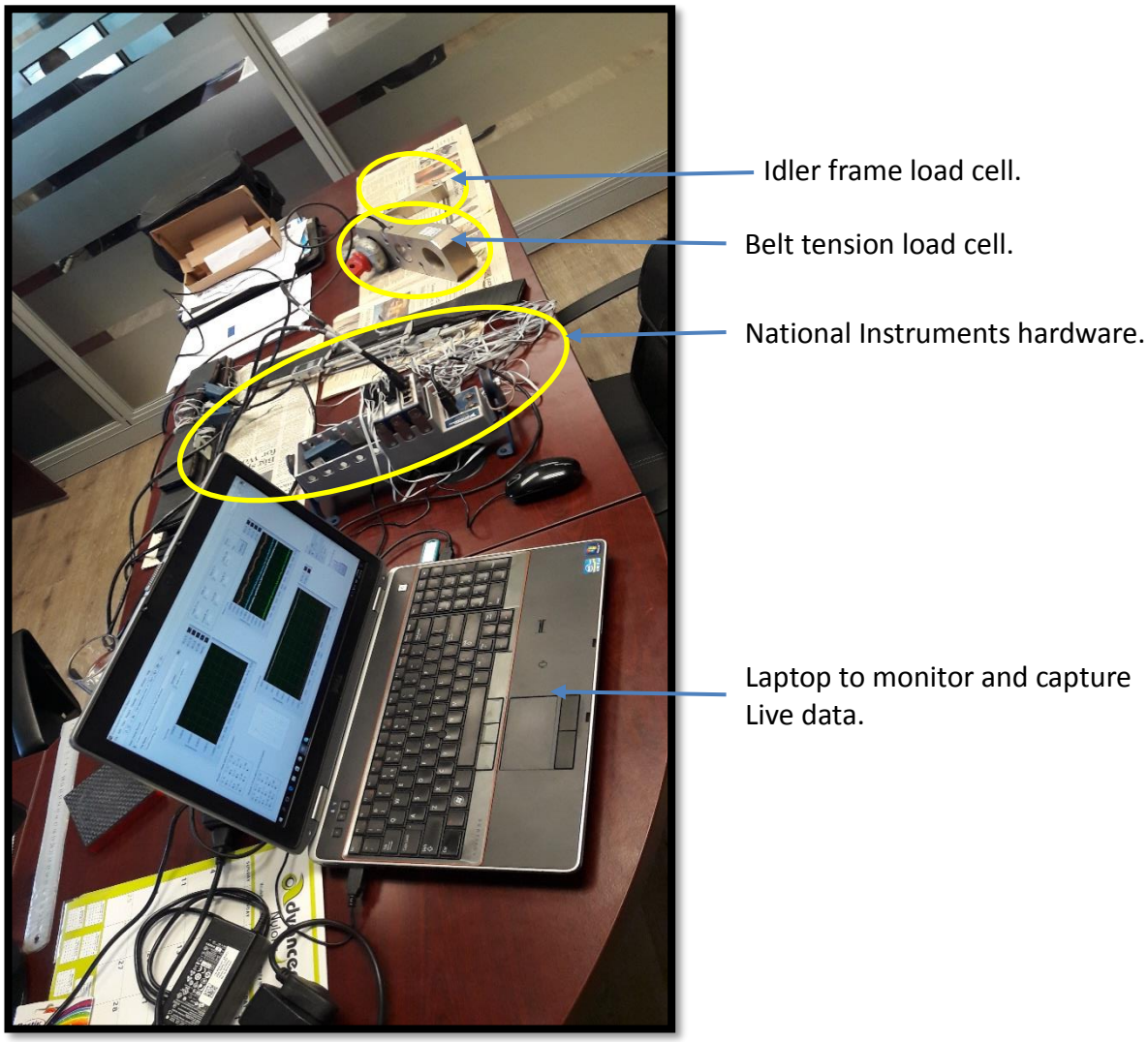


Figure 4-45: Labview and NI sample set-up to acquire data

5. The VFD (variable frequency drive) motor was inadequate in that the friction that needed to be overcome in bending the cables and the slack in the belt was more than the power the motor could deliver. It was envisaged that the 1.5 kW motor would be sufficient to move the cable and belt around the test facility but this was underestimated, see Figure 4-46 and Figure 4-47.

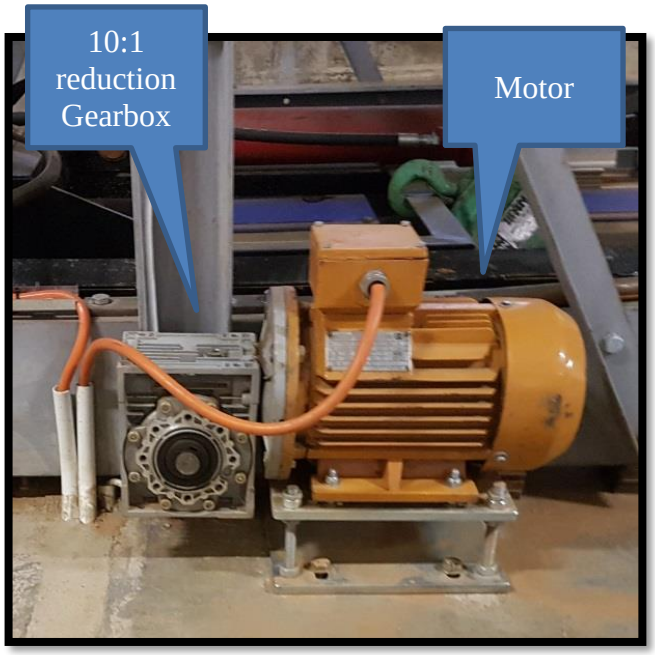


Figure 4-46: Motor used on the test facility.



Figure 4-47: VFD used on the test facility.

A temporary solution to overcome the additional tension was to use a tirfor attached to one side of the stationary frame, which can then be used to pull the belt and cable around the structure, see Figure 4-48. A permanent solution would be to have the belt and steel cables moved at a constant speed, this would eliminate the step change force that would be transmitted with every pull of the lever. A larger motor or higher reduction gearbox was not seen as a viable solution as the torque transmitted would be too large for the geared rack.

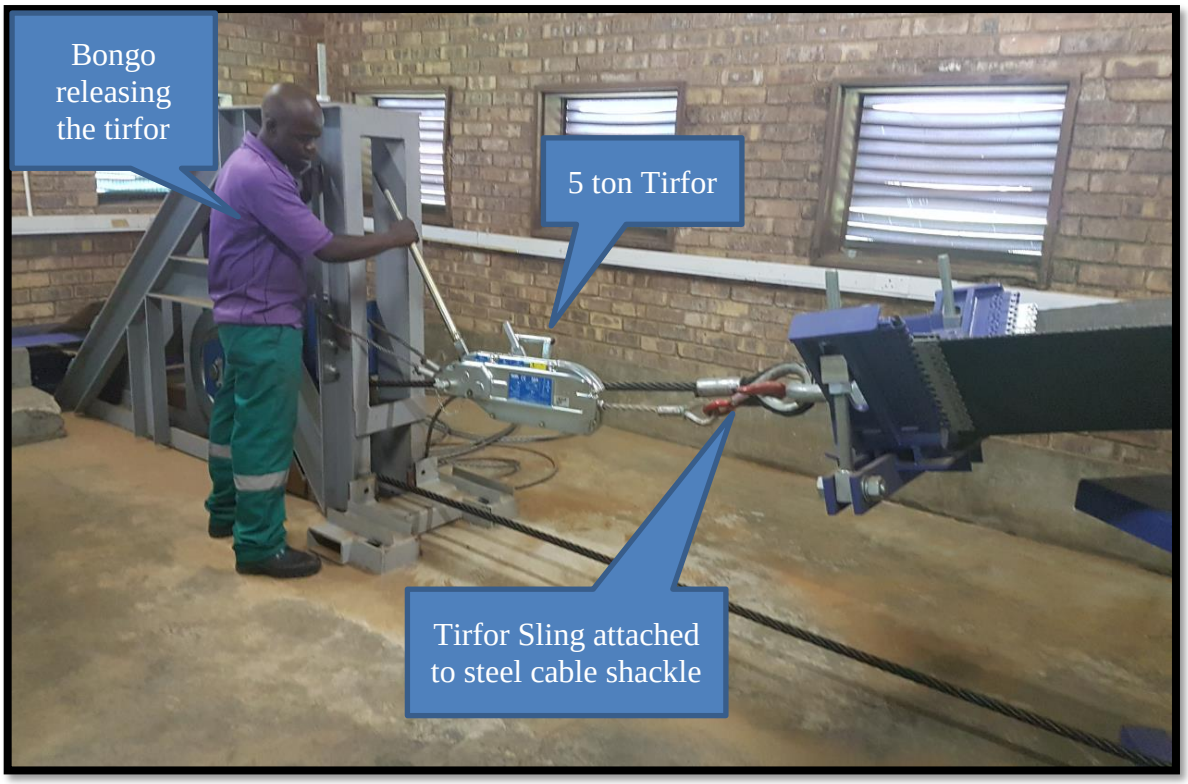


Figure 4-48: Tirfor used to move the cable and belt around the structure.

4.5 Safety Measures Designed into the Test Facility

Safety was a prime consideration in the design of the test facility equipment. There is a range of safety measures that have been designed into the test facility and on all critical items calculations and FEA analysis was conducted, see Appendices Section 8.1.2, 8.1.3 and 8.1.4 for details. Some of the most important design aspects were:

1. The selection of the steel wire cable over chain. The steel cable will give warning signs before failure while chain will fail suddenly.
2. The sheave frames are well secured into the ground and into the building. There are many mounting points in order to distribute the load.
3. The belt gantry lifter when loaded has a large support base to distribute the load into the ground and the hydraulics are secured by pins so that in case the hydraulic units fail the pins will restrain the entire unit. The belt gantry lift has a progressive lifting requirement so that even if the hydraulics fail, the unit will drop by up to 150 mm which is the maximum stroke of the jack. The hydraulic jacks are also secured in place within the system so that they cannot topple over. There is a mating hole in the top plate the aligns the jack and restraining plate through the sides that keep the jack steady.
4. The belt anchor is connected to the belt via mechanical joints and the belt will comb out of the mechanical joint in a progressive fashion. There will be no sudden catastrophic failure that would harm anyone.

4.6 Obstacles that were Overcome during the Commissioning Process

There were many challenges to the completion of this project and many of the most time consuming were of a non-technical nature. The largest challenge was to ensure that all the necessary resources were available that were required to properly complete this project. Many industry organisations were approached for assistance in terms of the products that they supply or for the financial assistance to be used for the erection of the test facility. This was a gruelling task that required much persistence to convince organisations of the value this project would bring. In the end sufficient resources were acquired for the successful completion of the project. Some of the most prominent technical challenges encountered were the following.

4.6.1 Sample Preparation

In order to ensure that the samples yield the most consistent results the samples were cut with a new geometry which had parallel sides instead of a curved sides and in an unconventional manner which was to have them waterjet cut. This gave them a much higher dimensional consistency.

4.6.2 Strain Gauge Constraints

There were several concerns that affected the strain gauges, these included, temperature effects which were negated with a full bridge configuration and with a dummy strain gauge arrangement on a quarter bridge configuration. There is permanent and elastic stretch in a belt. In order to overcome this problem, the permanent stretch of the belt has to be removed. This was done as per standard ISO 9856.

After cycling the belt 300 times it was seen that the permanent stretch was partially removed. This helped to mitigate this issue. It is recommended that the belt be cycled from 10% to 40% for 300 cycles to determine if this would remove most of the permanent stretch. There is a limit at which the strain gauges will be stretched beyond their elastic limit. The elongation should be contained within this limit.

The strain gauges have fatigue limit of 1000 micro strain for 10^7 cycles. However, it is not clear what the new fatigue limit would be as the strain exceeds 1000 micro strain. The way in which the strain limit will be circumvented is to only apply the gauges once the load has been applied to the belt and to remove the permanent stretch in the belt prior to testing.

At the start of a full scale test the strain gauges will have zero strain. The strain variation, across the belt, as the belt makes contact with the idler and moves passed the idler, will be measured. Figure 4-49 is repeated here for clarity. At the start of the test the belt will be roughly half way between the idlers with all the strain gauges readings set to zero; as the gauges move towards the idler the location of the higher stress locations can be determined.

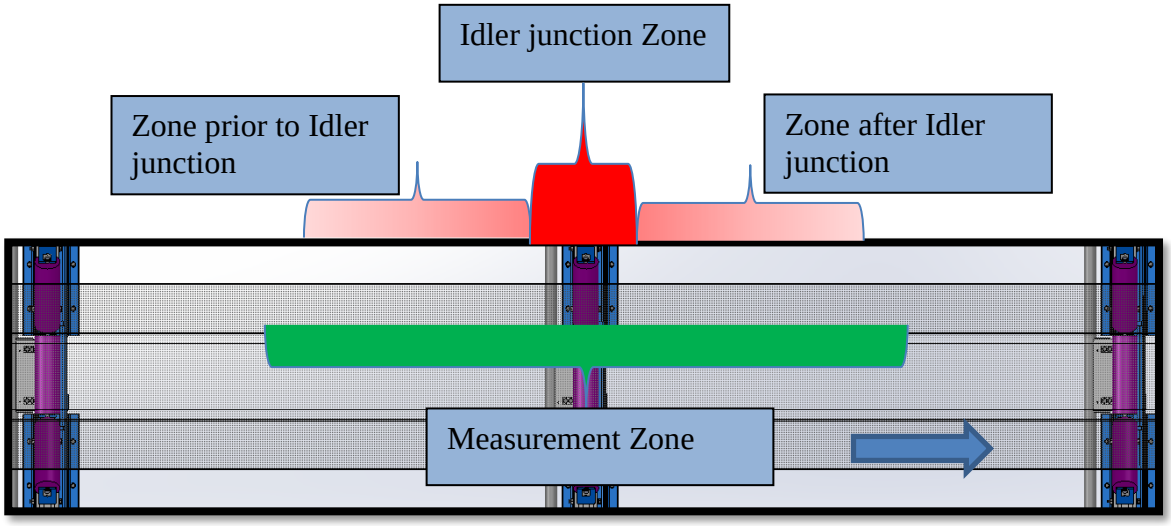


Figure 4-49: Illustration of important zones in the test setup, top view.

4.6.3 Lifting the belt under Tension

This is a direct consequence of the strain gauges being applied to the belt after the belt is tensioned. Again, this needs to be done for the reasons described in Section 4.6.2. The belt was required to be lifted with a large load applied to the belt, this posed safety and maintenance concerns. The design of the belt gantry was carefully considered in order to be suitable to overcome these challenges.

Tension in the system needs to be maintained, as a single test could run for an extended duration. There will be various parameters that need to be changed and each setup will require maintaining the tension, and the load will need to be maintained, even in the absence of external electrical power.

4.6.4 Test Facility Alignment

There were various items that needed to be accurately aligned on this test facility to remove as much uncertainty as possible. The belt profiler alignment was done by way of a water trough, which allowed for the water surface to be self-levelling. This allowed for a consistent baseline against which the entire belt profiler was levelled.

There were difficulties in reaching the manufacturing tolerances of some of the test facility components. This was particularly concerning for the universal idler, shown in Figure 3-3. These manufacturing concerns posed numerous challenges throughout the assembly process and rework was required to bring the parts back into specification. This added substantial delays to the project and were unfortunately picked up during the erection phase of the project.

5 DISCUSSION OF THE WORK CARRIED OUT

The objective of this research project was to design and construct a test facility to meet the research objectives, and then validate that all the equipment is fit for purpose. This was done by calibrating the instrumentation, ensuring that the various pieces of equipment are capable of the loads to which they will be subjected and that all the interfacing components of the test facility work together as expected.

The test facility in its current form can handle wing angles of 0 to 90 degrees and forward tilt of the wing rolls of 0, 2 and 5 degrees. The test facility provides a belt arc with a radius of up to 35 m, this convex curve will allow an additional component of downward force onto the idler set accentuating the issue of idler junction failure. Each of the universal idler frames is able to adjust independently and on the convex curve configuration each idler is set at 2.5 degrees relative to the adjacent idler. The belt profiler will allow the deformation of the belt to be measured accurately while the load and stress will be measured. The hydraulic system will provide the required tension.

A test facility that is modular enough to handle a variety of experiments, even beyond the scope of this project has been developed and constructed, a list of the various other topics that could be evaluated with this test facility are list in Section 5.1. This research will centrally focus on the stress effects that occur in and around the idler junction zone and will shed light on what effects the idler configuration has when the belt and idler make contact.

5.1 Range and Scope of the Test Facility

The test facility is flexible in a variety of ways; it can handle many different experiments. This report outlines one particular research application for the test facility. However, the versatile design allows for other projects to be conducted. Some of the range of tests that could be carried out are:

1. Idler junction testing on SANS standard 1050 belt width (which is the focus of this design project).
2. Investigate transition normalisation distance.
3. The test facility can accommodate idler roll length variations where the wing and the centre rolls can be of different lengths and diameters.
    a. The centre roll may be longer with a larger diameter and bearings to accommodate a higher load.
    b. Idler junction stress with different wing and centre roll dimensions.
    c. Does the roll diameter have an effect on the magnitude of the stress? In other words, would a larger roll diameter have a lower stress impact due to the larger contact area?
4. The effect of misalignment of the idlers can be more accurately quantified.
5. Different types of idler rolls can be used to determine stress effects, steel versus polymer rollers.
6. Determine the ideal idler junction gap and determine whether the gaps given in SANS 1313 specifications are appropriate.
7. Look at the effect of the pressure on the idler face with and without idler forward tilt.
8. Should the centre roll be leading or trailing? The force imparted into a belt may give an indication of tracking ability. This would determine if the centre roll should be leading or trailing in terms of the effect of stress experienced by the belt.
9. Look at friction factors between various troughing angles, is there a relationship between trough angle and friction factor?

5.2 Next Steps

Once the following work item points has been completed, the full scale tests can commence.

1. Continue with the belt sample testing, in order to fully understand which size of gauge will be most suitable (a 5mm or 10mm gauge). Also, which type of adhesive, a polymer (SC2000) or a cyanoacrylate (super glue) would yield the most consistent results?
2. Understand more thoroughly the stress variation across the belt sample and across the various sample pieces.
3. Consider the use of DIC (digital image correlation) techniques in order to understand how the entire belt sample experiences strain, does it vary across and along the belt sample?
4. Due to the large number of tests it would be ideal to refine current methods of measurement to more easily obtain data and convert the data into useful information, such as separating loading and unloading cycles to better extrapolate data to find better ways of obtaining trends which will be used on full scale testing.
5. Further investigate the ISO 9856 specification to determined how much permanent stretch is in a belt and how many cycles of testing are required in order to adequately remove this permanent stretch.

6 RECOMMENDATIONS FOR FURTHER WORK

This research report describes how the test facility has proven to be fit for purpose. It can be used to measure strain, force, displacement and temperature. The items described in Section 5.2 are the immediate next steps that should be completed along with ensuring that the hydraulic system can deliver the 20 ton output tension required and a system to move the belt and steel cables at a constant speed.

A full scale test programme with straight and a convex configuration can be initiated. The straight configuration would have five idlers all in a straight line while the convex configuration will have 9 idler frames in the shape of a convex curve. Various other parameters will be considered, such as the type of belt, ply belt or solidwoven. There will be various strength or classes of belt that will be tested. The various idler parameters would be tested, which would involve tilting the wing rollers forward and incrementing the trough angle in 15 degree increments.

The centre roll would be offset in increments of 25mm up to a maximum of 450mm and finally the load can be varied up to 120% of the operating tension. A control experiment will be used as a basis for evaluation, which would be the 0 degree configuration. The belt will be formed into the trough shape as the trough angle is increased in set increments. The stress within the belt will be determined by measurement and compared with the results obtained from FEA modelling. Ideally the comparison will validate the FEA studies, resulting in high levels of confidence in the use of FEA modelling to other belt widths and idler configurations. Ideally meaningful results from the data can be drawn to conclude whether an optimal distance for the offset distance between the centre idler roll and the wing roll exists for a given configuration.

7 REFERENCES

AC-Tek, 2017. *Sidewinder: Conveyor Design Software.* s.l.:AC-Tek (Advanced Conveyor Technologies).

Ckit, 2015. *Troughed Belt Conveyors.* [Online]
Available at: http://www.ckit.co.za/secure/conveyor/troughed/indextrough.htm
[Accessed 18 January 2015].

CKit, 2015. *Troughed Conveyor Belting.* [Online]
Available at:
http://www.ckit.co.za/secure/conveyor/troughed/belting/belting_basics.html
[Accessed 7 February 2015].

Ckit, 2017. *Profiles of Troughed Belt Conveyors.* [Online]
Available at: http://www.ckit.co.za/secure/conveyor/troughed/beginners-guide/bg30c.htm
[Accessed Jan 2017].

Conveyor Belt Guide, 2005. *Records: Longest Belt.* [Online]
Available at: http://www.conveyorbeltguide.com/LongestBelt.html
[Accessed 8 January 2015].

Dantec Dynamics, 2015. *Measurement Principles of (DIC).* [Online]
Available at: http://www.dantecdynamics.com/measurement-principles-of-dic
[Accessed 23 January 2015].

De, S. & White, J. eds., 1996. *Short Fibre-Polymer Composites.* Cambridge: Woodhead Publishing Limited.

EasiKit, 2012. *EasiKit: The History of the Conveyor.* [Online]
Available at: http://www.easikit.co.uk/news/uncategorized/the-history-of-the-conveyor
[Accessed 3 January 2014].

Egger M, S. D. a. K. H., 2002. Strain Gauges Applied to Conveyor Belts. *Bulk Solid Handling*, 22(1), pp. 42-45.

Faro, 2017. *Faro Gage.* [Online]
Available at: http://www.faro.com/en-us/products/metrology/measuring-arm-faro-gage/downloads-us#main
[Accessed Jan 2017].

Fayed, M. E. & Skocir, T., 1997. *Mechanical Conveyors: Selection and Operation.* Pennsylvania: Technomic Publishing Company Inc.

Fenner, 2016. *Fenner Data Center.* [Online]
Available at: http://www.fennerdrives.com/data-centers/
[Accessed Sep 2016].

Global Belting Technologies, 2015. *Knowledge Centre: General Belting Information.* [Online]
Available at: http://www.globalbelting.com/knowledge_gi.html
[Accessed 17 January 2015].

Graaff, R. d., 2016. *Troughability testing on troughed and pipe conveyor belts. Rapportnummer 2012.TEL.7695.*. [Online]
Available at: http://wbmttt.tudelft.nl/rapport/7695e.pdf

HabaTec, 2011. *Habasit.* [Online]
Available at:
http://www.habatec.net/HNET/HabaTEC.nsf/vwWebContent/B3AFDB9C92909C37

C12578BE002BB553?OpenDocument
[Accessed 12 December 2014].
Hannah R.L., R. S., 1992. *Strain Gauge Users Handbook.* First Edition ed. London, UK: Chapman & Hall.
Harandi, J., Kovousian, A., Parvini, M. & Soufian, M., 1992. *Rubber Chem Technol,* p. 697.
Henan Pingyuan Mining Machinery Co. Ltd., 2016. *Henan Pingyuan Mining Machinery Co. Ltd..* [Online]
Available at: http://www.pkmachinery.com/faq/conveyor-belt-damage-forms.html
[Accessed Jun 2016].
Hoffmann, K., 2015. *Applying the Wheatstone Bridge Circuit.* W1569-1.0 en ed. s.l.:HBM.
HYC, 2016. *HYC STraight Warp Conveyor Belt.* [Online]
Available at: http://www.hyc-king.com/en/product/p_straight_warp_conveyor_belt.html
[Accessed Sep 2016].
Interflex Conveyor Belts, 2012. *Multi-ply Conveyor Belt.* Nuffield, Springs, 1560: Interflex Conveyor Belts.
ISO 9856, 1989. *Conveyor Belts - Determination of elastic modulus.* s.l., International Standard.
Kadakia, M., 2009. *How to Design Take-up Travel for a Fabric Conveyor Belt,* Milwaukee: s.n.
Karak, N., 2009. *Fundamentals of Polymers.* New Delhi: PHI Learning Private Limited.
Kevra, 2016. *Kevra Advanced Composite Technology.* [Online]
Available at: http://www.kevra.fi/products/reinforcements/?lang=en
[Accessed Jun 2016].
Lemmon, R., 2015. *BELT TRANSITIONS ANALYSIS BY FINITE ELEMENT ANALYSIS.* Fourways 2055, Internation Materials Handling Conference, IMHC, Beltcon 17 Conference.
Lorbrand, 2008. *SABS Idler Catelogue,* Johannesburg: s.n.
Mac Steel, 2017. *STRUCTURAL STEELS in accordance with SANS 50025 / EN 10025.* [Online]
Available at: https://www.macsteel.co.za/files/en_10025_s275_s355.pdf
[Accessed Feb 2017].
Meijers, D. S., 2013. *Indaba 2013 Suppliment.* [Online]
Available at: http://www.elbengineering.co.za/downloads/news/elb_1_13b.pdf
[Accessed 8 January 2015].
MHEA, 1986. *Recommended Practice for Troughed Belt Conveyors.* s.l.:The Mechanical Handling Engineers' Association.
MHEDA, 2004. *The MHEDA Journal.* [Online]
Available at: http://www.themhedajournal.org/content/3q04/conveyors.php
[Accessed 3 January 2015].
Nisbett, R. G. B. a. J. K., 2011. *Shigley's Mechanical Engineering Design.* 9th ed. New York, NY 10020: McGraw Hill.
Pitcher, D., 2012. *Manufacture and Selection of Conveyor Belting,* Johannesburg: University of the Witwatersrand,
Pitcher, D., 2012. *Manufacture and Selection of Conveyor Belting,* Johannesburg: University of the Witwatersrand.
Pitcher, D., 2015. *Idler Junction Failure* [Interview] (15 January 2015).

Robinson, C. W., 2016. The indentation rolling resistance of spherically profiled idler rolls. *International Journal of Mechanical Sciences,* February, Volume Volume 106, pp. 363-371.
SANS 1173, (., 2013. *Conveyor Belting - General Purpose Textile-Reinforced Construction, (ED.3).* s.l.:SABS.
SANS 1313-1, P. 1., 2012. *Conveyor Belt Idlers - Part 1: Troughed Belt Conveyor Idlers (Metallic and Non-Metallic) for Idler Roller Rotational Speeds of Up to 750 Revolutions per Minute.* 4 ed. s.l.:SABS.
Satyendra, 2013. *Ispat Guru: Conveyor Belts.* [Online]
Available at: http://ispatguru.com/conveyor-belts/
[Accessed 17 January 2015].
SIG, 2017. *Siderflex.* [Online]
Available at: http://www.sig.it/SIDERFLEX/Siderflex_5.jpg
[Accessed Jan 2017].
Wheeler, C., 2012. *Belt Transitions and Vertical Curves.* Newcastle, Australia, TUNRA Bulk Solids Research Associates, The University of Newcastle, Australia..
Wheeler, C., 2012. *Overview of Main Resistances and Design Optimisation.* Newcastle, Australia: TUNRA Bulk Solids Research Associates, The University of Newcastle, Australia..
Wheeler, C., 2012. *Overview of Static Design Procedure.* Newcastle, Australia: TUNRA Bulk Solids Research Associates, The University of Newcastle, Australia..
Wikipedia, 2014. *Wikipedia: Conveyor belt.* [Online]
Available at: http://en.wikipedia.org/wiki/Conveyor_belt#History
[Accessed 12 December 2014].
Wombrose, 2014. *Wombrose: The History of Conveyor Belts.* [Online]
Available at: http://www.wombrose.co.uk/the-history-of-conveyor-belts/
[Accessed 3 January 2014].
Zhang, Y., 2015. *Conveyor Belt Bottom Cover Failure from Idlers and Pulleys.* Fourways 2055, Internation Materials Handling Conference, IMHC, Beltcon 18 Conference.

8 APPENDICES

8.1 Design Calculations

8.1.1 Determination of the Radius of the Convex Curve

Since Factor C and Factor D increase with an increasing trough angle, see Table 8-1, and given that the minimum convex radius is proportional to Factor C and Factor D, as shown in Equation 8-1 and Equation 8-2, only the calculation for a 45 degree trough angle is shown as it will yield the greatest minimum radius.

To prevent overstress of the belt edges (Wheeler, 2012)

$$R_{\min,1} = \frac{FactorC \times B^2 \times E \times p}{T_r - T_c} \qquad \textbf{8-1}$$

To prevent buckling of the centre of the belt (Wheeler, 2012)

$$R_{\min,2} = \frac{FactorD \times B^2 \times E \times p}{T_r - 5216B} \qquad \textbf{8-2}$$

Where

$R_{\min}$ = Minimum Convex Radius (m)

B = Belt width (m)

E = Modulus of elasticity of the conveyor belt ($N / m / ply$)

p = Number of plys in the belt (-)

T_r = Rated belt tension (N)

T_c = Tension at point of interest during normal running (N)

$FactorC$ = Factor provided (-)

$FactorD$ = Factor provided (-)

Table 8-1: Factors to calculate the minimum radius for various tough angles (Wheeler, 2012).

Trough Angle	*Factor C*	*Factor D*
20º	0.0756	0.0384
35º	0.1272	0.0636
45º	0.1572	0.0780

Table 8-2: Table of various belt class and its corresponding belt modulus (Interflex Conveyor Belts, 2012).

Belt class for number of plies				Belt Modulus kN/m	Full thickness breaking strength			
2	3	4	5		Class	Longitudinal direction kN/m width minimum	Transverse direction kN/m width minimum	Recommended maximum operating tension (kN/m)
160				880	160	160	63	16.0
200				1111	200	200	80	20.0
250	250			1390	250	250	100	25.0
315	315	315		1750	315	315	125	21.5
400	400	400	400	2220	400	400	160	40.0
500	500	500	500	2780	500	500		50.0
630	630	630	630	3500	630	630		63.0
800	800	800	800	4440	800	800	not	80.0
	1000	1000	1000	5550	1000	1000	specified	100.0
	1250	1250	1250	6940	1250	1250		125.0
		1600	1600	8890	1600	1600		160.0
					2000	2000		200.0
					2500	2500		250.0

It was assumed that the tension T_c is 70% of the rated tension. Table 8-2 provided values for the belt modulus for various belt classes. Table 8-3 provides calculations for the lowest and highest class belt that the research program will investigate. The greatest minimum radius is 30.56 m and the design value was selected at 35 m.

Table 8-3: Minimum radius for an increasing belt class.

Trough Angle (Deg)	Class (kN/m)	Belt Width (m)	E*p (kN/m)	T_r (kN)	$R_{min,1}$ (m)	$R_{min,2}$ (m)
45	315	1.05	1 750	33	30.56	8.53
45	1600	1.05	8 890	168	30.57	6.82

8.1.2 FEA Analysis of Key Components

A finite element analysis (FEA) was conducted on key components of the project. The results of the analyses shown below are on the worst-case conditions, so reasonable safety margin is built into all the components.

Base frame of the Universal Idler

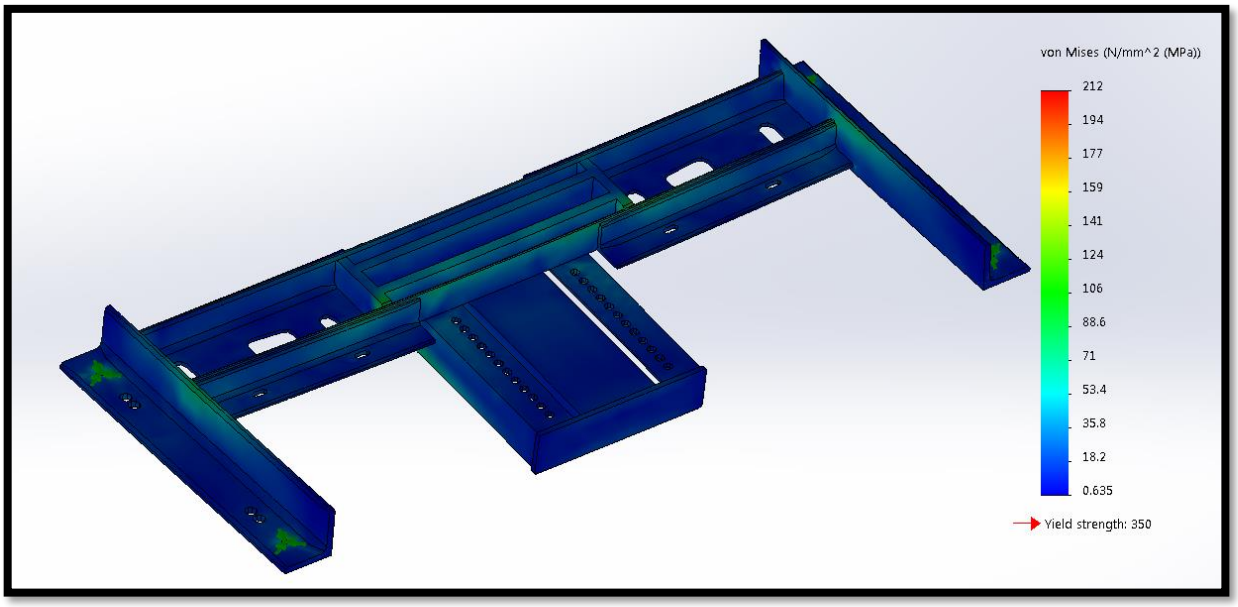


Figure 8-1: FEA analysis of the universal idler base frame.

Belt Attachment

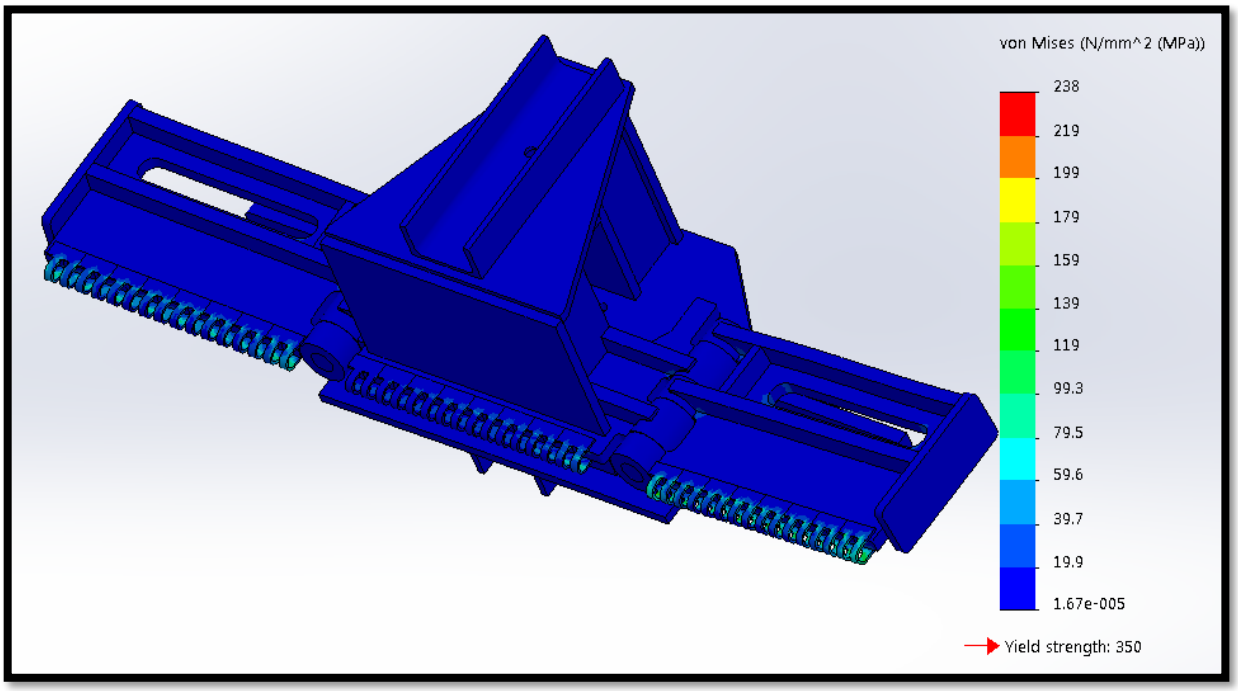


Figure 8-2: FEA analysis of the belt attachment.

Sheave Frame Structure

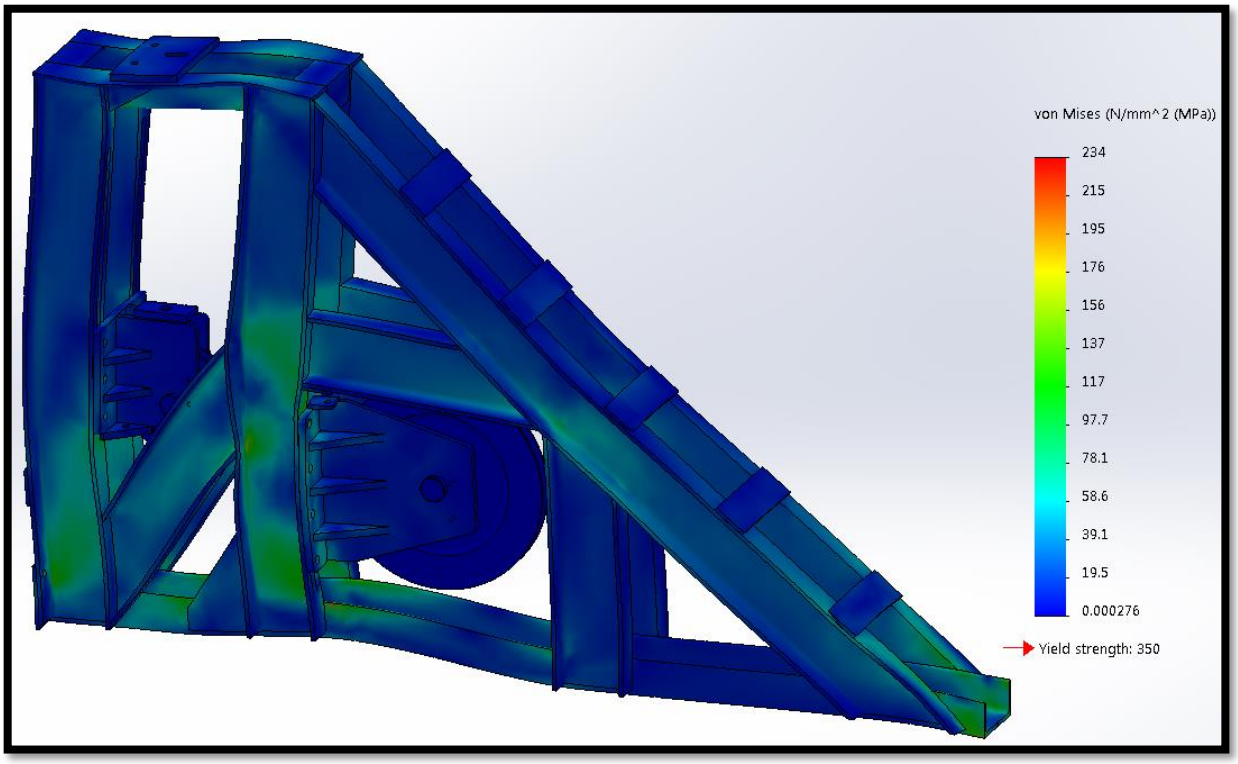


Figure 8-3: FEA analysis of the sheave frame structure.

8.1.3 Deflection Calculations

There were a few deflection of beam calculations that were used: the simple supports with centre loads and simple supports with a uniform load, Equation 8-3 and Equation 8-4 respectively (Nisbett, 2011).

$$y_{\max} = -\frac{Fl^3}{48EI} \qquad \textbf{8-3}$$

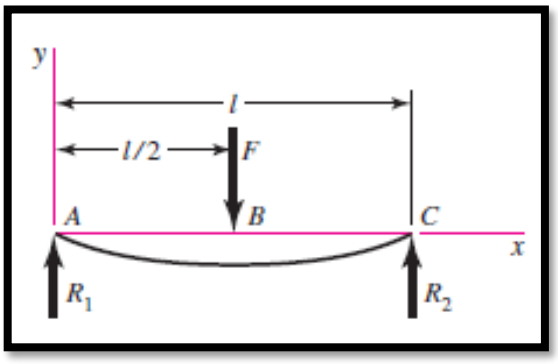


Figure 8-4: Simple supports with a centre load (Nisbett, 2011).

$$y_{\max} = -\frac{5\omega l^4}{384EI} \qquad \textbf{8-4}$$

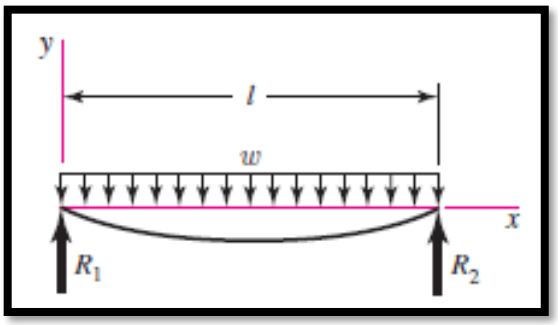


Figure 8-5: Simple supports with a uniformly distributed load (Nisbett, 2011).

Where

$y_{\max}$ = Maximum deflection (m)

F = Force (N)

l = Length of beam (m)

E = Modulus of Elasticity (Pa)

I = Polar Moment of Inertia (m^4)

ω = Uniformly distributed load (N/m)

Using the principle of superposition, Table 8-4, Table 8-5, Table 8-6 and Table 8-7 show the results for the total deflection of each one of the sections listed in Figure 8-8, Figure 8-9, Figure 8-6 and Figure 8-7.

Table 8-4: Deflection calculation for the I beam section, for the belt gantry lifter.

Load Type	F or ωl (kg)	L (m)	E (Pa)	I (m^4)	y_{max} (mm)
Centre Load	20000	3.0	2.10E+11	168.5E-6	3.12
Distributed Load	280	3.0	2.10E+11	168.5E-6	0.03
Total					**3.15**

Table 8-5: Deflection calculation for the double 180x90 aluminium beam section, for the belt profiler.

Load Type	F or ωl (kg)	L (m)	E (Pa)	I (m^4)	y_{max} (mm)
Centre Load	60	3.7	6.90E+10	148.7E-6	0.06
Distributed Load	215	3.7	6.90E+10	148.7E-6	0.14
Total					**0.20**

Table 8-6: Deflection calculation for the 90x90 aluminium beam section, for the belt profiler.

Load Type	F or ωl (kg)	L (m)	E (Pa)	I (m^4)	y_{max} (mm)
Centre Load	80	1.95	6.90E+10	2.11E-6	0.83
Distributed Load	15	1.95	6.90E+10	2.11E-6	0.10
Total					**0.93**

Table 8-7: Deflection calculation for the I beam section, for the belt profiler.

Load Type	F or ωl (kg)	L (m)	E (Pa)	I (m^4)	y_{max} (mm)
Centre Load	150	5.5	2.10E+11	52.8E-6	0.46
Distributed Load	180	5.5	2.10E+11	52.8E-6	0.34
Total					**0.80**

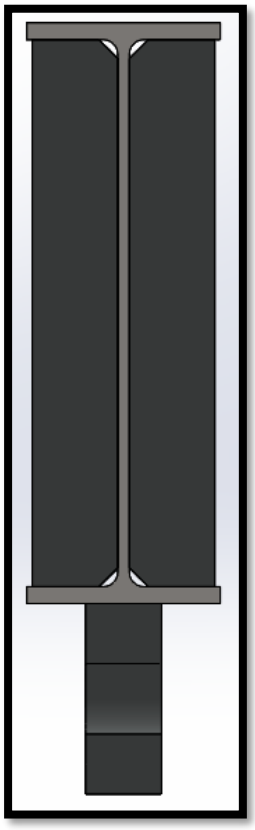


Figure 8-8: I beam section, for the belt gantry lifter.

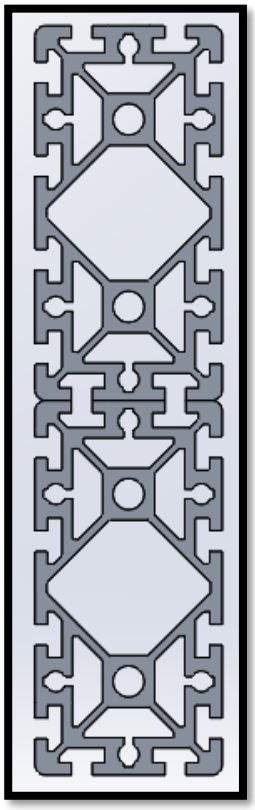


Figure 8-9: Double 180x90 aluminium beam section, for the belt profiler.

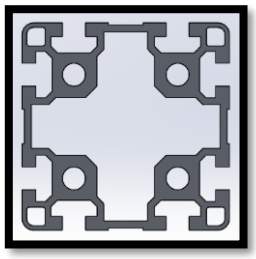


Figure 8-6: 90x90 aluminium beam section, for the belt profiler.

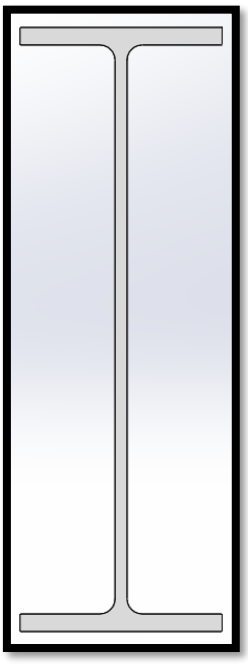


Figure 8-7: I beam section, for the belt profiler.

8.1.4 Stress Calculation in the Belt Gantry Lifter

The stress in the belt gantry lifter, section view shown in Figure 8-10, needed to be determined using Equation 8-5 and Equation 8-6 (Nisbett, 2011).

$$\sigma = \frac{My}{I} \qquad \textbf{8-5}$$

Where

σ = Bending Stress (Pa)

M = Bending Moment (Nm)

y = Perpendicular distance from neutral axis (m)

I = Polar moment of inertia (m^4)

$$\tau = \frac{V}{A} \qquad \textbf{8-6}$$

Where

τ = Shear stress (Pa)

V = Shear Force (N)

A = Area (m^2)

The results of the shear and bending stress is shown in Table 8-8. The maximum yield strength of the material the beam was made from (S355JR) is 355 MPa (Mac Steel, 2017). The design is safe since the yield limit exceeds the shear and bending stresses.

Table 8-8: Results for the Bending and shear stresses in the belt gantry lifter beam.

Bending Stress		**Shear Stress**	
M (Nm)	69367.18	V (N)	138734.35
y (m)	0.25	A (m^2)	31.78E-3
I (m^4)	168.47E-6	**τ (Pa)**	**4.37E+6**
σ (Pa)	**102.94E+6**		

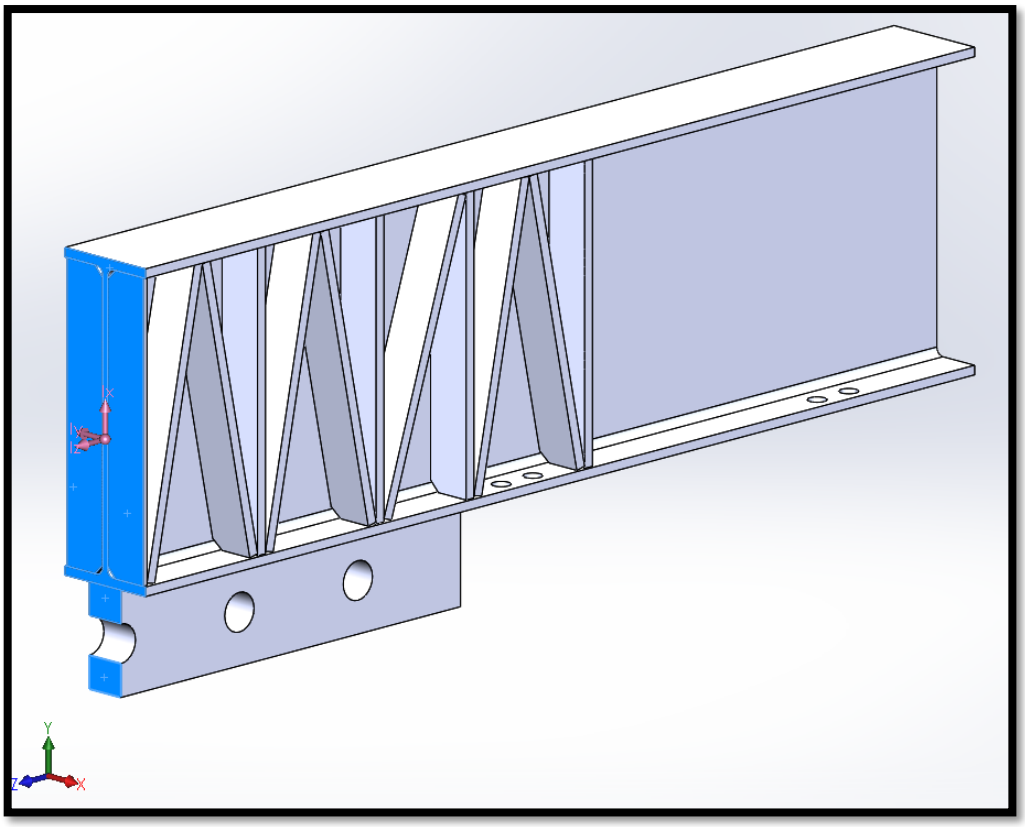


Figure 8-10: Sectioned view of belt gantry lifter beam.

8.2 Engineering Drawings

8.2.1 Test Facility Overview

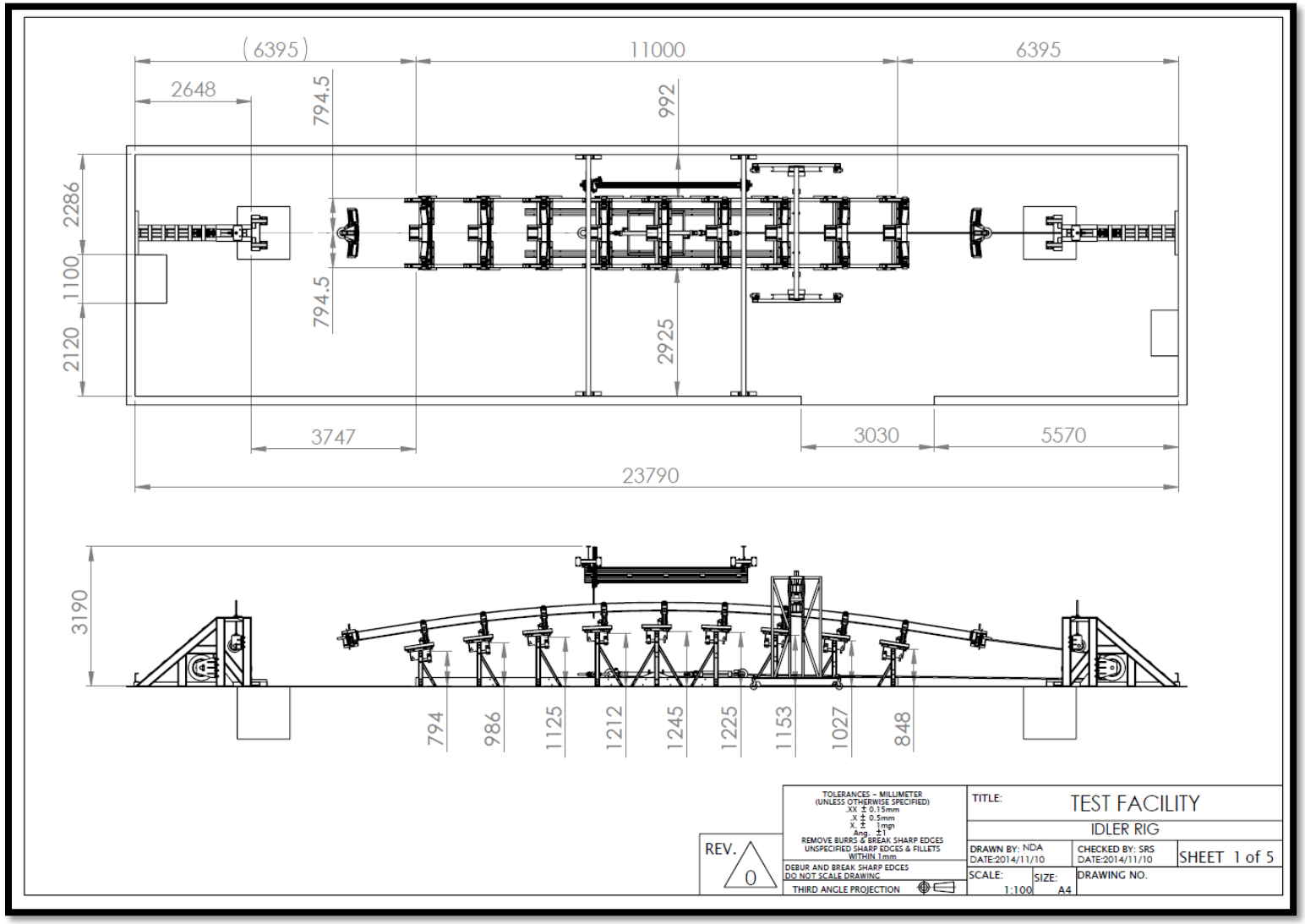


Figure 8-11: Overview of the convex test facility configuration.

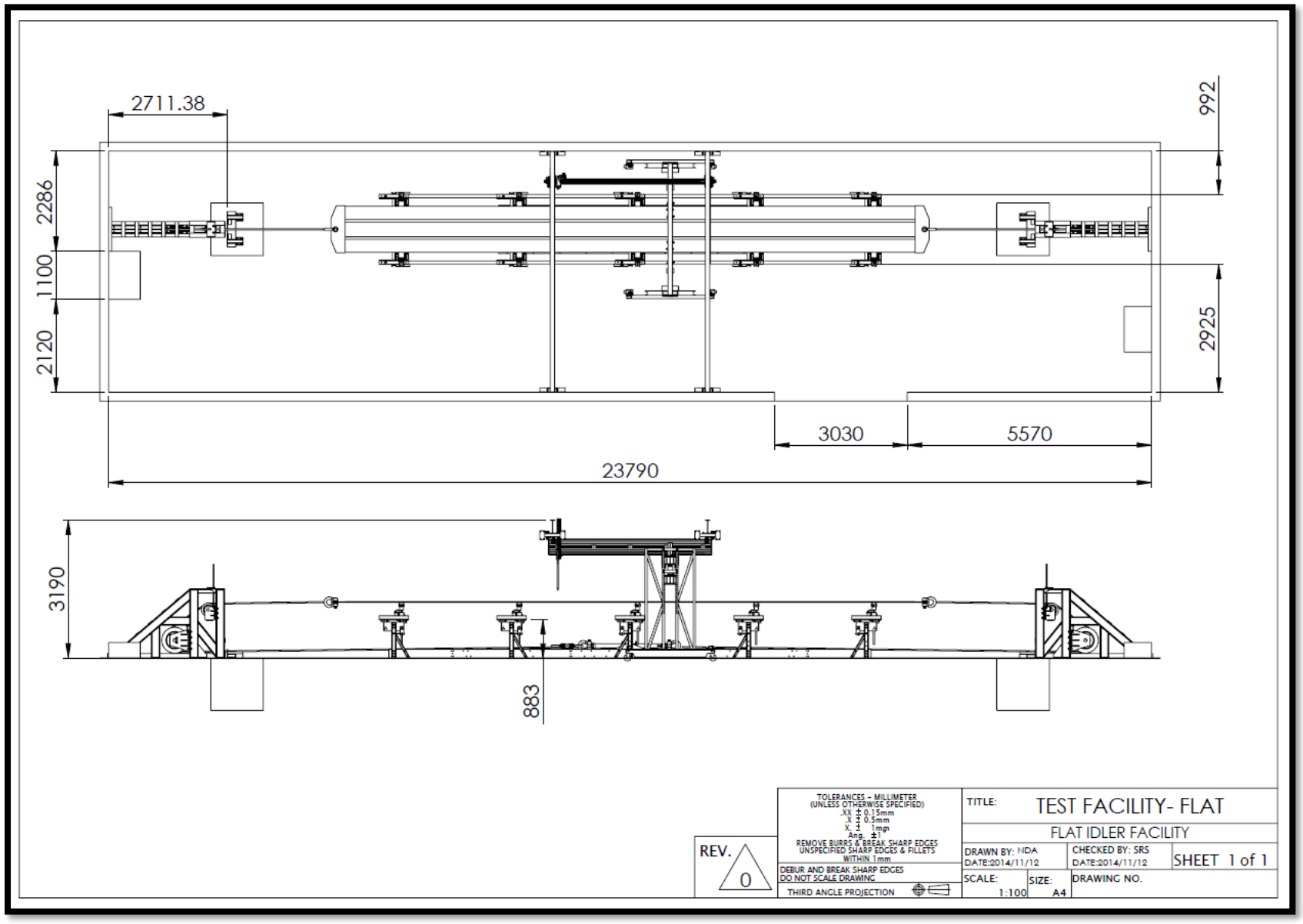


Figure 8-12: Overview of the flat test facility configuration.

8.2.2 Belt Attachment

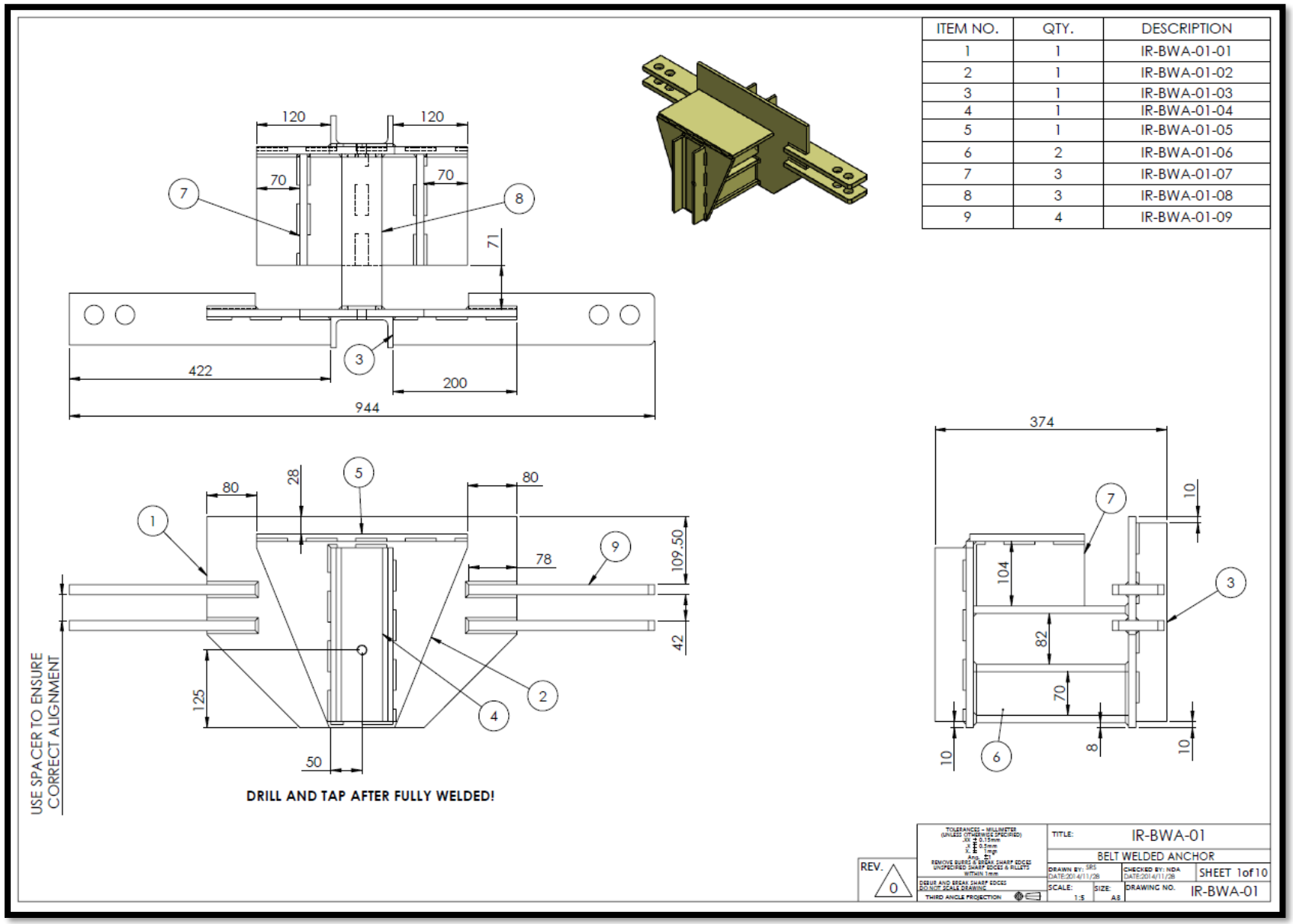


Figure 8-13: General arrangement drawing of the belt attachment.

8.2.3 Sheave Frame Assembly

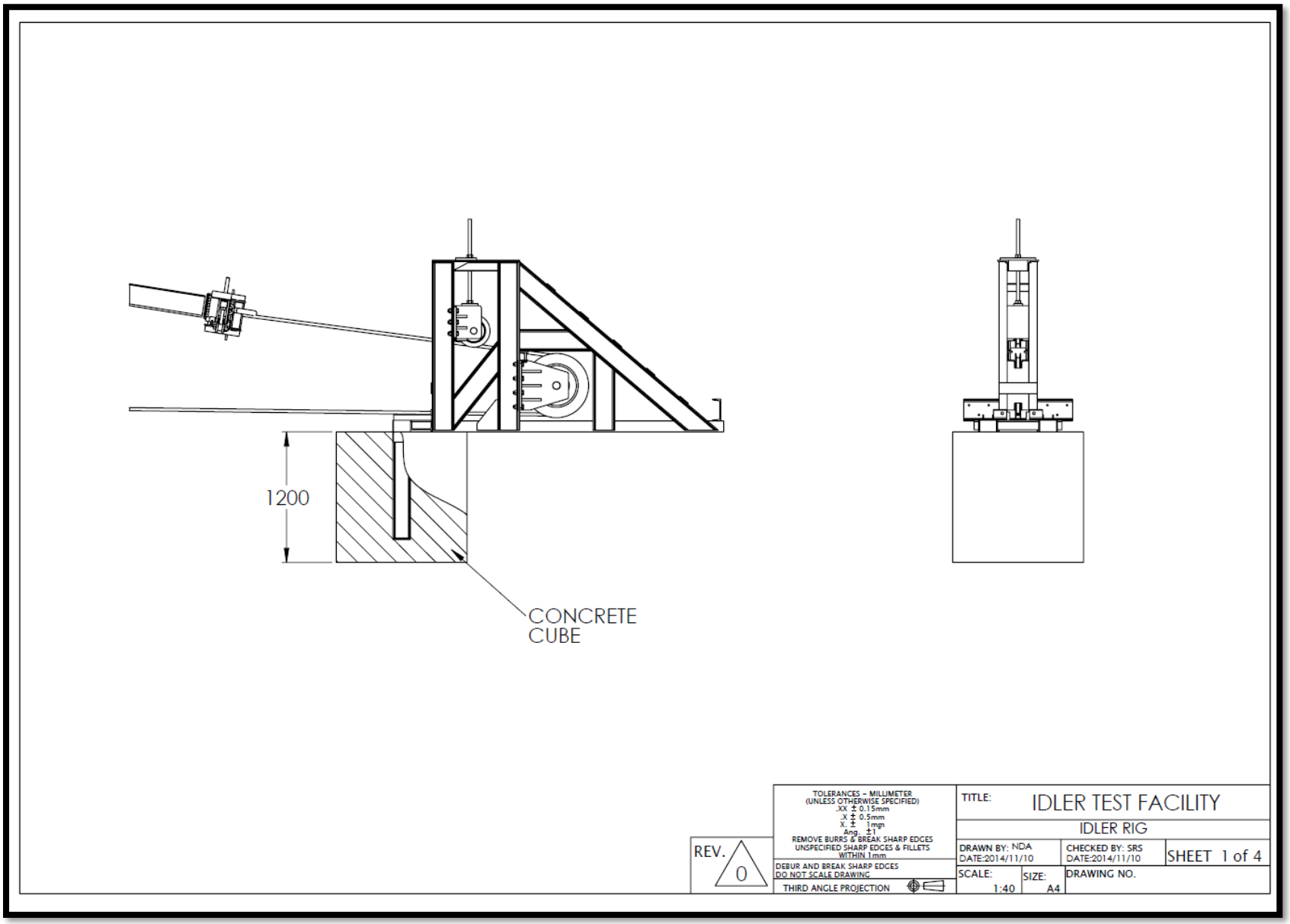
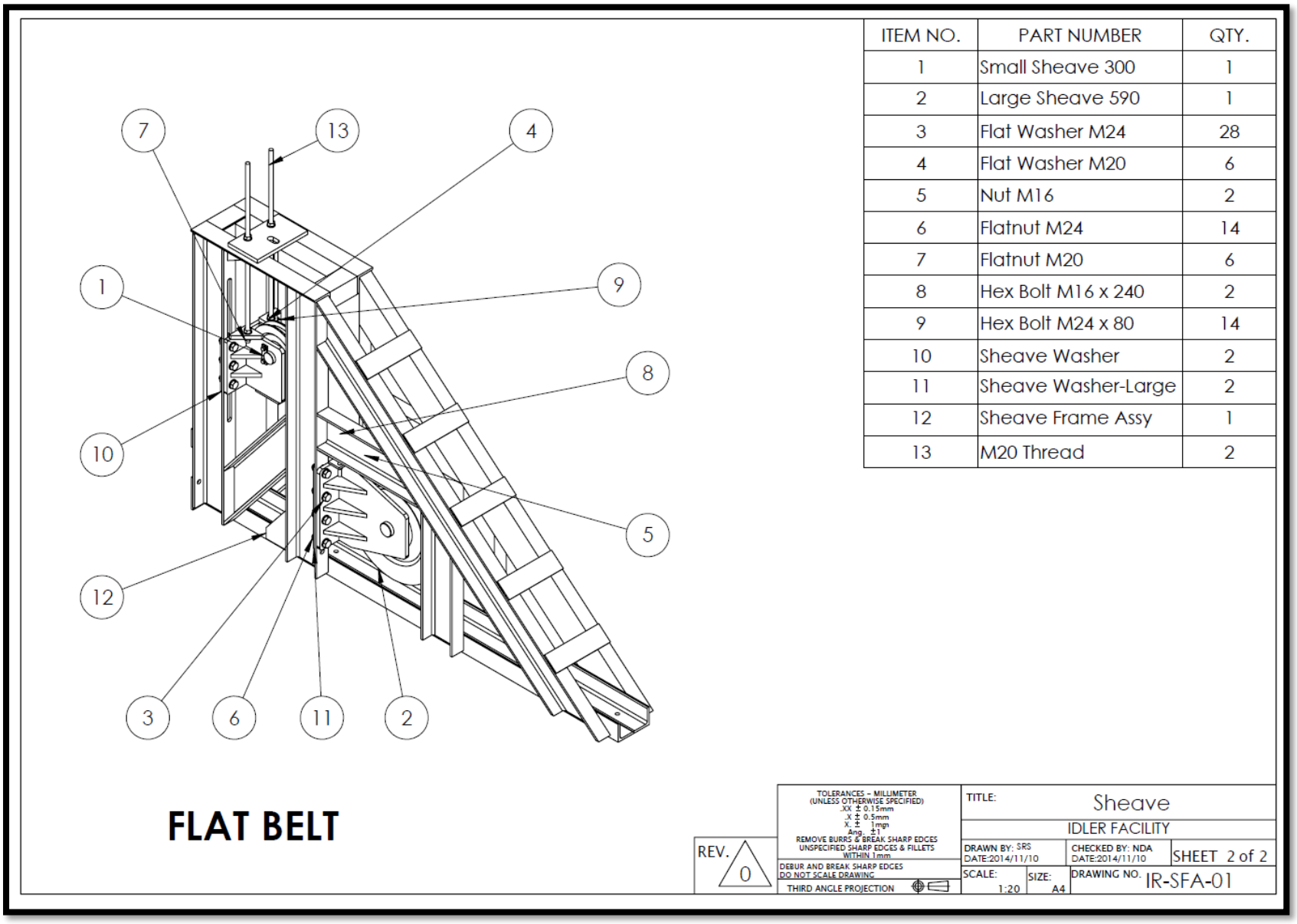


Figure 8-14: General arrangement drawing of the sheave frame section.



ITEM NO.	PART NUMBER	QTY.
1	Small Sheave 300	1
2	Large Sheave 590	1
3	Flat Washer M24	28
4	Flat Washer M20	6
5	Nut M16	2
6	Flatnut M24	14
7	Flatnut M20	6
8	Hex Bolt M16 x 240	2
9	Hex Bolt M24 x 80	14
10	Sheave Washer	2
11	Sheave Washer-Large	2
12	Sheave Frame Assy	1
13	M20 Thread	2

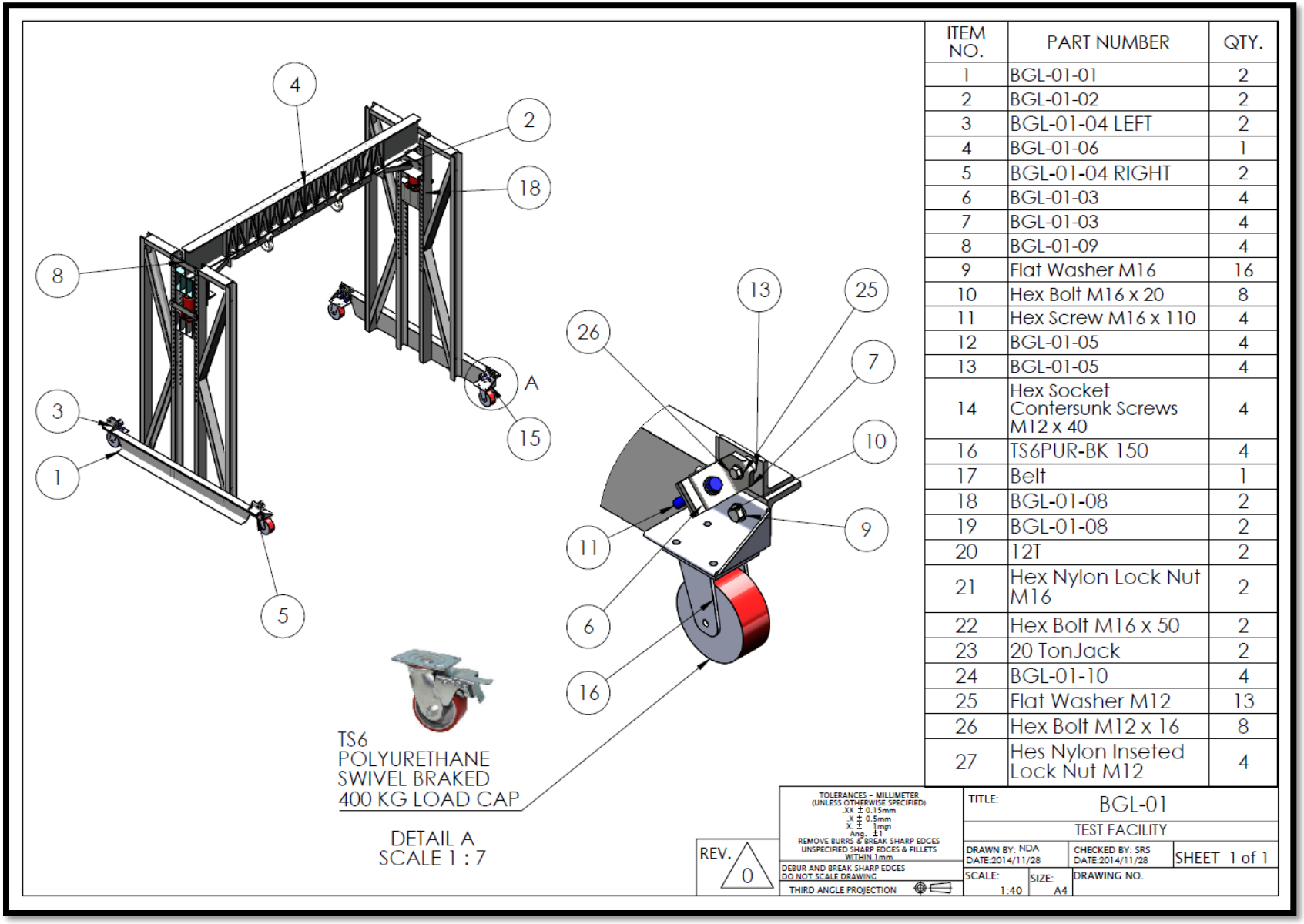
TOLERANCES – MILLIMETER
(UNLESS OTHERWISE SPECIFIED)
.XX ± 0.15mm
.X ± 0.5mm
X. ± 1mm
Ang. ±1°
REMOVE BURRS & BREAK SHARP EDGES
UNSPECIFIED SHARP EDGES & FILLETS WITHIN 1mm
DEBUR AND BREAK SHARP EDGES
DO NOT SCALE DRAWING
THIRD ANGLE PROJECTION

REV. 0

TITLE: Sheave
IDLER FACILITY
DRAWN BY: SRS DATE:2014/11/10
CHECKED BY: NDA DATE:2014/11/10
SHEET 2 of 2
SCALE: 1:20
SIZE: A4
DRAWING NO. IR-SFA-01

Figure 8-15: General arrangement drawing of the sheave frame assembly.

8.2.4 Belt Gantry Lifter



ITEM NO.	PART NUMBER	QTY.
1	BGL-01-01	2
2	BGL-01-02	2
3	BGL-01-04 LEFT	2
4	BGL-01-06	1
5	BGL-01-04 RIGHT	2
6	BGL-01-03	4
7	BGL-01-03	4
8	BGL-01-09	4
9	Flat Washer M16	16
10	Hex Bolt M16 x 20	8
11	Hex Screw M16 x 110	4
12	BGL-01-05	4
13	BGL-01-05	4
14	Hex Socket Contersunk Screws M12 x 40	4
16	TS6PUR-BK 150	4
17	Belt	1
18	BGL-01-08	2
19	BGL-01-08	2
20	12T	2
21	Hex Nylon Lock Nut M16	2
22	Hex Bolt M16 x 50	2
23	20 TonJack	2
24	BGL-01-10	4
25	Flat Washer M12	13
26	Hex Bolt M12 x 16	8
27	Hes Nylon Inseted Lock Nut M12	4

TOLERANCES – MILLIMETER (UNLESS OTHERWISE SPECIFIED) .XX ± 0.15mm .X ± 0.5mm X ± 1mm Ang. ±1
REMOVE BURRS & BREAK SHARP EDGES UNSPECIFIED SHARP EDGES & FILLETS WITHIN 1mm
DEBUR AND BREAK SHARP EDGES
DO NOT SCALE DRAWING
THIRD ANGLE PROJECTION

REV. 0

TITLE: BGL-01
TEST FACILITY
DRAWN BY: NDA DATE:2014/11/28
CHECKED BY: SRS DATE:2014/11/28
SHEET 1 of 1
SCALE: 1:40
SIZE: A4
DRAWING NO.

Figure 8-16: General arrangement drawing of the belt gantry lifter.

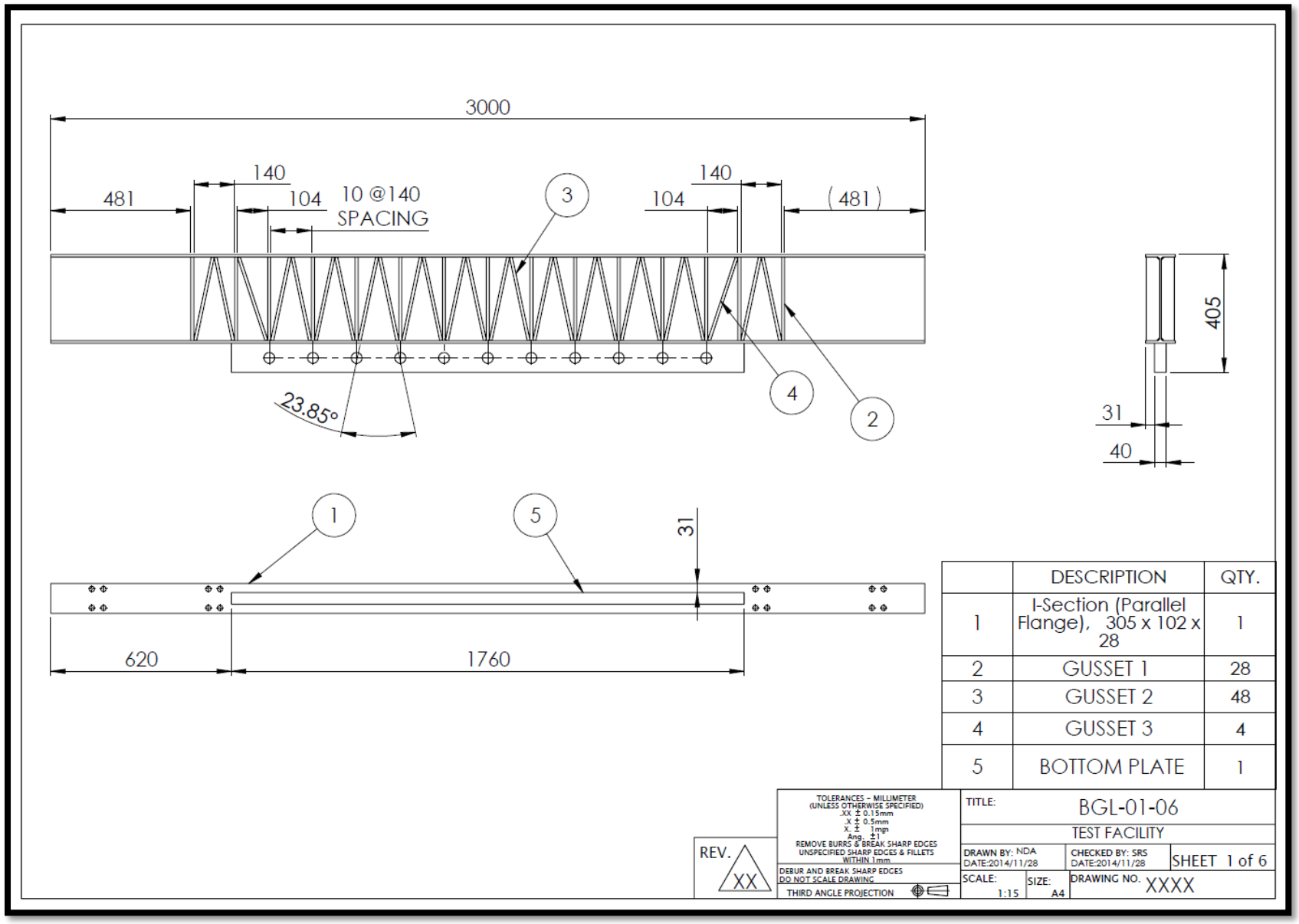


Figure 8-17: General arrangement drawing of the belt gantry lifter's main beam.

8.2.5 Column Supports

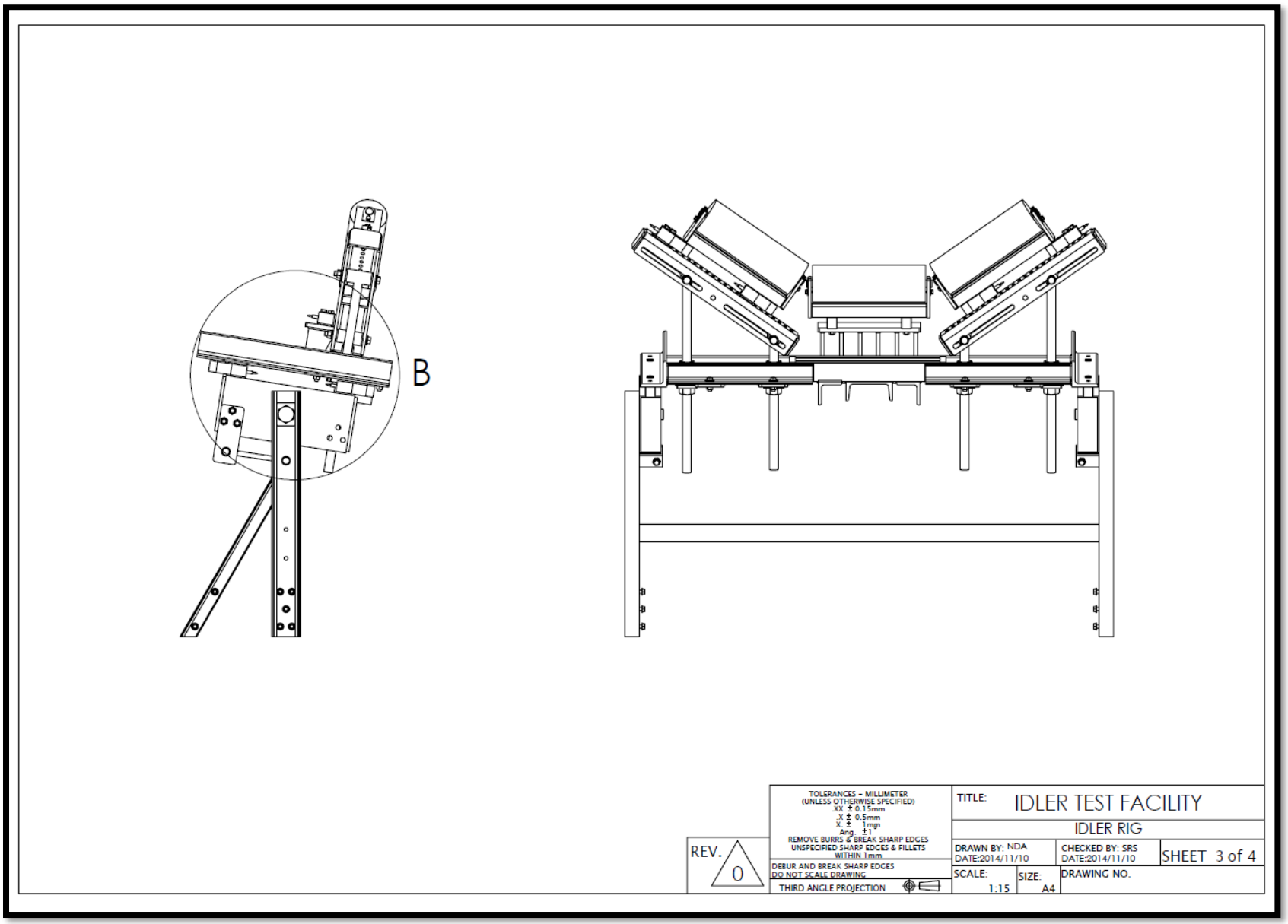


Figure 8-18: General arrangement drawing of the column support with the universal idler frame.

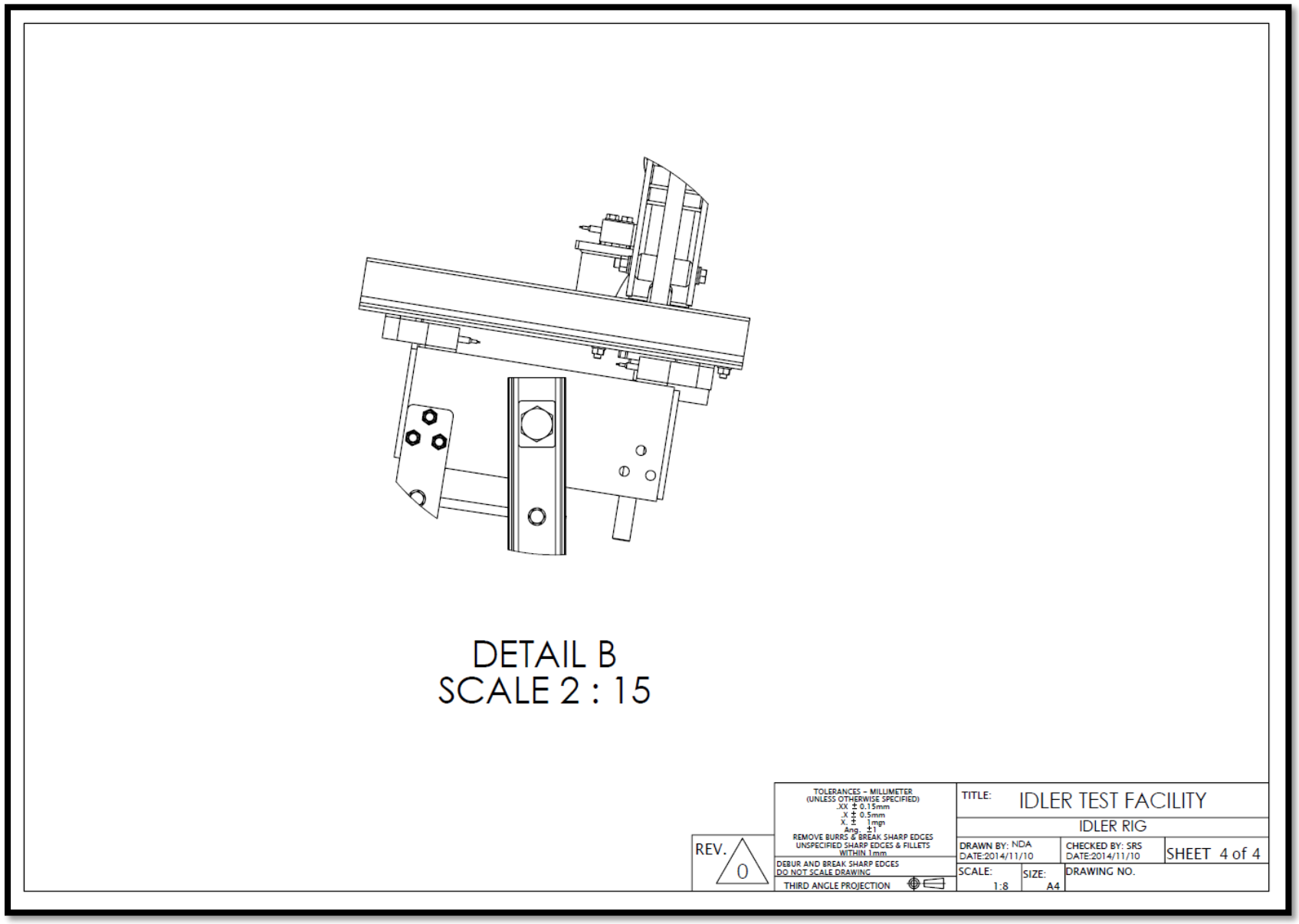


Figure 8-19: Detailed view of the column support with 2ton load cells.

8.2.6 Belt Profiler

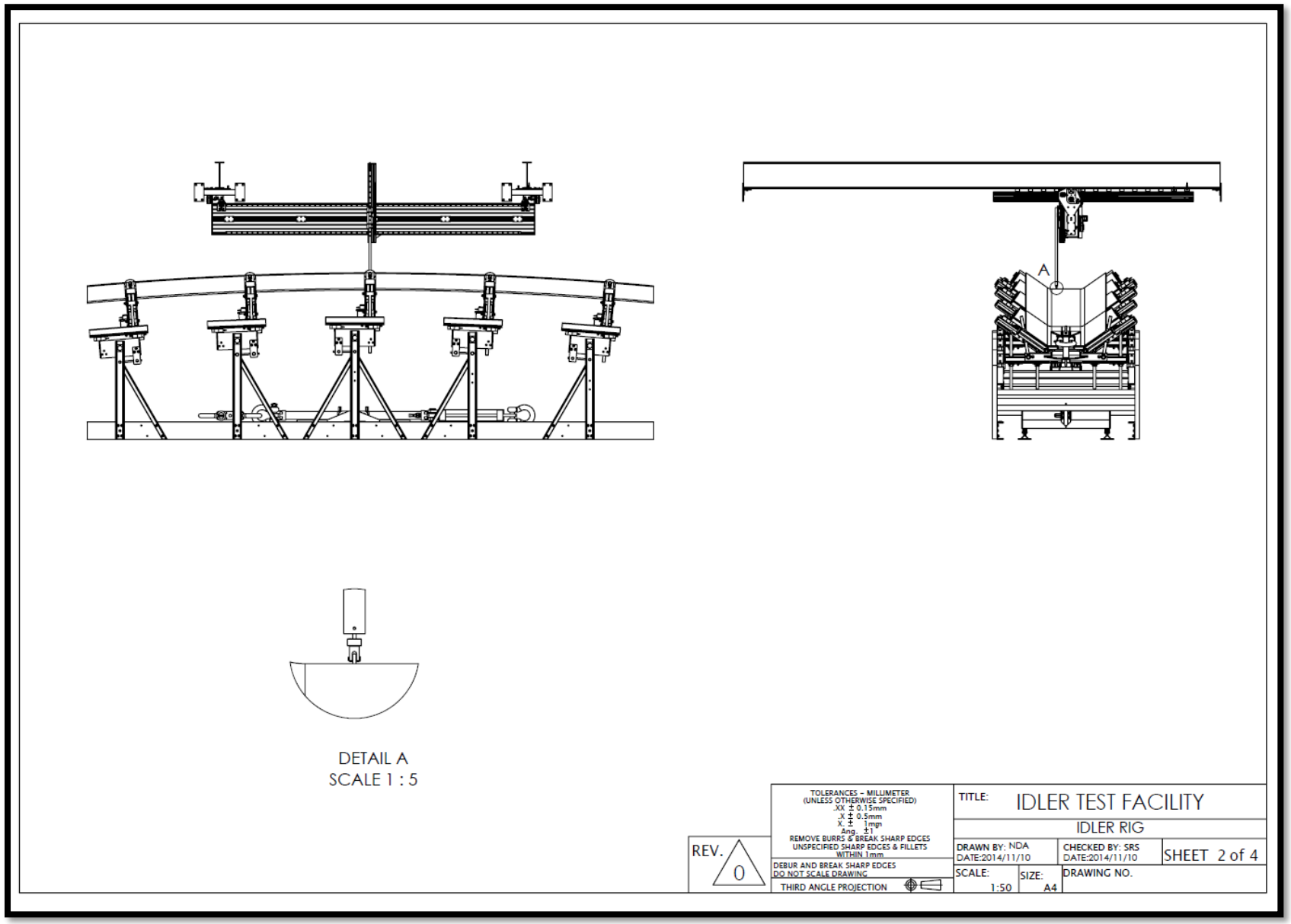


Figure 8-20: General arrangement drawing of the belt profiler.

8.3 Equipment Used

8.3.1 Test Instrumentation

There were various pieces of equipment used for the development of the project, these are listed in Table 8-9.

Table 8-9: Description of the instruments used for the project.

Type	Description	Notes
Strain Gauges	BE350-10AA-11 Zemic gages	5% Maximum elongation. Fatigue limit, 10^7 cycles at 1000 micro strain.
Strain Gauges	BE350-5AA-11 Zemic gauges	5% Maximum elongation. Fatigue limit, 10^7 cycles at 1000 micro strain.
Displacement Sensors	Magnetic Sensor MSK210	Magnetic Encoder.
Displacement Sensors	Magnetic Band MB200	Magnetic Encoder.
NI Chassis	cDAQ-9188	
NI Chassis	cDAQ-9178	
NI Module	NI 9401	Digital Module
NI Module	NI 9219	Multi-purpose Testing, Temperature and Strain
NI Module	NI 9236	350Ω Quarter Bridge Strain measurement
NI Module	NI 9237	Full Bridge Strain measurement
Loadcell	EB-20Ton: Tension Link Loadcell	
Loadcell	H8C-2Ton: Shearbeam Loadcell	
Temperature Sensors	Resistance Temperature Detector (RTD) (PT100) PR-20	

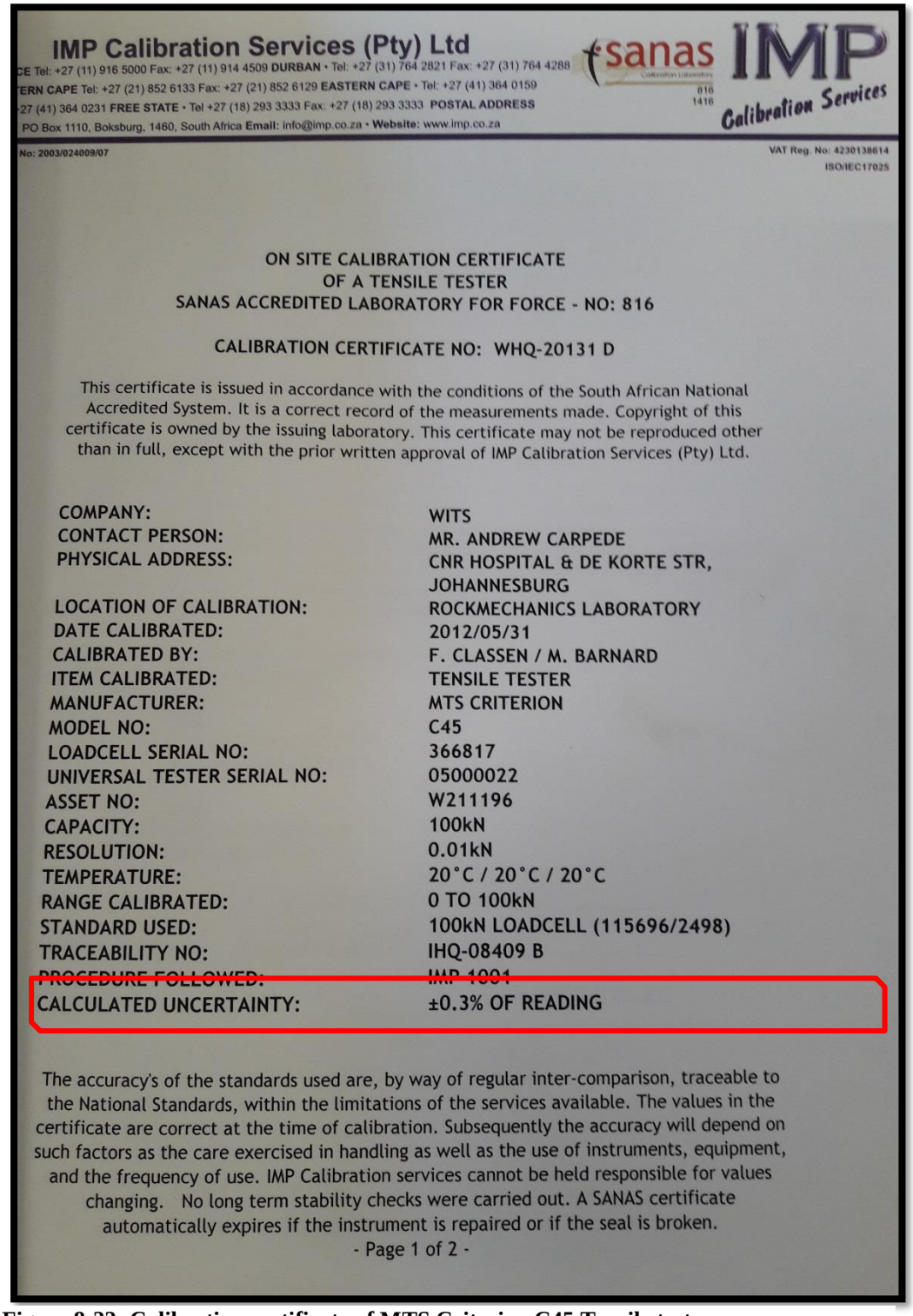
8.3.2 Calibration Instrumentation

Tensile Tester used to calibrate the 2 ton loadcells.



Figure 8-21: Illustration of an MTS Criterion C45 tensile tester.

Calibration certificate for the MTS Criterion C45 tensile tester.



IMP Calibration Services (Pty) Ltd

CE Tel: +27 (11) 916 5000 Fax: +27 (11) 914 4509 **DURBAN** • Tel: +27 (31) 764 2821 Fax: +27 (31) 764 4288
TERN CAPE Tel: +27 (21) 852 6133 Fax: +27 (21) 852 6129 **EASTERN CAPE** • Tel: +27 (41) 364 0159
·27 (41) 364 0231 **FREE STATE** • Tel +27 (18) 293 3333 Fax: +27 (18) 293 3333 **POSTAL ADDRESS**
PO Box 1110, Boksburg, 1460, South Africa **Email:** info@imp.co.za • **Website:** www.imp.co.za

sanas 816 1416

IMP Calibration Services

No: 2003/024009/07

VAT Reg. No: 4230138614
ISO/IEC17025

ON SITE CALIBRATION CERTIFICATE
OF A TENSILE TESTER
SANAS ACCREDITED LABORATORY FOR FORCE - NO: 816

CALIBRATION CERTIFICATE NO: WHQ-20131 D

This certificate is issued in accordance with the conditions of the South African National Accredited System. It is a correct record of the measurements made. Copyright of this certificate is owned by the issuing laboratory. This certificate may not be reproduced other than in full, except with the prior written approval of IMP Calibration Services (Pty) Ltd.

COMPANY:	WITS
CONTACT PERSON:	MR. ANDREW CARPEDE
PHYSICAL ADDRESS:	CNR HOSPITAL & DE KORTE STR, JOHANNESBURG
LOCATION OF CALIBRATION:	ROCKMECHANICS LABORATORY
DATE CALIBRATED:	2012/05/31
CALIBRATED BY:	F. CLASSEN / M. BARNARD
ITEM CALIBRATED:	TENSILE TESTER
MANUFACTURER:	MTS CRITERION
MODEL NO:	C45
LOADCELL SERIAL NO:	366817
UNIVERSAL TESTER SERIAL NO:	05000022
ASSET NO:	W211196
CAPACITY:	100kN
RESOLUTION:	0.01kN
TEMPERATURE:	20°C / 20°C / 20°C
RANGE CALIBRATED:	0 TO 100kN
STANDARD USED:	100kN LOADCELL (115696/2498)
TRACEABILITY NO:	IHQ-08409 B
PROCEDURE FOLLOWED:	IMP 1001
CALCULATED UNCERTAINTY:	±0.3% OF READING

The accuracy's of the standards used are, by way of regular inter-comparison, traceable to the National Standards, within the limitations of the services available. The values in the certificate are correct at the time of calibration. Subsequently the accuracy will depend on such factors as the care exercised in handling as well as the use of instruments, equipment, and the frequency of use. IMP Calibration services cannot be held responsible for values changing. No long term stability checks were carried out. A SANAS certificate automatically expires if the instrument is repaired or if the seal is broken.

- Page 1 of 2 -

Figure 8-22: Calibration certificate of MTS Criterion C45 Tensile tester.

Faro Gage used to level the belt profiler.

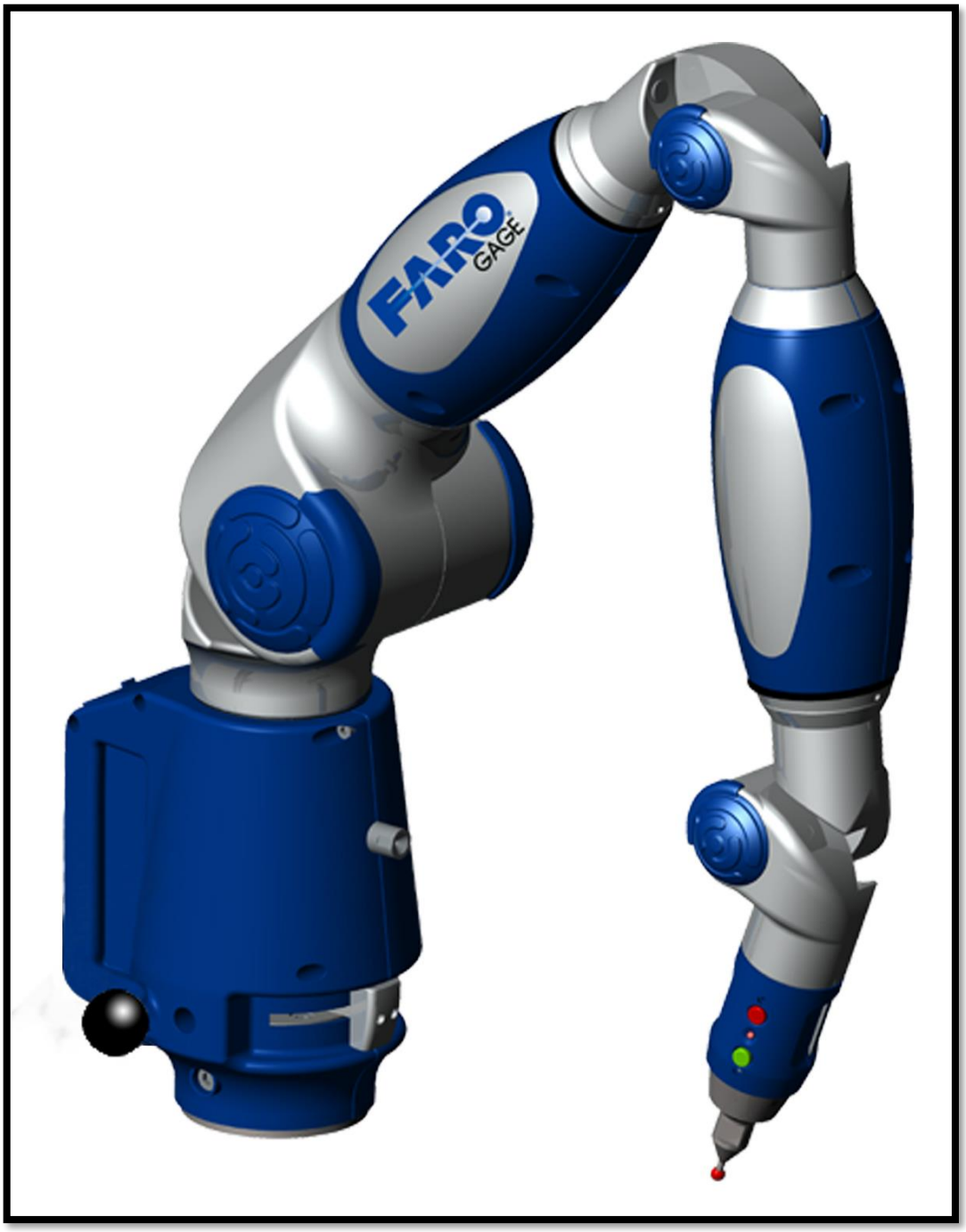


Figure 8-23: Faro gage used in the levelling for the belt profiler (Faro, 2017).

8.4 Load Cell Data

8.4.1 Readings for the 2 Ton Loadcells

Table 8-10: Calibration readings (in mV/m) for the 18, 2 ton load cells.

Force (N)	P111167	P174325	P109434	P174503	P109315	P179190	P225946	P174620	P178827	P110063	P109045	P022742	P111191	P278809	P178595	P178580	P108272	P109003
5	-2.17E-07	-2.16E-07	-2.36E-06	2.61E-07	-9.81E-09	-1.69E-09	2.14E-08	3.33E-07	2.64E-07	3.27E-07	3.10E-07	5.14E-07	2.05E-07	-3.32E-08	1.44E-07	-3.67E-08	-2.25E-07	3.64E-07
2500	1.92E-04	1.92E-04	1.90E-04	1.93E-04	1.92E-04	1.92E-04	1.93E-04	1.93E-04	1.92E-04	1.92E-04	1.92E-04	1.92E-04	1.92E-04	1.92E-04	1.92E-04	1.92E-04	1.92E-04	1.93E-04
5000	3.84E-04	3.84E-04	3.82E-04	3.85E-04	3.85E-04	3.84E-04	3.84E-04	3.85E-04	3.85E-04	3.85E-04	3.85E-04	3.84E-04	3.84E-04	3.84E-04	3.84E-04	3.86E-04	3.83E-04	3.84E-04
7500	5.76E-04	5.76E-04	5.75E-04	5.78E-04	5.78E-04	5.75E-04	5.74E-04	5.76E-04	5.77E-04	5.77E-04	5.77E-04	5.77E-04	5.77E-04	5.76E-04	5.77E-04	5.78E-04	5.77E-04	5.77E-04
10000	7.68E-04	7.69E-04	7.67E-04	7.70E-04	7.71E-04	7.68E-04	7.68E-04	7.69E-04	7.70E-04	7.70E-04	7.70E-04	7.70E-04	7.69E-04	7.70E-04	7.70E-04	7.69E-04	7.69E-04	7.69E-04
12500	9.62E-04	9.62E-04	9.61E-04	9.62E-04	9.63E-04	9.60E-04	9.60E-04	9.62E-04	9.63E-04	9.62E-04	9.63E-04	9.63E-04	9.62E-04	9.62E-04	9.62E-04	9.63E-04	9.62E-04	9.63E-04
15000	1.15E-03	1.15E-03	1.15E-03	1.16E-03	1.16E-03	1.15E-03	1.15E-03	1.15E-03	1.16E-03	1.15E-03	1.16E-03	1.15E-03	1.15E-03	1.15E-03	1.15E-03	1.16E-03	1.15E-03	1.16E-03
17500	1.35E-03	1.35E-03	1.35E-03	1.35E-03	1.35E-03	1.34E-03	1.35E-03	1.35E-03	1.35E-03	1.35E-03	1.35E-03	1.35E-03	1.35E-03	1.35E-03	1.35E-03	1.35E-03	1.35E-03	1.35E-03
20000	1.54E-03	1.54E-03	1.54E-03	1.54E-03	1.54E-03	1.54E-03	1.54E-03	1.54E-03	1.54E-03	1.54E-03	1.54E-03	1.54E-03	1.54E-03	1.54E-03	1.54E-03	1.54E-03	1.54E-03	1.54E-03
17500	1.35E-03	1.35E-03	1.35E-03	1.35E-03	1.35E-03	1.34E-03	1.35E-03	1.35E-03	1.35E-03	1.35E-03	1.35E-03	1.35E-03	1.35E-03	1.35E-03	1.35E-03	1.35E-03	1.35E-03	1.35E-03
15000	1.16E-03	1.15E-03	1.15E-03	1.16E-03	1.16E-03	1.15E-03	1.15E-03	1.15E-03	1.16E-03	1.15E-03	1.16E-03	1.15E-03	1.15E-03	1.15E-03	1.15E-03	1.16E-03	1.16E-03	1.16E-03

12500	9.63E-04	9.62E-04	9.61E-04	9.64E-04	9.64E-04	9.60E-04	9.61E-04	9.62E-04	9.63E-04	9.62E-04	9.62E-04	9.62E-04	9.62E-04	9.61E-04	9.62E-04	9.64E-04	9.63E-04	9.63E-04
10000	7.70E-04	7.69E-04	7.68E-04	7.71E-04	7.70E-04	7.68E-04	7.69E-04	7.67E-04	7.69E-04	7.71E-04	7.70E-04	7.70E-04	7.69E-04	7.70E-04	7.70E-04	7.71E-04	7.70E-04	7.70E-04
7500	5.77E-04	5.79E-04	5.76E-04	5.78E-04	5.78E-04	5.75E-04	5.77E-04	5.77E-04	5.78E-04	5.77E-04	5.77E-04	5.77E-04	5.77E-04	5.76E-04	5.77E-04	5.78E-04	5.77E-04	5.77E-04
5000	3.85E-04	3.85E-04	3.84E-04	3.86E-04	3.86E-04	3.84E-04	3.85E-04	3.84E-04	3.85E-04	3.84E-04	3.85E-04	3.85E-04	3.85E-04	3.84E-04	3.85E-04	3.85E-04	3.85E-04	3.85E-04
2500	1.93E-04	1.92E-04	1.90E-04	1.94E-04	1.93E-04	1.92E-04	1.94E-04	1.93E-04	1.93E-04	1.93E-04	1.94E-04	1.93E-04	1.93E-04	1.92E-04	1.94E-04	1.93E-04	1.93E-04	1.93E-04
5	7.42E-07	5.08E-07	-1.96E-06	9.00E-08	3.13E-07	3.20E-07	7.96E-07	9.07E-08	5.90E-08	3.06E-07	-2.55E-07	5.88E-07	9.23E-07	4.55E-07	3.16E-07	5.68E-07	2.86E-07	1.75E-07

8.4.2 Readings for the 20 Ton Loadcell

Table 8-11: Calibration readings (in mV/m) for the 20 ton load cell.

Force (kg)	Reading (mV/V)
18	1.6E-6
2000	99.8E-6
4000	197.0E-6
6000	295.0E-6
8000	393.0E-6
10000	492.3E-6
12000	589.1E-6
14000	686.2E-6
16000	783.5E-6
18000	881.0E-6
20000	978.2E-6
18000	881.3E-6
16000	783.6E-6
14000	686.2E-6
12000	590.3E-6
10000	492.3E-6
8000	393.0E-6
6000	295.4E-6
4000	197.2E-6
2000	99.9E-6
18	538.0E-9